

THESIS FOR THE DEGREE OF DOCTOR OF PHILOSOPHY

Non-intrusive instrumentation and estimation

-Applications for control of an additive manufacturing process

PETTER HAGQVIST

Department of Signals and Systems
Automatic control, Automation and Mechatronics
CHALMERS UNIVERSITY OF TECHNOLOGY
Göteborg, Sweden 2015

Non-intrusive instrumentation and estimation
-Applications for control of an additive manufacturing process
PETTER HAGQVIST
ISBN 978-91-7597-148-3

© PETTER HAGQVIST, 2015.

Doktorsavhandlingar vid Chalmers tekniska högskola
Ny serie nr 3829
ISSN 0346-718X

Department of Signals and Systems
Automatic control, Automation and Mechatronics
Chalmers University of Technology
SE-412 96 Göteborg
Sweden
Telephone + 46 (0)31 – 772 1000

Typeset by the author using L^AT_EX.

Chalmers Reproservice
Göteborg, Sweden 2015

For my girls

Measure what is measurable and make measurable what is not so.
- Galileo Galilei *

*Most often attributed to Galileo, although evidence suggests that he may not in fact be the source of the quote [1].

Acknowledgements

There are very many people beside myself that have contributed to me being able to pursue a doctoral degree. My supervisors Anna-Karin Christiansson and Bengt Lennartson should be saluted for their patience with me and for the guidance they have provided me with. Almir Heralić deserves a very special mention, as he is very much responsible for the creation of the technology that is LMD-w. His deep understanding of the process and detailed knowledge of nearly all things concerning LMD-w has been essential in this work. I would also like to address a special thanks to Fredrik Sikström who has been a mentor for me in both temperature measurements and control theory. I would also like to mention my gratitude towards Hans Dahlin and his electrical wizardry. Thanks also to Kjell Hurtig who has been very patient and understanding with all my questions concerning welding. And also for acting as a living prop during the Researcher's Grand Prix final.

Wei Jan Wang at IKV, Tommy Ive at Chalmers MC2, Per Nylén and Morgan Nilsen have been most helpful with testing and commercialising the ECSP technology. Especially I would like to thank Per for not only managing the projects and investing his precious time in my idea, but also for mentoring me throughout the process. Peter Jonsson, Per Thorin and other very competent professionals at GKN Aerospace in Trollhättan have my appreciation for giving both an industrial viewpoint, as well as sharing tricks of the trade with an outsider.

I also address special thanks to: Jeroen De Backer, Patrik Broberg, Isabelle Choquet, Jack Donoghue, David Filipiak, Emile Glorieux, Camilla Martinsson, Alireza Javidi Shirvan, Ali Keyvani, Jeff Resnick, Lisa Simonsson, Edvard Svenman and Victoria Sjöstedt along with my other colleagues at Production Technology Center who have been available for discussions and questions.

Funding for this thesis has been received from the European Community's Seventh framework Programme FP7 2007-2013 under grant agreement 266271 - Merlin Project. Also, projects funded by Tillväxtverket and Vinnova have contributed to funding my research.

The last and deepest thanks goes to Klara and Eva-Lena, for everything else.
Vad funkar bäst? –Teamwork!

PETTER HAGQVIST
Trollhättan, January 2015

Preface

If someone would have asked me if I wanted to pursue doctoral studies when I was still studying for my M.Sc. I would most likely have replied something like:

” Getting a Ph.D. is just for the ones who fail to get a real job.”

It was a longstanding joke among me and my friends whenever we were taught by an eccentric doctor or doctoral student, that pursuing an academic career was for those who did not quite cut it in ”the real world”. In retrospect it is more of a joke on us that the great majority of me and my friends from Linköping now either have, or are about to earn, our Ph.D. degrees.

Also, if someone would have asked me whether I would have considered automation as a subject, I would most likely have been skeptical to say the least. My master’s degree is in Engineering Biology and before I got to University West I had never been acquainted to anything similar to production technology or automation. Then, one might wonder, how did I end up replacing biosensors and macromolecular chemistry with robot programming and welding? I have asked myself the same question many times for the past years. I guess the answer is related to my curiosity and ambition to learn a bit about everything. Anna-Karin challenged me, but also believed that it was possible for me to change horses in midstream, and I guess that this book serves as proof that she was correct, as usual.

I am convinced that I am not the first to develop a love-hate relation to my thesis subject. Many days when I was going to the lab, I have felt a pressing feeling of anxiety as to ”what is going to break or go wrong today?”. But also when things have actually worked, more or less the way they should, I have been literally dancing around and cheering outside the cell. During the most stressful and hard periods, Anna-Karin’s encouragement and never-ending positive attitude has helped a lot. Although I have at times almost felt provoked by your way of always seeing the best in situations and people, Anna-Karin, I have learnt a lot from it.

I have really enjoyed the past years and I will always cherish the great working environment at PTW created by my dear colleagues. There will surely be times when I will miss being a Ph.D. student, with many possibilities and still quite few responsibilities, but today I long for the next step.

PREFACE

Since this thesis is the most concrete result of my work, I would like to give some encouraging words to whoever you are attempting to read it. If it seems hard to grasp, difficult to understand or just quite boring, you are more or less sharing the feelings I had when I wrote it. In that case, I recommend making yourself a cup of good tea and putting on some music that you like. Then when you return to reading again, the text will be no easier to understand, and it will not miraculously have turned into great literature. But while you keep struggling, you will at least have something good to drink and to listen to. Happy reading!

PETTER HAGQVIST

Trollhättan, January 2015

Publications

This thesis is based on the following appended papers:

- Paper 1** P. Hagqvist, F. Sikström, and A-K. Christiansson, Emissivity estimation for high temperature radiation pyrometry on Ti-6Al-4V, *Measurement*, **46(2)**:871-880, Feb 2013.
- Paper 2** P. Hagqvist, F. Sikström, A-K. Christiansson and Bengt Lennartson, Emissivity compensated spectral pyrometry for varying emissivity metallic measurands, *Measurement Science and Technology*, **25**:025010 2013, Feb 2014.
- Paper 3** P. Hagqvist, F. Sikström, A-K. Christiansson and Bengt Lennartson, Emissivity compensated spectral pyrometry - algorithm and sensitivity analysis, *Measurement Science and Technology*, **25**:025011 2013, Feb 2014.
- Paper 4** P. Hagqvist and A-K. Christiansson, *Proceedings of IECON 2013 - 39th Annual Conference on IEEE Industrial Electronics Society*. pages 2384-2389, Vienna AUT, Nov 2013.
- Paper 5** P. Hagqvist, A. Heralić, A-K. Christiansson and Bengt Lennartson, Resistance measurements for control of laser metal wire deposition, *Optics and Lasers in Engineering*, **54**:62-67, Mar 2014.
- Paper 6** P. Hagqvist, A. Heralić, A-K. Christiansson and Bengt Lennartson, Resistance based iterative learning control of additive manufacturing with wire, resubmitted after revision to *Mechatronics*, Jan 2015.

PUBLICATIONS

The following publications, not appended, are relevant to the work presented in this thesis.

P. Hagqvist, A method for measuring temperature, PCT patent application, PCT/EP2012/071393.

P. Hagqvist, H. Kristoffersen, A-K. Christiansson, Temperature monitoring of induction hardening using spectral pyrometry, in *Proceedings of SPS14 - 6th Swedish Production Symposium*. Gothenburg SWE, September 2014.

Contents

Acknowledgements	i
Preface	iii
Publications	v
Contents	vii
Abstract	xvii

I Introductory chapters

1 Introduction	1
1.1 Background	1
1.2 Previous work within LMD-w	8
1.3 Process monitoring and control of AM processes	9
1.4 Scope of work	10
1.5 Research questions	11
1.6 Limitations	12
1.7 Contributions	12
1.8 Outline	14
2 The laser metal wire deposition process	15
2.1 Deposition process	15
2.2 Equipment	17
2.3 Difficulties in laser metal wire deposition	23
2.4 Summary	26
3 Process measurements and actuators	27
3.1 Limitations	27
3.2 Implemented systems	28
3.3 Prospective technologies for measuring geometry in LMD-w	30

CONTENTS

3.4	Actuators	32
3.5	Summary	34
4	Process control of LMD-w	37
4.1	Previously implemented control strategies	37
4.2	Resistance in-process control	39
4.3	Temperature control	40
4.4	Summary	43
5	Temperature measurements	45
5.1	Contact thermometry	45
5.2	Radiation thermometry fundamentals	45
5.3	Emissivity	46
5.4	Pyrometry	49
5.5	Summary	52
6	Emissivity compensated spectral pyrometry	53
6.1	ECSP functionality	54
6.2	Algorithm	56
6.3	Weights and filtering	58
6.4	Calibration	59
6.5	Sensitivity analysis	60
6.6	ECSP results	66
6.7	ECSP for LMD-w monitoring	67
6.8	Summary	68
7	Summary of included papers	71
8	Conclusions and future work	75
	Appendix	79
A	The importance of Planck's law for ECSP	81
	References	86
II	Included papers	
Paper 1	Emissivity estimation for high temperature radiation pyrometry on Ti-6Al-4V	103
1	Introduction	103
2	Theory	105

2.1	Narrow Wavelength Radiation Pyrometry	105
2.2	Difficulties in Spectral Radiation Pyrometry	106
2.3	Methods for Emissivity Measurements	107
2.4	Emissivity of Ti-6Al-4V	107
2.5	Reference Paints	108
3	Method for Emissivity Estimation	108
4	Experimental procedure	109
5	Calibration Results and Discussion	111
5.1	Implications on Trial 1	112
5.2	Uncertainty in Emissivity and Temperature	112
5.3	Resulting uncertainty in temperature measurement	114
5.4	Phase transitions	115
5.5	Modelling of Emissivity Behaviour	116
5.6	Implications on Trial 2	118
6	Conclusions	119
	References	120
Paper 2 Emissivity compensated spectral pyrometry for varying emissivity metallic measurands		127
1	Introduction	127
2	Thermal radiation	129
3	Proposed method	130
3.1	Prerequisites	130
3.2	Measurement scenario	131
3.3	Algorithm	132
4	Experimental setup and results	133
4.1	Equipment	133
4.2	Experimental procedure	135
4.3	Algorithm implementation	136
4.4	Results	136
4.5	Emissivity variations	138
5	Conclusions and future work	139
	References	140
Paper 3 Emissivity compensated spectral pyrometry - algorithm and sensitivity analysis		147
1	Introduction	147
2	Theory	148
2.1	Emissivity	148
2.2	Temperature measurement method	149
3	Sources of uncertainty	154
3.1	Instrument calibration	154

CONTENTS

3.2	Error model	156
3.3	Estimation of relative standard deviation	156
3.4	Practical signal levels and weighting with β	157
4	Principle experimental setup	158
5	Sensitivity analysis through simulations	158
5.1	Implementation	159
5.2	Sensitivity to noise	159
5.3	Sensitivity to emissivity changes	161
5.4	Sensitivity to temperature change rate	162
6	Conclusions and discussion	163
	References	164
Paper 4 Automatic detection of material phase transitions from spectroscopic data		169
1	Introduction	169
2	Background	170
3	Materials and experiment	171
4	Phase change detection methods	173
4.1	Identification of oxide cap formation	173
4.2	Method I: Sectioning with derivatives	175
4.3	Method II: Identification of radiance steady state	175
4.4	Method III: Cross correlation	176
4.5	Weighting for wavelengths	176
5	Results	177
5.1	Method I: Sectioning with derivatives	177
5.2	Method II: Identification of radiance steady state	177
5.3	Method III: Cross correlation	179
6	Conclusion	179
	References	180
Paper 5 Resistance measurements for control of laser metal wire deposition		185
1	Introduction	185
2	Control strategy	187
3	LMD-w system	188
3.1	Hardware	188
3.2	Software and communication	189
3.3	Material	189
3.4	Deposition	190
4	Resistance model	190
4.1	Model creation	191
4.2	Resulting model	191

5	Distance controller	192
6	Results and discussion	193
7	Conclusions and future work	195
	References	196

Paper 6	Resistance based iterative learning control of additive manufacturing with wire	201
1	Introduction	201
1.1	The LMD-w process	202
1.2	Previous work	204
1.3	Motivation	204
2	Materials and methods	205
2.1	Resistance to distance model	205
2.2	Resistance measurement system	205
2.3	Filtering of resistance signal	206
2.4	Control system	207
2.5	Actuators	207
2.6	Iterative learning controller	208
2.7	Implementation	211
2.8	Experimental procedure	212
3	Results and discussion	213
4	Conclusion	215
	References	216

Nomenclature

Although consistency of notation has been a target when writing this thesis, some notation may not be consistent between the papers. This is since the readers of the different publications expect a certain, and in their opinion standard, notation. It is only when these notations that are used in different fields clash that the notation in this thesis is inconsistent. One example is θ which is used both for denoting a polar angle, which is standard in mathematics and physics, and for denoting a regression vector, which is standard in control science.

Abbreviations

AM	Additive Manufacturing
A/D	Analog to Digital
Alloy 718	Nickel based precipitation hardening super-alloy
BLUE	Best Linear Unbiased Estimator
CAD	Computer Aided Design
CAM	Computer Aided Manufacturing
CCD	Charge Coupled Device
ECSP	Emissivity Compensated Spectral Pyrometry
ILC	Iterative Learning Control
IR	Infra Red
LMD-p	Laser Metal Deposition with powder
LMD-w	Laser Metal Deposition with wire
MAG	Metal Active Gas, a welding technology
MBE	Molecular Beam Epitaxy
MIG	Metal Inert Gas, a welding technology
NIR	Near Infra Red
PCT	Patent Cooperation Treaty
PLC	Programmable Logic Controller
PTW	Production Technology West, research group at University West
SLM	Selective Laser Melting

CONTENTS

SMD	Shaped Metal Deposition
SNR	Signal to Noise Ratio
TCP	Tool Center Point
Ti6Al4V	High performance titanium alloy used in aerospace and medical applications
TIG	Tungsten Inert Gas, a welding technology
TOF	Time-Of-Flight
UV	Ultra Violet
UV-Vis	Ultra Violet and Visual
WAAM	Wire and Arc Additive Manufacturing

Mathematical Notation

x	Scalar valued variable x
\mathbf{x}	Vector variable \mathbf{x} , wavelength resolved ($n \times 1$) unless otherwise stated
\mathbf{X}	Matrix variable \mathbf{X} , $n \times n$ unless otherwise stated
$N(\mu, \sigma)$	Gaussian distribution with first moment μ , and second moment σ
$\mathbf{x} \circ \mathbf{y}$	Hadamard element-wise multiplication of vectors \mathbf{x} and \mathbf{y}
$\mathbf{x} \oslash \mathbf{y}$ and $\frac{\mathbf{x}}{\mathbf{y}}$	Hadamard element-wise division of vectors \mathbf{x} and \mathbf{y}
\tilde{x}	$x - \hat{x}$, the estimation error
$\underline{\mathbf{x}}$	Normalisation into a vector from 0 to 1: $(\mathbf{x} - x_{min}) / (x_{max} - x_{min})$

Latin letter variables

A_c	Cross sectional area of deposited bead
B_e	Bias error of spectrometer calibration matrix
d	Distance between nozzle and substrate
d_{nom}	Nominal d
e	Error in reading from sensor
F_t	Time-domain filter
F_λ	Wavelength-domain filter
G	Function which predicts current spectral emissivity from history
G_ε	Function creating an emissivity estimation from temperature and radiance
G_T	Function creating a temperature estimation from emissivity and radiance
H	Difference measure, translates a vector of differences to scalar value
I	Electrical current
j	Layer iterator in ILC

k	Discrete time instance
l	Wire stick-out length
n	Number of wavelength channels in spectra
N	Total number of samples
$n + \kappa i$	Complex refractive index, note that this n differs from that above
P_L	Laser power
r_P	Blackbody radiance, scalar value
\mathbf{r}_P	Blackbody radiance, spectral vector value
r_E	Emitted radiance, scalar value
\mathbf{r}_E	Emitted radiance, spectral vector value
r_k	Measured scalar radiance at sample k
\mathbf{r}_k	Measured spectral radiance at sample k
R	Resistance
T	Absolute temperature
T_P	Temperature as measured by a pyrometer
\hat{T}	Estimated temperature
\tilde{T}	Temperature estimation error, i.e. $\hat{T} - T$
\mathbf{u}	Control signal consisting of m individual control signals $[u_1, u_2 \cdots u_m]$
v_t	Traverse speed of robot
v_w	Wire feed rate
V	Voltage
z	Weighted difference scalar, argument to H
\mathbf{z}	Weighted difference vector, argument to H
Greek letter variables	
α_L	Laser incidence angle relative to substrate
α_w	Wire incidence angle relative to substrate
β	Weights used in ECSP algorithm
γ_k	Relative Standard Deviation at sample k , γ is also used for denoting learning gains in an ILC context
Γ	Reflectivity
ε	Emissivity, scalar value
$\boldsymbol{\varepsilon}$	Emissivity, spectral vector value
$\boldsymbol{\varepsilon}^Q$	Compound spectral emissivity
$\hat{\boldsymbol{\varepsilon}}_{k k-1}^Q$	Estimated compound spectral emissivity at instance k given information up until $k - 1$

CONTENTS

θ	Polar coordinate system angle for describing radiance emission direction, also used as a regression vector in resistance to distance modelling
τ	Atmospheric transmission
λ	Wavelength
Λ	Wavelength range, $\lambda_1.. \lambda_n$
μ_k	Sensor distribution mean value at sample k
ν	Filter window/kernel size
ξ	Function for describing spectral emissivity in multispectral pyrometry
ρ	Optical path spectral attenuation
σ	Theoretical sensor standard deviation
σ_χ	Actual sensor standard deviation, due to χ
ϕ	Polar coordinate system angle for describing radiance emission direction, also used as a regression vector in resistance to distance modelling
χ	Biased spectrometer calibration matrix

Abstract

For integration of additive manufacturing into industrial production, there is a need for capable yet robust automation solutions. Such solutions are to ensure consistent process outputs, both with regard to deposit geometry and material properties. In this thesis, instrumentation and control solutions have been investigated for the laser metal wire deposition additive manufacturing process. This particular process is promising with regard to e.g. high deposition rates and negligible material waste. However, due to its inherent dynamics, it requires automatic control in order to prove competitive.

A large number of process parameters affect the resulting quality of the deposit. Successful control of these parameters is crucial for turning laser metal wire deposition into an industrially tractable process. This requires relevant and reliable process information such as the temperature of the deposit and the positioning of the tool relative to the workpiece. Due to the particular requirements of instrumenting the process, only non-intrusive measurement methods are viable. In this thesis, such measurement solutions are presented that advance automatic control of the laser metal wire deposition.

In response to the need for accurate temperature measurements for the process, a new temperature measurement method has been developed. By adopting the novel concept of temporal, rather than spectral, constraints for solving the multispectral pyrometry problem, it opens up for temperature measurements which compensates for e.g. an oxidising deposit.

For maintaining a good deposition process in laser metal wire deposition, control of tool position and wire feed rate is required. Based on measurements of resistance through the weld pool, a simple yet well performing control system is presented in this thesis. The control system obtains geometrical input information from resistance measurements made *in-situ*, and feeds this information to an iterative learning controller. This results in a robust, cheap and practical control solution for laser metal wire deposition, which is suitable for industrial use and that can easily be retrofitted to existing equipment.

Keywords: Additive Manufacturing, Automation, Emissivity, Emissivity Compensated Spectral Pyrometry, Laser Metal Wire Deposition, Metal Deposition, Pyrometry, Resistance Feedback Control, Thermometry

Part I

Introductory chapters

Chapter 1

Introduction

1.1 Background

Metal additive manufacturing (AM) comprises of technologies which produce net-shaped or near net-shaped components in metal. These components may be solid or hollow and of various geometrical complexities, but they are all produced as a means of manufacturing a final product and not only for prototyping. The components are typically built up layer by layer through melting or fusing material in a certain two dimensional pattern as indicated in Figure 1.1. Several layers with suitable patterns are deposited on top of each other resulting in the component's final shape. The metal additive manufacturing technologies,

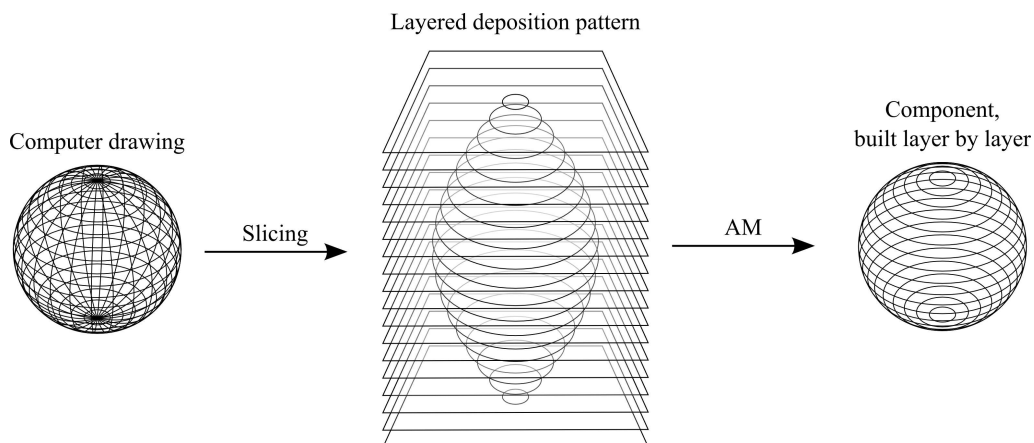


Figure 1.1: Illustration of the AM principle. A computer drawing of a component is sliced into several two dimensional layer patterns. These patterns are deposited on top of each other, forming the component's geometry.

throughout this thesis simply referred to as AM-technologies, excluding polymer and ceramic AM technologies, are based on a number of different energy sources and material feedstocks. They provide extended means for the manufacturing in-

dustry to cut lead times and production costs substantially, especially for small series [2]. AM technologies even allow for completely new concepts of manufacturing components, which combine several different manufacturing technologies and maximises the strengths of each of them. Additive manufacturing provides enabling technologies that can provide the last building block required for replacing conventional manufacturing technologies, such as machining and casting, for certain applications [3]. Some of the AM technologies are also very well suited for repairwork and modifications of preexisting component geometries [2, 3].

Metal additive manufacturing has existed for several decades and been implemented in many forms during that time [2, 4]. The advent of the industrial lasers and developments in welding technology caused an increase in research, publications and patents in the 1980's. During the last decennia, the technologies have been further developed and commercialised and are even sold as turn-key systems [5–8].

Motivations for additive manufacturing

AM technologies offer a lot of advantages when compared to the alternatives. AM provides the possibility to quickly produce finished components which only require moderate post-processing, if any at all. For applications where flexibility is vital, the ability of AM technologies to adapt production to today's or tomorrow's requirements is most desirable. Typically, an operator should only have to upload a CAD/CAM file to the AM system and the component is produced without intermediate steps. The ability to perform AM in-house might also reduce dependence on subcontractors and reduce transports needed both inside and outside the production facility [2].

Compared to machining, material waste and production times can be reduced considerably. Casting is another competing technology which has significant weaknesses compared to AM, especially for small series. In some cases components produced by AM exhibit better material characteristics than castings and AM-parts do not have to be produced at a foundry [3]. Also, AM offers possibilities of producing more complex geometries than what would be advisable for casting. The improved material characteristics and increased design freedom allow for more optimal component design with reduced weight and material usage, which in turn lead to more sustainable product.

For repair applications, the benefits are quite obvious. Instead of scrapping an entire component, the damaged portion is removed, usually by machining away material. The removed material is then replaced with new, added material, restoring the component geometry. AM also allows for graded composition of materials where costly high performance materials are only used where needed, and cheaper materials are used for bulk and low stress areas of the component [2,

3].

The drawbacks of AM mainly comes down to a few points:

- Depending on the process, the resulting material quality may vary throughout the component due to process disturbances, such as temperature buildup.
- Mitigating such disturbances by employing a control system has proven challenging [2, 3], a situation which is illuminated also in this thesis.
- AM systems have typically been aimed at smaller components and these systems do not scale up easily.
- Investment costs for investing in a physical system and for training might deter the industry from adopting AM.
- Being new and somewhat untested technologies, AM systems are not as well established as their conventional alternatives. In addition, manufacturing standards for AM are not yet agreed upon except for certain applications. The safe route might therefore be to go with what is trusted and known when a decision on how a components should be manufactured is made.

AM is not suited for replacing conventional manufacturing processes in all or even a majority of the cases. But for some applications, the adoption of AM technologies is very rewarding. For the developers and suppliers of AM systems, identification of these applications might however prove to be just as a challenging task as technology development itself.

Available technologies

There is a wide range of technologies available on the market and under development. Their main differences lie in how the material is conveyed to the process and which power source is used for restructuring or melting the material.

Powder bed systems

The perhaps most well developed technology within AM, with many commercial systems available, is the powder bed based system. A thin layer of metal powder is distributed on a platform and is selectively melted by means of a power source and re-solidifies, fusing the powder into the desired geometry. Another powder layer is placed on top of the previous one and is selectively melted just like the layer before. Through this stepwise procedure of distributing powder layers and selectively melting them, it is possible to manufacture very complex parts. Hollow, or even counter-intuitive geometries, such as the Klein bottle



Figure 1.2: Klein bottle manufactured using a powder bed process.

shown in Figure 1.2 can be created with these methods. Usually powder bed AM systems give very good geometrical accuracy and allow for very high degrees of design freedom [9]. However, surface finish, size limitations and production speed might be substantial problems when utilising these methods.

Electron beam power source Arcam AB, is a Swedish company, which has developed the combination of powder bed and electron beam technology. They have been very successful in producing orthopaedic implants [10], and also market products towards the aerospace industry [7]. Because of these application areas, Arcam has specialised in titanium and cobalt-chrome alloys. Processing takes place in a low pressure processing chamber and resulting material is claimed to be better than cast material and comparable to wrought material [11]. The use of electron beams offers the possibility of tuning surface parameters such as porosity and roughness. The largest build envelope offered by Arcam today is $\varnothing 350 \times 380$ mm with their Q20 machine [12].

Laser power source The use of a laser power source together with powder bed technology is a relatively well established technology with a number of companies offering complete solutions [4, 13–16]. They all share strengths and weaknesses. These systems, often denoted Selective Laser Melting (SLM), are well suited for smaller components with complex geometries, thin walls, hollow structures etcetera. For some applications however, surface roughness is rela-

tively high due to entrapped semi-molten powder particles. Hence, the finished component might require post-processing such as milling. The use of a process chamber also severely limits the size of produced components. This, along with a relatively slow production speed, makes the technology mostly useful for smaller components manufactured in small series. Using laser as a power source allows for use in atmospheric pressure since it is not deflected, like an electron beam is, by gas residing in the chamber. Considering the resulting material, studies have shown that static mechanical properties are, although somewhat anisotropic, comparable to those of wrought material while the fatigue strength is decreased compared to conventional materials [9]. The previously used range of materials include stainless steel, tool steel, cobalt-chrome, titanium and aluminium alloys.

Laser powder deposition

There are quite a few suppliers of systems which rely on powder being fed through a nozzle into a weld pool which is created by a laser source [2, 17, 18]. Material is deposited, by melting and subsequent solidification, side-by-side and layer upon layer. This technology, in this work referred to as laser metal powder deposition (LMD-p), enables buildup of larger components than what is possible with powder bed solutions while still retaining good dimensional accuracy. Usually, a powder delivery system delivers the powder through a nozzle which is more or less integrated with the laser optics. The deposition tool can be mounted onto either a robot or a NC-type movement actuator. The downsides of this technology lie in the fact that the use of powder might result in porous material if not enough care is taken tuning the process. Furthermore, the handling of powder requires health and safety precautions along with a powder collection system for excess powder not fused into the deposit. Recycling of powder is currently investigated by powder suppliers but proves hard to certify for high spec applications. Material used with this technology include: mild steel, Al-, Nb-, Ni-, Co-, Cu- and Ti-based alloys. Due to the technology's potential for processing exotic materials which are otherwise hard to process, much work has been spent investigating high temperature materials such as highly alloyed Ni [2]. The material characteristics are highly dependent on process parameters and may be tuned to suit the target application. In general terms, laser powder deposition allows for larger build envelopes and higher deposition rates than powder bed solutions. In turn, the solutions based on nozzle-fed powder achieve lower dimensional accuracy and less control of deposit material characteristics.

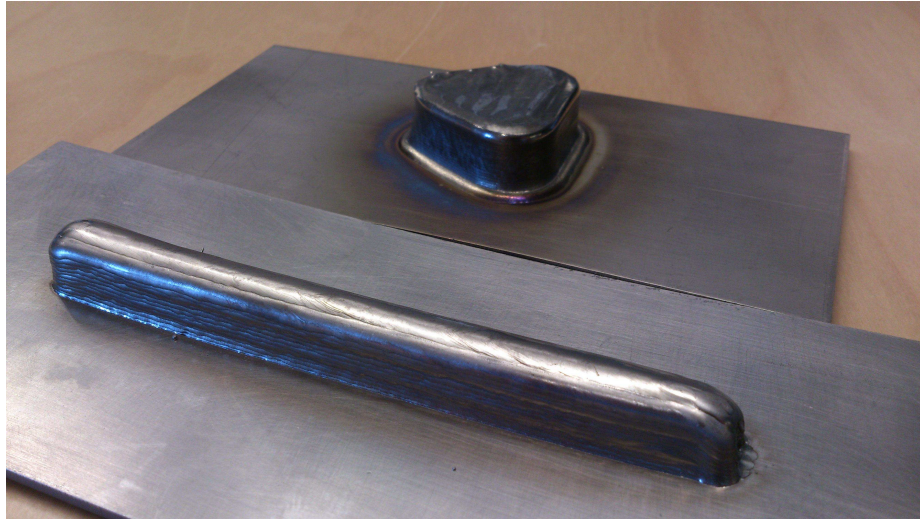


Figure 1.3: Examples of laser wire deposition components manufactured at University West.

Wire deposition

The main advantages of the wire deposition processes are due to that, since wire is used, all material is utilised and high deposition rates are possible. However, the wire processes prove hard to control and commercial systems are typically less developed than the powder based methods [19, 20]. Similarly to LMD-p, described above, the build envelope of wire deposition technologies is typically only restricted by the reach of the manipulator robot or gantry.

At University West in Trollhättan Sweden, a long-standing cooperation with GKN Aerospace (formerly Volvo Aero) has resulted in a technology called robotised laser metal wire deposition, in this work abbreviated LMD-w. The technology has proven to give aerospace specification grade deposits of titanium alloy [3] and is today used by GKN in production. Standard laser welding equipment such as a 6 kW fibre laser, focusing optics and a robot is combined with custom monitoring and control systems for successful deposition. This system, although not yet productified, has proven to overcome some of the process' inherent difficulties such as weld pool instability, poor material fusion and poor geometrical accuracy [3]. This technology also requires little or no post-machining of parts for geometrical accuracy and surface finish. Examples of titanium deposits made with LMD-w are shown in Figure 1.3. This technology and the associated process is at the center of this thesis and the subject of study. Similar, but independently developed, technologies has been investigated and described by Miranda et al. [21] as well as Syed et al. [22, 23]. Brandl et al. have also investigated combined use of laser with wire feedstock for additive manufacturing [24–26]. The company Norsk Titanium uses another power source

for depositing titanium. A plasma is used for melting the wire, which allows for cheaper hardware and possibly a process which is less susceptible to disturbances than when using a laser [27]. However, deposited components require post-process machining due to oxide scaling of the material. Despite this drawback, Norsk Titanium has proved that plasma based wire deposition is a viable business case with high value for the customer. A critical element in this is to quickly generate parts directly from a CAD-model without any manual adjustments.

Another wire deposition technology, which is developed by Sciaky Inc. is the use of an electron beam together with wire. Automatic processing of CAD-models and their deposition technology allows for easy prototyping and production of large scale components as large as $5.5 \times 1.2 \times 1.2$ m directly from the computer to the ready-for-machining component [8].

Cranfield University and Rolls Royce Inc. have jointly developed a technology for depositing wire using a Tungsten Inert Gas (TIG)-weld source called shaped metal deposition (SMD). A robotic arm is used together with path generation algorithms and automatic control of deposition. Much effort has been addressed to material properties and evaluation [28–31]. This technology has been extended and further developed by Cranfield University into the Wire and Arc Additive Manufacture (WAAM) process. The WAAM technology encompasses a variety of arc energy sources such as Cold Metal Transfer (CMT), DC and AC TIG, Tandem Metal Inert Gas (MIG) as well as plasma [32, 33]. A number of academic publications describe the WAAM technology, both with regard to material properties [34–39] and with regard to the process and process control [34, 40–43].

Fabrication strategies with additive manufacturing

The ability to use additive manufacturing technologies allows designers much greater freedom when designing components, both with regard to load dimensioning, materials used and possible geometries. Instead of casting or machining entire components, geometrically complex parts of the component can be cast or machined and then welded together or onto high strength sheet or bar material. Smaller features such as stiffeners or welding preps can then be deposited with AM. The possibilities and benefits of this fabrication strategy are many. Weight can be saved through using higher specification materials, which allow for weight optimised components. Higher geometrical freedom gives possibilities to manufacture near optimal structures instead of being limited by a conventional manufacturing method. Minimising the use of castings will decrease the reliance on foundries and enable a larger part of the component value to be generated within one manufacturing plant. Even though more processing steps

might be introduced, the steps performed might still be faster than machining or casting an entire component. When introducing a fabrication concept into production and design, AM technologies are essential for adding component parts which are not easily manufactured with any other method. AM is very well suited for creating flanges and stiffeners due to the ability to add material onto existing parts whereas most other processing methods removes material [3].

1.2 Previous work within LMD-w

Using wire as filler material for laser metal deposition shows great potential when prioritising relatively simple geometries deposited at high speed. No complete LMD-w systems are however available as a ready to use products, which can be bought as of today to the author's knowledge. One of the main reasons for this is the very nature of the process which is typically hard to predict and control. A good result has up until recently been totally dependent of a skilled operator. In 2012 Almir Heralić defended his thesis "*Monitoring and Control of Robotised Laser Metal-Wire Deposition*" in which he describes a way to use an automatic geometry control system [3]. This control system is shown to give a stable process, which results in a deposit with dimensions well within tolerances.

Control of laser metal wire deposition

When developing LMD-w further, there are quite a few hurdles to overcome. Ensuring a stable process when the deposition speed is varied is one challenge. Another challenge arises when processing different materials. Different materials behave differently, for example their melting temperatures, surface tension and specific heat capacities differ [44]. In addition to these inherent physical properties, different materials require different thermal management strategies in order to control e.g. hardening and crack formation [45]. These effects require tailoring of process parameters to each new material processed. Also, since the geometry of the deposit and the fixture used will affect the thermal dissipation and buildup of temperature, process parameters might have to be adjusted during deposition depending on the specific deposit and fixture.

One major prerequisite for mitigating the problems mentioned above is the ability to measure critical process parameters such as weld bead shape and tool-to-workpiece distance. Another of these important parameters is temperature. Measuring temperature accurately is however not a simple task since contacting temperature measurement methods are not an option. This is due to the LMD-w process itself. It is impossible to use contact thermometry on a structure which is built up during processing. Also, the deposited material must not be contaminated by any foreign material such as a contacting temperature probe. Further,

laser reflexes which may damage sensitive equipment and limited space for attaching instruments make the problem even more intricate.

Previously, Heralić has implemented cameras for monitoring and automatic droplet detection. A laser diode and a laser line scanner have been introduced for height measurements, and a thermal camera for temperature field monitoring [3]. The laser line scanner and the cameras required cooling and protection from laser reflexes, in order to operate successfully in within the processing chamber.

1.3 Process monitoring and control of AM processes

In this section, measurement and control solutions for AM processes, excluding LMD-w , are described in order to give an overview of related work. Some comments on the methods' suitability for LMD-w are also given. Due to the inherent nature of the AM processes, non-contact measurement methods are essential in understanding and monitoring laser metal deposition processes. However the powerful laser and the blackbody radiation from the weld pool demands careful filtering and smart positioning of measurement instruments and devices.

Cameras

A number of articles make use of cameras for geometrical observations of AM processes: [46–53]. Cameras are used for estimation of angles, weld pool dimensions, positioning of the nozzle and estimation of powder velocities. In the related field of laser welding monitoring, specialised camera solutions have previously been employed to give insight into the fluid flow and dynamics of the melt established by the laser [54].The main problem in using cameras as sensory equipment is to find placements that will not interfere with the deposition process. Since the goal of camera monitoring typically is to gain information about the actual processing, the camera should be aimed at the weld pool. Placing the camera close to the laser optics, onto the manipulator tool, makes the camera follow the weld pool and allows for good resolution due to the short distance to the weld pool. A placement parallel to the laser gives a lot of space for the robot to move around, if a robot manipulator is used, but it will only give a top view of the process. Attaching a camera perpendicular to the laser will give a much better view, but on the other hand it restricts manipulator movement and requires a large chamber, if a chamber is used. Saturation of CCD-sensors due to thermal radiation and high power laser reflexes also cause problems that are best countered with careful filtering and positioning.

Pyrometers

Pyrometers have found extensive use in previously reported works [46,51,52,55–57] for temperature monitoring. The main use of pyrometers is to monitor weld pool temperature automatically while depositing material. The weld pool temperature affects resulting deposit material properties and the weld pool geometry in all three dimensions. The main problem with pyrometers is the wavelength and temperature dependent emissivity of the material as explained in Paper 1. Using a multi-wavelength pyrometer or spectrometer together with careful calibration could possibly resolve this issue as described in Paper 1 and Paper 2.

Photodiodes

In papers by Leong et al. and Bi et al., photodiodes are used for temperature measurement [58, 59]. However, as the signals received are very difficult to calibrate to true temperature values, they only give temperature dependent signals and not absolute temperature signals. Such temperature dependent signals may however be analysed for e.g. derivatives, transients and trends. Photodiodes are also limited by low spatial resolution, which makes it hard to attribute readings to any particular location in or near the weld pool [56].

Automatic AM process control

There are several articles discussing automatic control of laser deposition processes [31, 50, 52, 60–64]. Toyserkani and co-authors describe several systems in their book "*Laser Cladding*" [2]. Most of the articles discuss LMD-p in two dimensions (thin wall/arced wall) and use geometry and temperature information for automatic control, typically in feedback configurations.

For the TIG-based SMD process, many systems for automatic control have been implemented [28, 30]. Cameras, microphones, IR-phototransistors, thermal cameras, and voltage measurements are used for automatic control of e.g. input power or material feed rate.

1.4 Scope of work

In many ways, the LMD-w process challenges automation efforts. It is a sensitive and typically unstable process with high demands on precise control [3]. At the same time, instrumentation proves difficult due to demands on non-contact instruments, high temperatures and the presence of laser reflexes. This thesis is focused on instrumentation and estimation solutions for the LMD-w process, which are able to give essential information when it comes to either controlling the process or relating key parameters to a certain result. Quite a lot of effort

has been put into identifying suitable instrumentation solutions. Out of many concepts and ideas, two are investigated within the scope of this thesis.

The larger portion of the thesis addresses non-contact temperature measurements and varying emissivity, due to the complexity of the subject. Resistance measurements are discussed to a lesser extent, but it is based on concepts that are more familiar for readers with a general technical background, and therefore require less introduction.

Temperature measurements

With temperature being a very important parameter within LMD-w and other processes, the question of accurate temperature measurements is given much attention in this work. Questions of instrument calibration with regard to emissivity and emissivity variations are discussed in depth. Sources of emissivity variation such as oxidation, surface restructuring and temperature dependences are introduced and related to their relevance for industrial applications. How multispectral information can be used to overcome problems associated with varying emissivity is investigated and compared to conventional methods. This multispectral concept is interesting both for LMD-w and for other industrial applications, since temperature is a parameter that is often monitored or controlled for material quality purposes. In addition to the multispectral method itself, an auxiliary signal processing procedure is presented, which strengthens the technology's position in terms of implementation in industry.

Resistance measurements and control

One method, which is investigated for LMD-w control, is monitoring of the wire and weld-pool resistance. How this can be measured in practice and how the signal can be filtered and integrated into the control system is discussed. Implementations of process control solutions, based upon resistance based measurements, are carried out and discussed from practical perspectives. The integration of resistance measurements into an iterative learning control scheme, previously utilised with laser scanning data, is investigated and is also the topic of Paper 6.

1.5 Research questions

The fundamental initial research question, established early in this work was:

What measurement solutions could prove beneficial for LMD-w process control and diagnostics?

With time, this general question was simplified and refined into the following research questions that constitute the subject of this thesis:

- Q1** How can measurement systems for LMD-w be implemented and evaluated in order to extract the essential information from the process?
- Q2** How can temperature be accurately measured for the LMD-w process?
- Q3** In the case of an oxidising metal object, how can accurate non-contact temperature measurements be made despite the varying emissivity?
- Q4** How can resistance measurements be used for monitoring or controlling the LMD-w process?

1.6 Limitations

The main limitation of this thesis is that the work performed stems from the requirements on non-intrusive instrumentation and estimation of the LMD-w process. This is the setting in which the work has been conducted, resulting in the direction of this thesis and the papers included. The applications of the results of this thesis is not limited to only LMD-w, but the reader should keep in mind that the developed technology was first intended to benefit monitoring and control of LMD-w.

The scope of this thesis does not include control strategies in a control theory sense. Such methods have been previously developed by Heralić [3] and are only briefly discussed in this work. Process controllers, which prove to be functional, are implemented in Paper 5 and Paper 6, but a thorough study on their suitability is not conducted. Further, discussions on laser welding, welding in general, and materials science are left out of this work. These subjects, along with others, are however very important when developing LMD-w, and the author has spent a considerable amount of time and effort penetrating these areas, even though they are not discussed in this thesis.

The equipment available to the Production Technology West (PTW) research group at University West has limited some of the work. For example, ellipsometric measurements, for which PTW lacks equipment, could have further strengthened the hypotheses in Paper 1. The material and equipment used at University West are described in detail in Section 2.2. In addition to the experiments performed at PTW, a handful of tests have been performed at the Department of Microtechnology and Nanoscience at Chalmers and together with Swerea IVF in Mölndal.

1.7 Contributions

The contributions of this thesis are listed below. Their relations to the research questions and the publications are presented in Table 1.1.

1.7. CONTRIBUTIONS

		Implementation for LMD-w	Temperature measurements for LMD-w	Temperature measurements with varying emissivity	Resistance measurements
		Q1	Q2	Q3	Q4
Pyrometer calibration	C1	Paper 1	Paper1		
Emissivity of Ti6Al4V	C2		Paper 1		
Multispectral method	C3		Paper 2	Paper 2&3	
Validation of multispectral method	C4		Paper 2	Paper 2&3	
Automatic calibration method	C5	Paper 4	Paper 4	Paper 4	
Resistance measurement	C6	Papers 5&6			Papers 5&6
Resistance for ILC	C7	Paper 6			Paper 6

Table 1.1: Contributions and their relations to research questions and papers.

- C1** A procedure for pyrometer calibration using thermocouples and induction heating.
- C2** An investigation of the varying emissivity of Ti6Al4V and its impact on non-contact temperature measurements between 750 K and 1550 K.
- C3** A multispectral temperature measurement method that compensates for variations in emissivity.
- C4** Validation of the method in C3 in terms of experiments and simulations.
- C5** An automatic method for calibrating the multispectral temperature measurement method in C3.
- C6** A method using resistance measurements for monitoring and control of LMD-w.
- C7** Resistance measurements used as input to an iterative learning controller (ILC) for wire feed rate control of the LMD-w process.

1.8 Outline

The remainder of this thesis is outlined as follows. First, the LMD-w process is introduced in Chapter 2. Following that, process measurements and process control are discussed in Chapters 3 and 4 respectively. Temperature measurements are then discussed with emphasis on non-contact thermometry methods in Chapter 5. In Chapter 6, a novel temperature measurement method, developed as part of this thesis, is presented. Following those theory oriented chapters is a summary of the included papers in Chapter 7. Part I ends with the conclusions and discussions on future work in Chapter 8.

In Part II, a total of six peer reviewed scientific papers are included. One of these is a conference contribution and five of them are journal contributions. Out of the journal contributions, one is currently resubmitted after revision while the others are published.

Chapter 2

The laser metal wire deposition process

In this chapter, the LMD-w process is presented briefly. The process and the equipment used are introduced. The measurement and control strategies for LMD-w are discussed in Chapters 3 and 4 respectively.

2.1 Deposition process

Laser metal deposition with wire (LMD-w) is a process wherein a metal wire is melted onto a substrate to form resolidified weld beads. These beads are placed side-by-side and layer-upon-layer to form a deposit as indicated in Figure 2.1.

Performing laser metal deposition with wire as filler material is a far from trivial task. Assuming a suitable system is available, an operator will first have to establish parameters for deposition. Such parameters might be laser power P_L , traverse speed v_t , as actuated by a robot manipulator, wire feed rate v_w , wire and laser incidence angles relative to the substrate, α_w and α_L respectively, as well as wire stick-out length l as indicated in Figure 2.2. When employing hot-wire techniques, which introduce energy in the form of resistive heating to the weld, also wire current has to be set appropriately. Once such parameters are available, through former experience or through a trial-and-error procedure, a deposition pattern has to be created. It could be generated automatically, as described by Ericsson et al. [65], or created manually by the operator. In addition to manual creation of deposition patterns and robot code, software for pattern generation has been developed by the author in MATLAB, later discussed in Section 2.2. This software allows the operator to design a pattern semi-automatically. The operator is able to script the generation of a geometry or generate it manually by adding positions one-by-one, visualise the geometry and generate the robot code automatically.

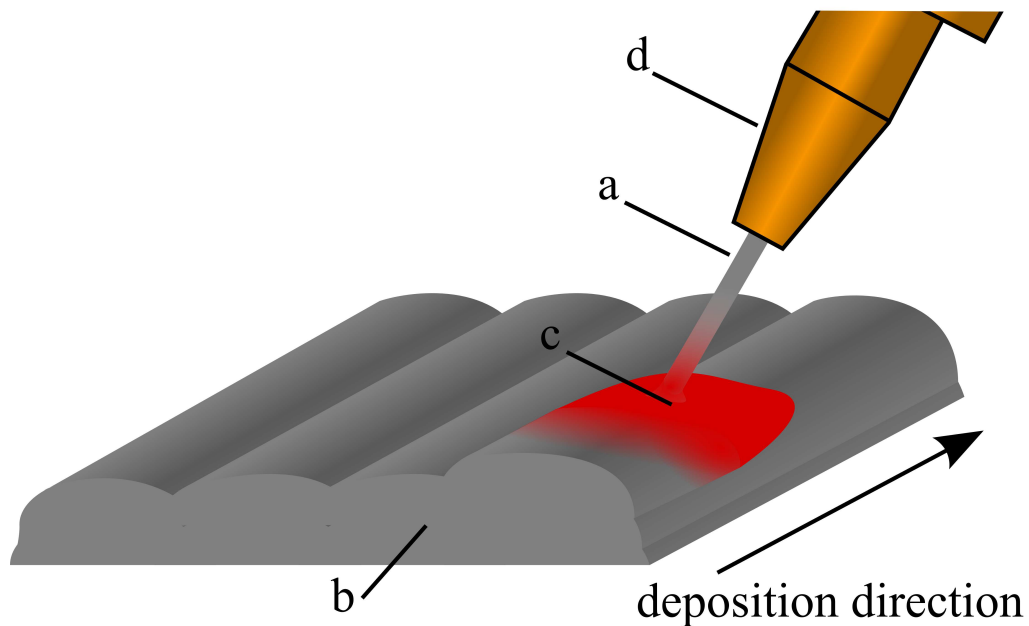


Figure 2.1: Build-up of deposit by layer-wise deposition of weld beads. The high-power laser radiation (omitted from illustration) melts the wire (a) and the substrate (b) as wire is fed into the weld pool (c) by the nozzle (d). The deposition direction indicated is the relative movement of the wire feeder nozzle to the substrate/deposit.

A deposition pattern should not only result in a desirable geometry but also incorporate acquired knowledge regarding heat build-up, weld pool flow, possible laser reflections and productivity strategies among other issues. Such a pattern must then be translated into robot instructions, which with the system used at University West, means ABB RAPID code. With a set of generated robot instructions, it is possible to start deposition performing the following steps.

1. Upload the robot code to the robot controller. In order to minimise oxidation, fill the process chamber with argon gas and await sufficiently low oxygen levels.
2. Initialise the deposition system by engaging the laser source and beam switch, camera cooling, weld source, oxygen meter and other control and security systems.
3. Deposit a bead of molten material onto the substrate or previous layer. Repeat until a whole layer is deposited. If resistance measurements are made, these are collected and stored during this step.
4. Optionally, scan the deposited layer geometry if using a laser scanner.

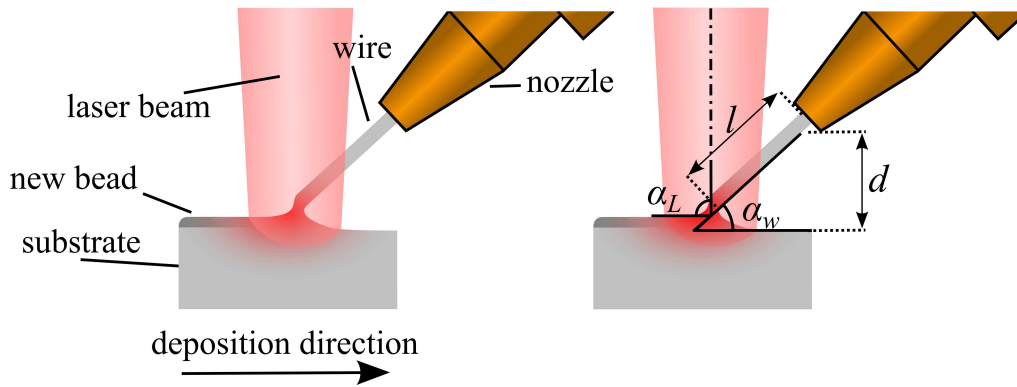


Figure 2.2: Left: wire plunged into weld pool (red) by tool nozzle. Right: geometrical parameters.

5. Compute a control signal for next layer, either based on laser scan result or on resistance measurements.
6. If not enough layers have been deposited, return to step 3, otherwise deposition is finished.

2.2 Equipment

A large number of components constitute the system used for LMD-w at University West, used by the author. The most important ones are discussed in this section. Due to the high power laser used for deposition, all monitoring, supervision and control must be performed from outside the processing cell. This situation requires reliable instruments, which can supply an operator and the control system with information with minimal time lag. In Figure 2.3, the equipment described in the sections below is showed in context relative to the other equipment in a schematic illustration.

Material

When performing deposition trials, plate material with dimensions $300 \times 100 \times 3.6$ mm were used along with wire with a diameter between 0.8 mm and 1.2 mm. The material used was either Ti6Al4V or Alloy 718.

Process chamber

In order to prevent oxidation of the metal substrate and deposit, all trials took place in a process chamber made from transparent flexible plastic sheet filled with argon. It is sealed to a stainless steel base with metallic adhesive tape and

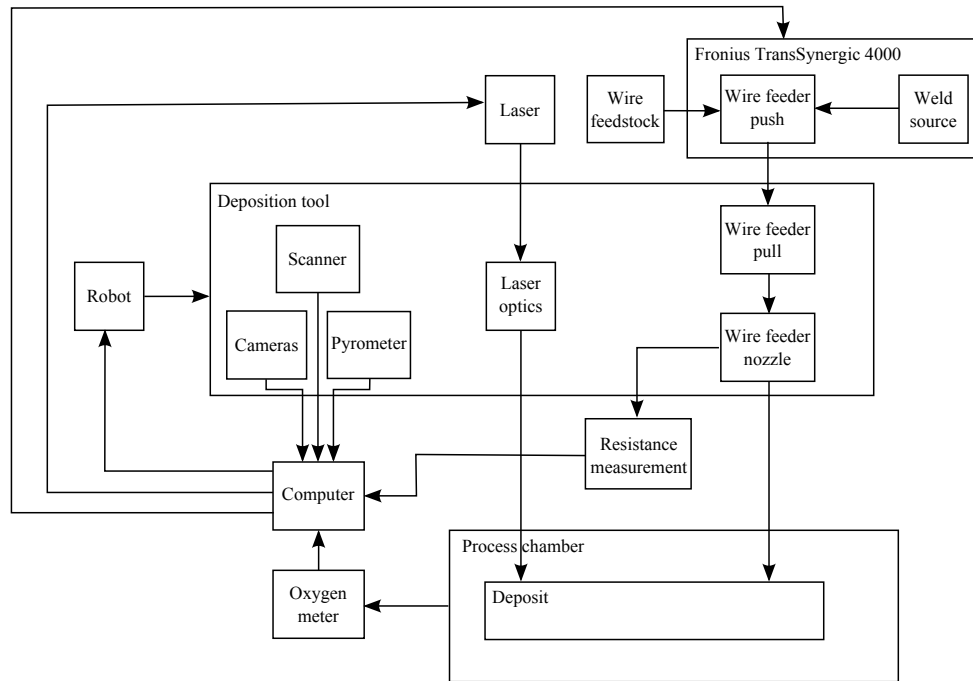


Figure 2.3: Schematic illustration of the equipment used for LMD-w and their inter-connections. Connecting lines indicate connections which are electrical, optical, data or mechanical. The arrowheads indicate the flow of material, energy, mechanical action or information.

is made easily accessible through zippers. A picture of the process chamber is shown in Figure 2.4.

Laser

The laser power used for melting the wire is provided by a 6 kW Ytterbium fibre laser system from IPG Photonics with emission wavelengths between 1070 and 1080 nm.

Laser optics

The laser optics used for LMD-w at University West, is currently a laser welding optical assembly manufactured by Permanova Lasersystems AB, Gothenburg Sweden. It has collimating lens with a focal length of 120 mm and a focusing lens with a focal length of 300 mm. The optics are used for obtaining an out of focus laser spot with a size of approximately $\varnothing 3$ mm when coupled to a 600 μ m diameter fibre.

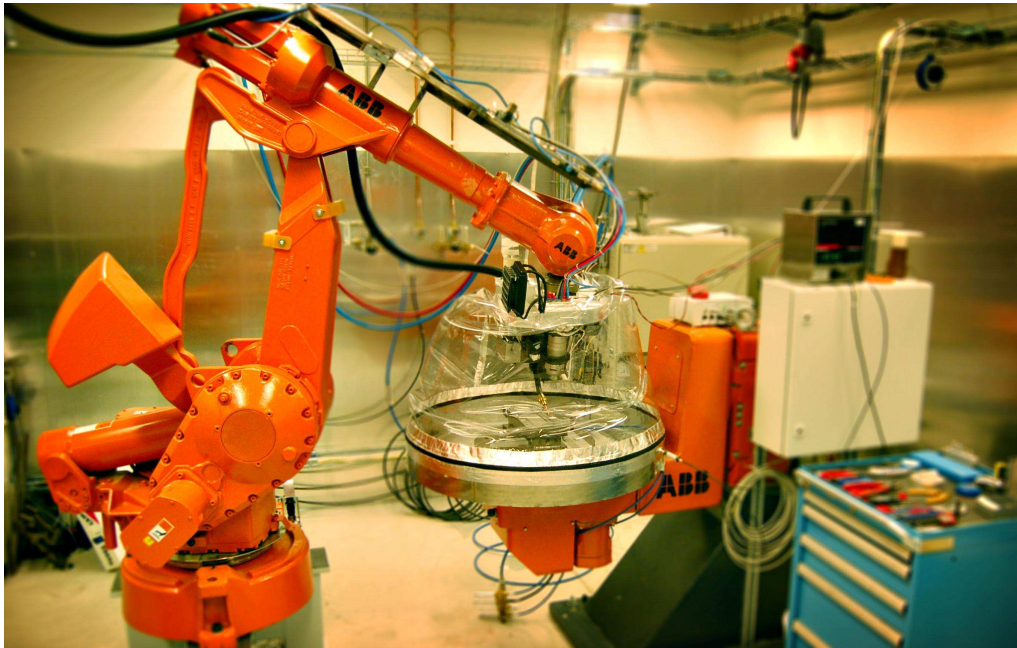


Figure 2.4: Picture of robot with tool and process chamber. Photograph courtesy of Almir Heralić.

Robot

An ABB IRB 4400 6-axis robot arm with an IRC-5 controller is used for manipulating the deposition tool described below. With the deposition tool the robot manipulates the laser optics, the wire feeder nozzle and the attached measurement instruments.

Wire feeder and weld source

A Fronius TransSynergic 4000 is used for providing wire feeding capabilities as well as acting as a welding current source. It is capable of providing up to 400 A to the weld by the means of a current passing through the wire and the weld pool. The integrated wire feeder has a push-pull design, which encompasses feeding mechanisms both on the feedstock side and close to the nozzle. This design gives smoother feeding and gives better control of feed rates.

Oxygen meter

An Oxy 3 residual oxygen meter from Orbitec gives oxygen level readouts between 0 and 999 ppm.

Cameras

A total of three cameras are used for surveillance of the processing cell, the chamber and the weld pool. For monitoring the cell and the processing chamber, C9000 QuickCam Pro and C920 HD Pro webcams from Logitech are used. Weld pool visual feedback is provided by a Marlin F131B CMOS camera with a mirror which reflects process laser radiation but transmits visual range radiation. The mirror protects the camera from high power reflexes from the highly reflective metal which would otherwise ruin the detector.

Optical scanner

An laser line scanner from Micro Epsilon with software created in-house is used for collecting geometrical data from the deposit. It has a specified depth accuracy of 10 μm and is attached to the robot via a pneumatic arm which can lower the scanner into position for scanning. The pneumatic arm has been found to be highly repeatable and an insignificant contribution to uncertainty when compared to the robot's positional accuracy.

Pyrometer

The pyrometer used for measuring temperature of either the substrate or the deposit is a single waveband pyrometer: Impac IGA 5-LO MB25, with a wavelength range of: $\{1.45..1.8\} \mu\text{m}$.

Deposition tool

Mounted onto the robot is the deposition tool. It is an assembly of the wire feeder nozzle, the laser optics and cameras for monitoring the weld pool as well as the process chamber. Onto this deposition tool, sensors such as the optical scanner and the pyrometer is attached when required. Within the robot controller, the Tool Center Point (TCP), is calibrated as the point in space, relative to the robot's sixth axis, where the wire intersects the laser beam. The geometry of the tool defines the TCP and it is the TCP which moved around by the robot manipulator during deposition. In Figure 2.1, the TCP may be thought of to be in the weld pool.

Data acquisition hardware

Modular hardware from National Instruments is used for data acquisition from certain instruments, such as the pyrometer, and for communication over the field

bus protocol Profibus. Such modules are also used for the resistance measurements described in Paper 5 and Paper 6. The measurement and communication modules are placed in a cDAQ-9172 rack, which is accessed over USB from the control system computer.

PLC system

A Programmable Logic Controller (PLC) system from Beckhoff Automation with custom control software from Permanova Lasersystems is used for ensuring secure operation in terms of enabling power sources only when certain prerequisites are met, etcetera. The PLC also acts as a Profibus master node for Profibus communication between the robot, weld source, laser and computers.

Computers

Off the shelf PC:s, running Windows XP or Windows 7 are used for controlling and monitoring most of the deposition process and logging data. A total of 4 computers are used in parallel for different tasks.

Software

Custom made software written in LabVIEW, MATLAB, MySQL, ABB RAPID and AutoHotkey have been developed especially for the LMD-w system at University West. The LabVIEW system is used for time synchronised data acquisition, process monitoring and control. All instrument inputs are relayed through LabVIEW software. During deposition, all relevant data is logged to the MySQL database. MATLAB is used for analysing scanner and resistance data, calculating controller response, designing deposition patterns and for automatically generating ABB RAPID robot code. The developed graphical user interfaces developed for the deposition pattern design tool is illustrated in Figure 2.5.

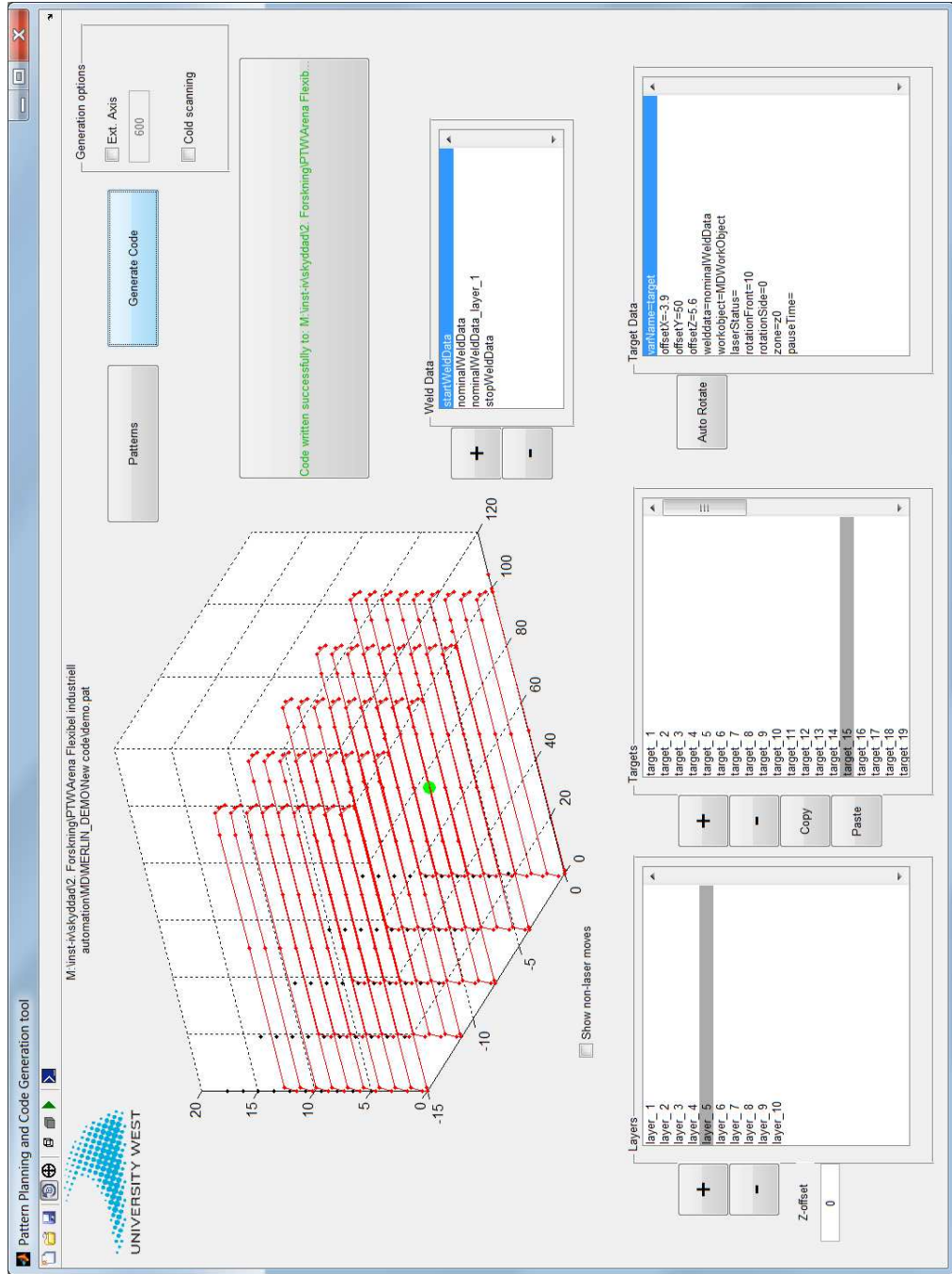


Figure 2.5: Graphical user interface for designing deposition paths and generating robot code. In this case, a rectangular bar, five beads in width and ten layers high is programmed.

Before the start of each deposition run, the robot code and controller software source code are uploaded to the same database, which is used for logging process data. This is for version handling and for making sure that it is possible to restore all software used for a particular deposition trial. AutoHotkey executables are used for downloading and uploading robot code to the database as well as for initiating surveillance cameras.

2.3 Difficulties in laser metal wire deposition

During LMD-w processing, there are a number of factors which may cause problems if not handled properly by the control system or the operator. In this section, these difficulties in LMD-w are listed and described.

Wire position relative to weld pool

When introducing wire into the weld pool, which is created by the laser irradiation, it is of uttermost importance that it enters both in a good position relative to the pool and with a good feeding rate. A good positioning allows the wire to absorb some laser radiance and thus being heated before entering the pool in order to be fully melted. Please refer to Figure 2.2 and Figure 2.6 for illustrations of the wire entering the weld pool. While absorbing some of the laser radiation, the wire must not shade the pool so much that the weld pool gets too cold and solidifies prematurely. The wire should enter the weld pool in the pool's symmetry axis, which is parallel to the deposition direction. It also must not enter the pool too close to the front or the back of the pool, in which case the wire might easily leave the weld pool and the smooth material transfer might be broken.

The ability to use the hot-wire technique decreases the importance of pre-heating the wire with the laser. The wire is heated resistively before it enters the weld pool and also resistive power is introduced to the weld pool itself, thus helping to sustain it. Positioning of the wire is affected by the robot position relative to the substrate in all three dimensions. As long as the wire incidence angle, α_w as indicated in Figure 2.2, is not normal to the substrate, any change in robot-substrate distance, d as indicated in Figure 2.6, will cause the wire to enter the weld pool at a different place. Also, d will affect the geometry of the weld pool and the material transfer mode as indicated in Figure 2.6. With a too large distance, as illustrated in the rightmost part of Figure 2.6, there is a significant risk that the material link will be broken. The laser will gradually melt the wire and a droplet will build up at the wire tip. As the droplet grows, gravitational pull will eventually exceed surface tension forces and the droplet will enter the weld pool causing an uneven deposit in the form of the solidified droplet. For a short time, the transfer link is re-established only to be broken

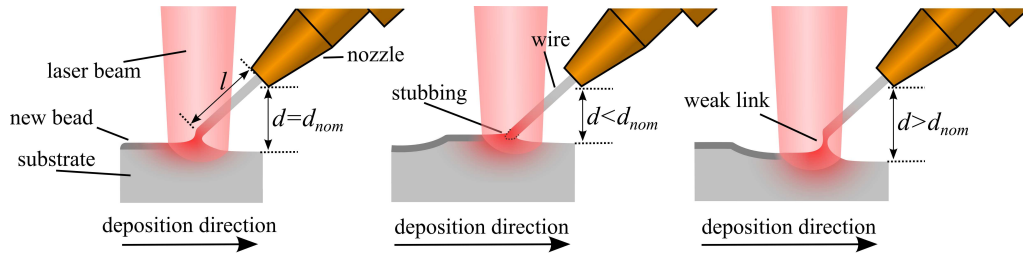


Figure 2.6: Transfer modes, to the left: desired transfer with $d = d_{nom}$. In the centre: $d < d_{nom}$ causes stubbing. To the right: $d > d_{nom}$, with risk of droplet formation.

again. A new droplet will build up and so forth. This causes a transfer mode, which may not give inherently bad material properties but surely will give an uneven deposit making subsequent layers harder to deposit [3]. In the case where d is too short, the wire will not completely melt when introduced to the weld pool, but instead protrude through the liquid state into the unmolten substrate as seen in Figure 2.6, middle part. This causes so called stubbing, where the wire tip scrapes against the substrate and moves rapidly from side to side. The incomplete melting of the wire causes bad material properties and stubbing must be avoided in order to maintain a sound process with good deposit quality. As the substrate height may vary due to an uneven base substrate or uneven previously deposited layers, d will vary throughout the deposition. Even if the surface topology is known, there is still a problem with positioning the tool by the means of the industrial robot manipulator. The robot's positional accuracy and step response to position changes determine how well d can be adjusted during deposition. Apart from the physical limitations of the robot, the robot controller software utilised is limited with regard to rapid adjustments in a certain direction while performing a nominal movement.

Wire feeder

The wire feed rate, v_w , at which the wire is fed into the weld pool is another parameter which is beneficial to control. Weld pool material flow might cause uneven surface profiles that have to be mitigated by adjusting v_w . When properly controlled, v_w can be used to fill troughs and to flatten ridges for consecutive layers [3]. Proper control leads to controlled final geometries and also facilitates subsequent layer deposition. Bad control leads to an inability to perform layer-by-layer deposition while maintaining geometrical stability.

Laser power

Laser power affects the process in a number of ways. It determines the deposited bead cross-section geometry as well as size and temperature of the weld pool.

2.3. DIFFICULTIES IN LASER METAL WIRE DEPOSITION

Raising the laser power, apart from affecting the aforementioned properties, also increases the probability of high power reflexes which may cause damage to the equipment. The absorptivity of the metal material limits the laser efficiency and a lot of power is lost in the form of reflected laser radiation. Power added resistively, in terms of increasing the current through the wire and the weld pool, has higher energy efficiency compared to laser power for adding energy to the weld pool. Resistive power also does not alter the geometry of the weld pool as much as laser power [66, 67]. By balancing laser and resistive power, it is thus possible to somewhat tailor bead cross-section geometry to suit the application.

Deposit material

The material used for deposition affects the process in a number of ways. Its liquidus temperature, enthalpy of fusion and surface tension greatly affects the process behaviour. In trials performed by the author and Almir Heralić, not reported in this thesis, deposition of Alloy 718 was compared to that of Ti6Al4V. It was found that the higher surface tension of Alloy 718 [68], made the process a lot less "smooth" compared to Ti6Al4V. Higher energy input was needed in order to successfully deposit Alloy 718 and the parameters which previously proved to be suitable for Ti6Al4V deposition were not useful for depositing Alloy 718. Likewise, it may not be expected that process parameters, suitable for one particular material, are suitable for deposition of other materials.

Deposition pattern

When depositing geometries such as round bosses which cannot be divided into single straight beads [3], the deposition direction must differ from that shown in Figure 2.2 if the tool cannot be rotated freely. Since the tool is attached to the laser fibre and the wire feeder, together with a lot of other cables and tubes, it cannot be rotated around its axis in order to maintain a constant deposition direction in its current configuration. Changing the deposition direction effectively changes positioning of the wire relative to the weld pool and the process windows becomes narrower [3]. Thus, when it is not able to arbitrarily rotate the tool, the process will become more sensitive when depositing in any direction different from that indicated in Figure 2.6. Utilisation of a tool with coaxially fed wire such as the COAXwire developed by Fraunhofer IWS could possibly mitigate these problems [19], however such a setup demands more precise control of the wire feed rate in order to avoid stubbing or droplet formation.

2.4 Summary

The LMD-w process is a relatively complex AM-technique, which is inherently hard to control. It consists of many hardware subsystems, which are off-the-shelf equipment with the exception of the optical scanner casing and the deposition chamber. The hardware is tied together using a number of communication interfaces, such as Profibus, and custom made software in order to form a functional LMD-w system. In order to deposit material with high quality, the process must be supervised and controlled. This of course requires reliable process measurements and actuators, topics which are discussed in the following chapter.

Chapter 3

Process measurements and actuators

Fundamental requirements for controlling the LMD-w process are the abilities to measure process related entities and to actuate adjustments if needed. In this chapter, measurement systems and actuators for LMD-w are discussed.

3.1 Limitations

With the aim of the LMD-w process development being to find solutions and strategies which allow an LMD-w system to be utilised in an industrial setting, there are many limitations on possible measurement systems. These restrictions are both cost related and related to the harsh physical conditions. Generally, instruments must be non-contacting and built to withstand high temperatures, fumes and possible high power laser reflexes. Contacting instruments could both introduce contaminants into the deposit and would also need repositioning as the deposition process progresses.

The aforementioned limitations exclude many types of sensors such as thermocouples, thermistors, strain-gauges and indentation probes. The measurement systems must rely on either electromagnetic radiation of some kind, acoustic emissions, physically sampling the process chamber gas, reading internal data from a deposition system module or exploit the process in itself as a sensor. This latter approach can for example be realised by exploiting the fact that the weld pool geometry changes when d changes, as indicated in Figure 2.6, and that weld pool resistance can be related to geometry and indirectly d as shown in Paper 5 and Paper 6.

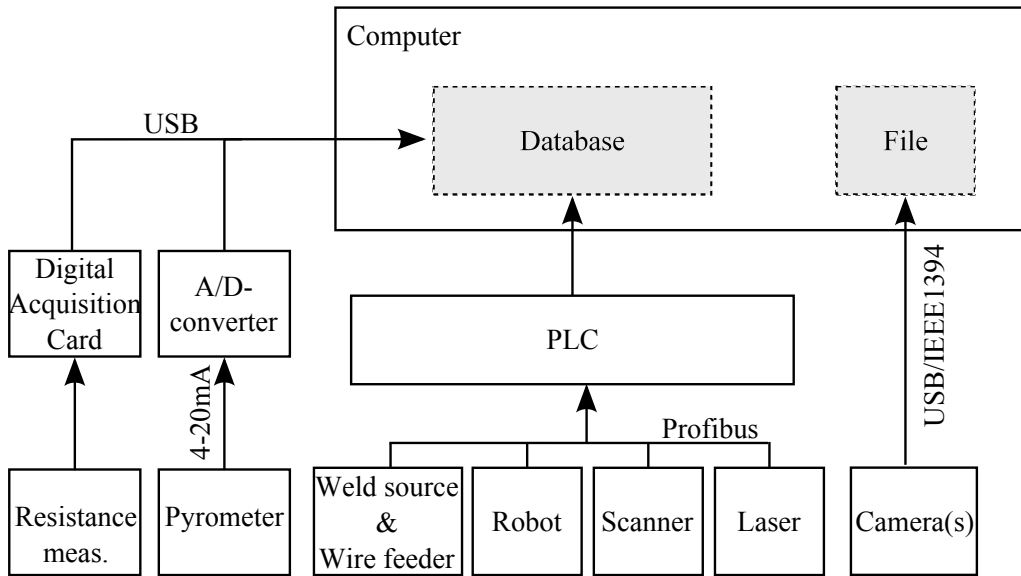


Figure 3.1: Flow of input information to control system computer.

3.2 Implemented systems

A number of measurement systems of varying complexity are integrated into the LMD-w deposition cell at University West. The input information flow is illustrated in Figure 3.1. The readings from most of the subsystems and instruments are logged in a common database. The recorded videos from the cameras are however handled differently due to their large data sizes and stored as separate files.

Optical scanner

The optical line scanner is mounted onto the deposition tool and is used for recording the topography of the deposit. Its main purpose is to give height input to the automatic control systems previously developed by Heralić [3]. It is described in more detail in Section 2.2.

Pyrometer

The pyrometer fitted to the deposition tool is a single waveband pyrometer further detailed in Section 2.2. It was used for measurements both in Paper 1 and Paper 2. As outlined in Section 5.4, pyrometers are not always well suited for determining the true absolute temperature of an object. This, and the problems associated with relating surface temperature in a single point to an appropriate control action, further elaborated on in Section 4.3, limit the use of pyrometer

measurements. Pyrometer measurements are therefore typically used only for comparison between trials during process development and for monitoring purposes rather than for direct in-process control.

Robot position information

As a task running in parallel with the actual deposition task in the robot controller, the robot system introduced in Section 2.2 sends the current position of the deposition tool to the control system. This information is vital since most other measurements are related to the robot position. Successful deposition is dependent on both robot position in the substrate plane, i.e. the plane parallel to the substrate, as well as the tool-to-workpiece distance d described in Section 2.3. Reliable position information is thus one of the most important inputs to an LMD-w control system.

Cameras

A total of three cameras are mounted in the deposition cell. Two are strictly for monitoring the deposition procedure from a security and supervision perspective. One surveys the cell as a whole and the other is used for monitoring the deposition chamber and the tool as detailed in Section 2.2. The output from these cameras are usually not saved in any way. The third camera is used for weld pool and process monitoring. The video recorded from this camera is saved, with process information such as elapsed time and position superimposed, as a separate video file.

Oxygen meter

The oxygen level information, given by the oxygen meter described in Section 2.2, is not used for control of the process. Its sole purpose is to ensure that a sufficiently low oxygen content has been reached before commencing deposition and is kept during processing. Too high oxygen levels might lead to material oxidation with oxide inclusions in the final deposit and poor deposit material properties. For traceability purposes, the oxygen might also be included in the database along with the other process data.

Weld pool resistance metering

In Paper 5, a current is fed through the wire and weld pool using the welding source. The current is measured along with the applied voltage. From these measures, the total resistance of the weld pool and the wire stick-out is calculated. Through an empirical model, resistance is related to the distance between

the wire feeder nozzle and the substrate. This distance is crucial for controlling the LMD-w process as discussed in Section 2.3. Resistance metering can thus be used for controlling the process and maintaining a stable process as described in more detail in Section 4.2. The resistance can be especially useful for detecting detachment of the wire from the pool. The detachment is a very clear indication of an unstable process and is easily identified through the absence of current transferred through the weld pool.

In the follow-up paper, Paper 6, the concept was developed further. Partially due to signal disturbances experienced in Paper 5, and partially due to a desire to reduce the current through the weld pool, the measurement method was improved by introducing a wheatstone bridge. This is an electrical circuit seen in Figure 3.2 where the weld pool resistance is measured as R_x and the other resistance values are known. The setup enables very accurate readings of resistance and did result in somewhat reduced noise levels compared to what was achieved in Paper 5. But more importantly, the current could be reduced to below 1 A. This meant that the input energy due to the current needed for measuring resistance is negligible compared to the laser input. This is beneficial when "hot-wire" preheating of the wire is not desired.

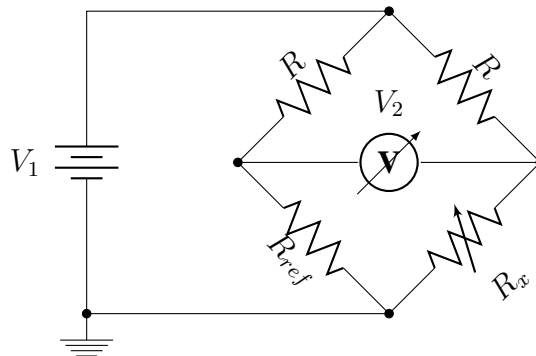


Figure 3.2: Circuit for measuring R_x .

3.3 Prospective technologies for measuring geometry in LMD-w

In this section, a compilation of measurement technologies which may be used for geometrically monitoring the LMD-w process is listed in Table 3.1 along with comments on their suitability. Since the main challenge in further automating LMD-w is process stability, only solutions aimed at maintaining a stable process, and thereby geometry, are listed. Their suitability is judged with respect to ease of application, robustness, cost and maturity. Already implemented tech-

3.3. PROSPECTIVE TECHNOLOGIES FOR MEASURING GEOMETRY IN LMD-W

Technology	Information provided	Suitability
Laser line scanning	Accurate surface topography	Proven performance, but time consuming and lacks accuracy for chamfered edges
Resistance in-process measurements	Deposition height profile along the deposition pattern	Proven performance, but further investigations into limitations required
Spectral domain optical coherence tomography [69]	Very accurate distance measurement through laser beam	Only point measurement and complex setup
3D Time-of-Flight camera [70]	Surface topography with accuracy > 0.2 mm	Camera with picosecond exposure time required
Scanning physical probe	Point-wise distance measurement	Requires physical scan in 3 dimensions

Table 3.1: List of prospective control technologies

nologies such as resistance in-process control and laser scanning are included for comparison.

The technologies which only provide point-wise measures of built height are limited for deposition patterns which include rotation of the tool, i.e. non-straight beads. For depositing straight beads, point-wise distance measurements can be used for control, but otherwise the benefit of such technologies is limited. For a generally applicable control system, point-wise distance measures are not sufficient. It is necessary to provide a control system with distance information for all directions in the x-y plane so that stability can be maintained even while rotating the tool, or with a distance measure which follows the deposition path such as available with resistance in-process distance measurements. A solution where an instrument for point-wise measurement is physically manipulated for scanning is possible, albeit very impractical, for integration with an LMD-w tool. Hence, the only two technologies listed in Table 3.1 which show real promise for a versatile control system are the 3D Time-of-Flight (TOF) camera and resistance in-process measurements. TOF technology, with the desired resolution, however requires an ultrafast camera with exposure times in the pico second range and a pulsed illumination laser [70]. The reported resolution in depth (0.2 mm) might prove enough for certain applications but is still a step back from that of the laser scanner (10 μ m). Application of 3D TOF measurements during processing is another possible limitation since a scan takes several seconds to perform and the light generated by the process might cause disturbances. This leaves scanning in between layers much alike what has been previously done with the laser line

scanner. The only remaining advantage of the TOF system is then that a scan can be performed in just a few seconds compared to the laser scan which takes up to a minute. In regard to this, it might be more resource efficient to aim to hasten the scanning procedure rather than investing in an advanced, expensive and untested 3D TOF system in order to decrease scanning time. Tailoring a scanning solution to the LMD-w process, rather than buying one off-the-shelf, might open up new possibilities regarding determination of surface topography, even during processing.

For the resistance based measurements however, hardware is cheap and available as off-the-shelf components. As mentioned in the discussion in Paper 6, further investigations are required for discerning the method's sensitivity to tool rotation and other process parameters. Possibly could the dynamics of the resistance, as a function of geometry, be more accurately modeled and coupled into the control system design. Another benefit of the resistance based measurements is that the profile information translates directly to deposition pattern coordinates. There is no need to, like with the 3D scanning methods, translate a topography map into deposition coordinates before calculating control action.

3.4 Actuators

In order to actuate control signals for the process, a number of actuators are integrated to the deposition system. The actual hardware is described in Section 2.2, which is why only their properties are described in this section. A schematic overview of the different actuators and the process parameters which they control are shown in Figure 3.3.

Wire feeder

The wire feeder, described in Section 2.2, with its push-pull design enables accurate control of wire feed rate, v_w , at the feeder nozzle outlet. The feed rate affects the cross-sectional area, A_c as illustrated in Figure 3.4, of the deposited bead due to the mass balance required

$$\frac{v_w \pi (\varnothing/2)^2 [\text{m}^3 \text{s}^{-1}]}{v_t [\text{m s}^{-1}]} = A_c [\text{m}^2] \quad (3.1)$$

where \varnothing is the wire diameter. However, the step response of the wire feeder with deposit geometry as the output is not a causal one [3]. This is because the weld pool redistributes material backwards relative to the deposition direction. This makes it seem as if there is a change in build height even before the change in feed rate was made when evaluating the bead geometry. The redistributive behaviour of the weld pool along with surface tension effects might also give unexpected results, especially when depositing patterns with multiple adjacent beads

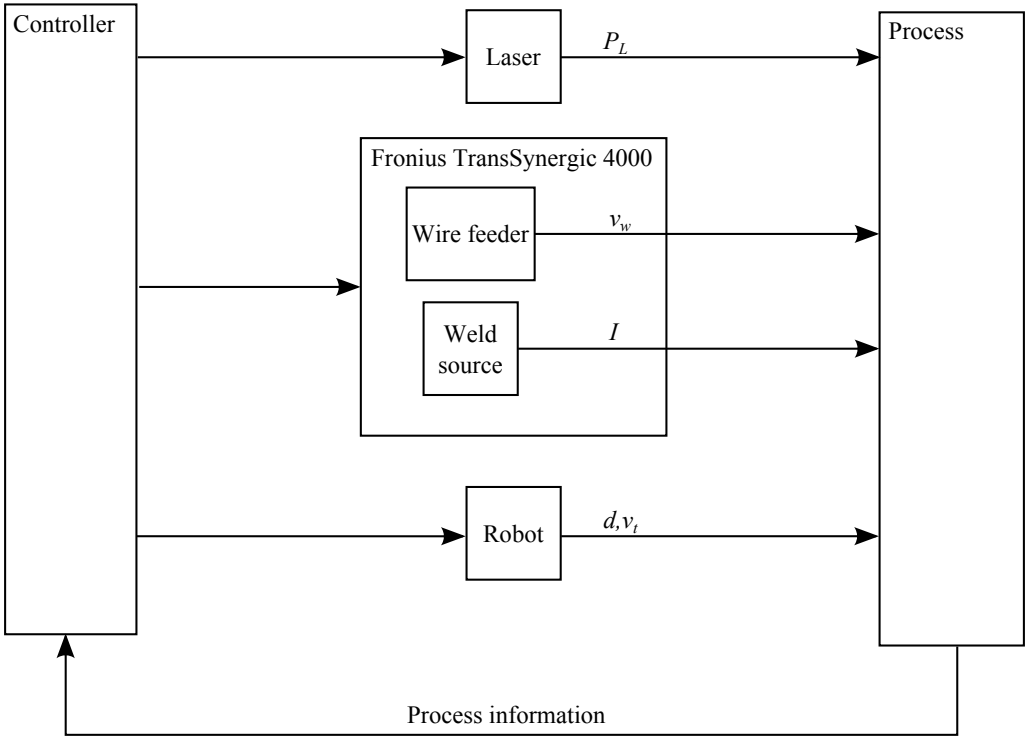


Figure 3.3: Schematic illustration of actuators and controlled parameters.

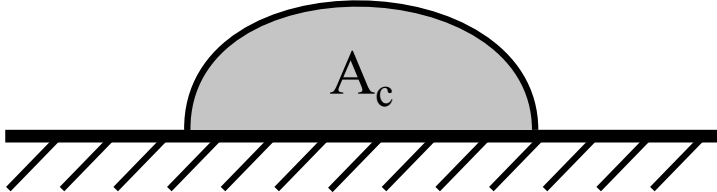


Figure 3.4: Illustration of A_c as seen in an imagined bead cross-section.

since the weld pool might redistribute material to neighbouring beads. These complex plant dynamics is why the iterative learning control scheme, introduced in Section 4.1, has proven to be useful for such situations [3].

Robot

The robot, detailed in Section 2.2, is used for maintaining correct tool-to-workpiece distance d as well as actuating the traverse speed v_t , which affects geometry as seen in (3.1). The former, d , is achieved by raising the robot in a direction normal to the substrate. The robot has got good positioning repeatability but poorer absolute accuracy [71]. This, and the limitation in running parallel tasks on the robot controller has proven to cause some problems with positioning and synchronisation when developing the LMD-w system.

Laser

The laser power source, which is described in Section 2.2, can be controlled in many ways. It may operate in pulsed or continuous mode. In pulsed mode, the pulses may be tailored with regard to rise-times, pulse width etc. In continuous mode, which has been used for the work in this thesis, the controllable parameter is the power output. Laser power, P_L , is typically set *a-priori* for a certain deposit geometry and not varied throughout a deposition process. However, for finding suitable laser power settings for a geometry, power settings are typically changed in-between deposition trials based on the operator's experience and possibly also metallurgical evaluation.

Weld source

The weld source described in Section 2.2, with the configuration used in this work, operates on a principle of constant current. A maximum voltage is typically set to 10 V, and the current is automatically controlled by the weld source voltage in order to maintain the desired current. Desired current level settings are treated much like laser power in that they are not controlled during deposition but iteratively adjusted in between deposition trials.

3.5 Summary

Due to the nature of the LMD-w process, the possibilities for instrumentation are limited to non-contact instruments. Complicating things even more is the fact that actuators often affect more than one process parameter. Adjustments to many actuator control signals will have to be made in order to, for example,

3.5. SUMMARY

decrease the bead width or preventing droplet formation. The availability of process information from measurements and the ability to actuate control output does not however guarantee a good result. A successful deposition also requires a good process control strategy implemented in the control system. Control systems for LMD-w are presented in the following chapter.

Chapter 4

Process control of LMD-w

In order to ensure a stable LMD-w process, resulting in a deposit with a geometry within tolerances and with deposited material exhibiting desired properties in terms of limited amounts of cracks, pores, lack-of-fusion flaws etc., some control scheme is required [3]. For very simple geometries such as single beads and for a few layers, the process might prove stable enough without any control, provided suitable parameter settings. For more than a handful layers or more complex structures however, adjustments have to be made during deposition. The two parameters, which have proven most successful to control are the distance between robot and workpiece, d , as indicated in Figure 2.2, and the wire feed rate, v_w [3]. Basically, a correct d ensures that the wire is always in contact with the weld pool but not scraping the unmolten substrate. A correct v_w -value ensures that the correct amount of material is deposited. By necessity, these two parameters rely on correct laser power settings, tool tilting, traverse speed and, if used, wire preheating power.

4.1 Previously implemented control strategies

In order to control the LMD-w process, several different control strategies can be used. They vary in implementation complexity, from manual control based on real-time video of the process, to off-line processing of scanner or resistance data in between layers for obtaining iterative learning control actuator responses.

Manual control

A skilled operator is able to successfully deposit material using LMD-w, based on the appearance of the weld pool as it is captured by the weld pool camera described in Section 2.2. The operator controls the tool-to-workpiece distance d , by adjusting the robot's z-position, and the wire feed rate, v_w , by adjusting the wire feeder's setpoint feed rate, to ensure stable deposition. The main drawback

of this control strategy is that it relies on a skilled operator. It takes time to train an operator who also gets tired from concentrating long periods of time. Further, different deposition patterns and different materials will require the operator to adapt her or his actions to the process at hand. Reproducibility might be another issue for manual control, along with the fact that the number of parameters which could be simultaneously controlled by an operator is limited. A fully automated system might be more reproducible and able to control more parameters simultaneously, but on the other hand might not be as versatile and able to adapt to new situations.

Iterative learning control

As described by Heralić [3], the concept of Iterative Learning Control (ILC) can be employed for controlling LMD-w. Due to the process nature which propagates disturbances over several layers, the ability of ILC to adapt control actions and to learn the disturbance patterns is most valuable. Measurements of deposit height are used for controlling deposition parameters. In Heralić's implementation, height measurements are made with a laser line scanner after each deposited layer. Wire feed rate, v_w , and d are adjusted accordingly as the ILC-system learns where and when disturbances occur and how these should be mitigated. In his studies of the application of ILC to LMD-w, Heralić shows that with a conservative selection of ILC learning gain parameters, it is possible to achieve stable control of the LMD-w process.

The laser scanning solution used by Heralić has a few distinct limitations however. Mainly, the scanning cannot be performed during deposition. After a layer is deposited, the scanner is activated and positioned by the robot. This procedure takes time from the actual deposition, thus limiting process productivity. The scanner also exhibits limitations when it comes to scanning highly reflective surfaces and chamfered edges [3].

For production where several identical components are produced, the above method is well suited. The first component is processed with ILC and laser scanning while all parameters are recorded. These recorded parameters are then used for subsequent components without any need for topography scanning, provided no unexpected disturbances. However, for continuous in-process control, combining a laser scanner with ILC proves to be of limited use. However, this is only due to the limitations of the laser scanner. If geometry data is provided to the ILC in another way, without the laser scanner's limitations, the benefits of applying ILC to LMD-w can be exploited even for continuous in-process control.

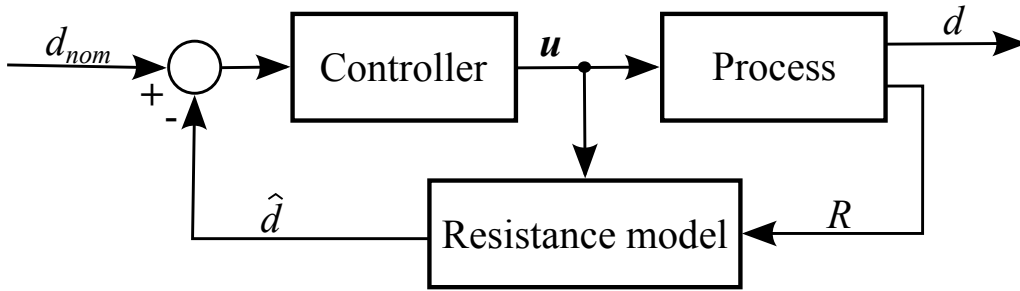


Figure 4.1: Control strategy as implemented in Paper 5, control signals u are generated in order to keep the distance, d equal to the nominal distance d_{nom} . The resistance model outputs a distance estimation, \hat{d} , based on resistance and control signals.

4.2 Resistance in-process control

As previously described in Section 2.3, the tool-to-workpiece distance d is very important in order to avoid wire stubbing or droplet formation. A manual control system with operator feedback based on real-time process video and the ILC-system are both attempts to resolve the issue with d -control described by Heralić [72, 73]. In Paper 5 in this thesis, another method is proposed for d -control which is based on measurements of resistance, R . When current is led through the wire and the weld pool, the length of the wire stick-out l and the weld pool geometry will affect the resulting resistance as described in Paper 5. The weld pool geometry is, as illustrated in Figure 2.6, very dependent on d . Wire stick-out, l , is related to d by the wire incidence angle, α_w , as indicated in Figure 2.2. Through either empirical or analytical modelling of the relation between R and d , the tool-to-workpiece distance can be measured indirectly from measurements of R and the created model. The obtained estimate \hat{d} , of d , can then be used for controlling the process and stabilising d . The controller input \hat{d} can either be used for feedback control as demonstrated in Paper 5 and illustrated in Figure 4.1, or with a control strategy which calculates actuator adjustments before deposition such as the ILC system implemented in Paper 6. An on-line feedback controller could, if it only makes adjustments when stubbing or droplet formation is detected, aid in manual deposition as an automatic auxiliary function of the control system. In the implementation presented in Paper 5, the resistance feedback control is shown to successfully adjust the robot position in order to maintain a nominal deposition distance d_{nom} using a simple PI-controller. As indicated in Section 4.1 above, replacing the laser scanner input data with something else is regarded to be beneficial. The significant contribution in Paper 6 from a control perspective, is the coupling of the height information obtained through resistance measurements to an Iterative Learning Controller for LMD-w previously developed by Heralić for controlling LMD-w. The concept is based on adapting to the

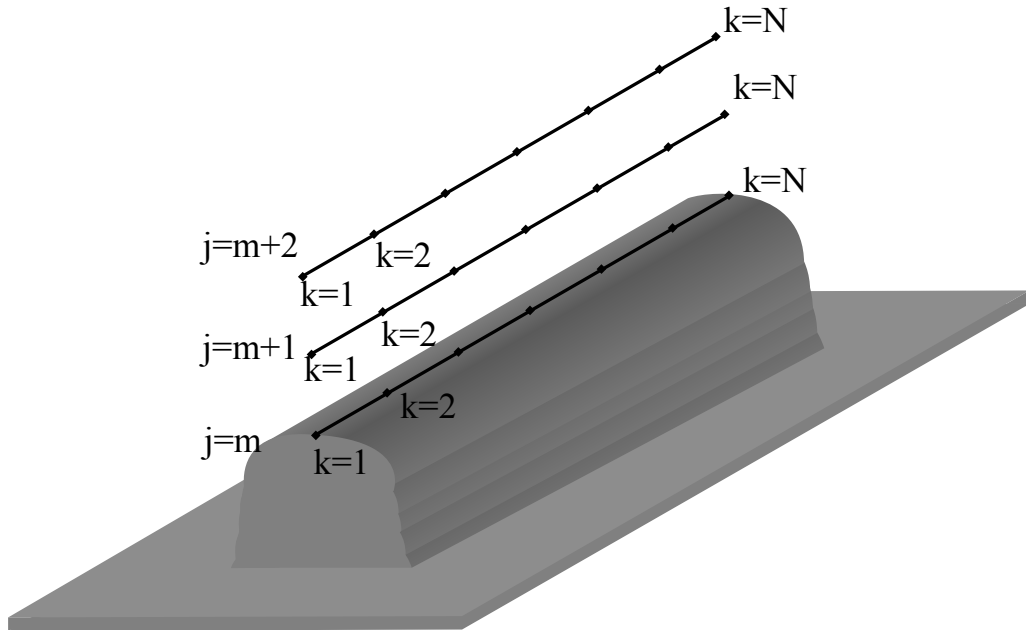


Figure 4.2: Illustration of ILC iteration domain with index j . Control signal is updated in between iterations in order to minimise deviations in the deposition process.

periodical behaviour of the process, corresponding to deposition of beads on top of each other as illustrated in Figure 4.2 for some layer iterations j . Disturbances are mitigated by feed-forwarding errors from previous layers when creating the control signal for the current layer, at specific positions along the pattern (k), as indicated in Figure 4.3. In Paper 6, the controller parameters such as plant and learning gains were chosen according to Heralić's previous studies [3, 73]. The same ILC parameters were used when replacing the laser scanner data in [3, 73], with topography data from resistance measurements in Paper 6, resulting in good process control. There is however room for improvement of the controller with more accurate tuning in the future.

4.3 Temperature control

For LMD-w in general, and especially for depositing Alloy 718, it is beneficial to survey and control temperature in some way. The motivation for this being that a too hot deposit might melt and that material properties might be affected by the temperature history. The thermal history of Alloy 718 is especially sensitive since cracks, due to the formation of brittle phases, might form as a result of prolonged periods with temperatures slightly below solidus temperature, which is approximately 1600 K (1327 °C) [45, 74].

Although a 3D temperature map of the entire deposit and the substrate would

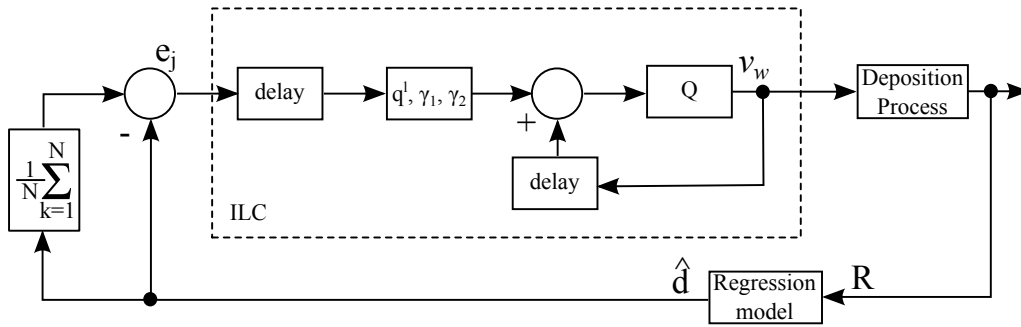


Figure 4.3: ILC architecture as implemented in Paper 6. The delay is in the iteration domain and v_w is the nominal wire feed rate. A description of the parameters is found in Paper 6.

be preferable, especially for estimating and predicting material properties [45], there are no available measurement methods that can provide such information. Generally, one is restricted to measurements of surface temperature, especially during LMD-w processing since no holes may be drilled into the bulk during deposition.

Temperature measurements on hot metals are preferably conducted with contacting probes for cost and accuracy reasons. More detailed descriptions of the available methods are found in Section 5.1. For LMD-w, in-process temperature measurements using contacting methods are not viable alternatives. The motivation for this being that contacting temperature probes might contaminate the deposit material as described in Paper 1. Also, difficulties in attaching probes during processing and the successive build-up of the deposit prevent the use of contacting instrumentation. This leaves only non-contact temperature measurement methods, which are further elaborated upon in Chapter 5 (Section 5.4) and in Chapter 6. Temperature information ideally consists of absolute temperature measurements, which have to be given by a correctly calibrated pyrometer as described in Paper 1 or by an Emissivity Compensated Spectral Pyrometry (ECSP) instrument developed by the author, presented in depth in Paper 2 and Paper 3. If no ECSP measurements are possible, or if no correctly calibrated pyrometer can be utilised due to e.g. oxidation, as discussed in Paper 1, relative temperature information can still be collected with a pyrometer or even with a photo diode [2, 75, 76]. This information is useful only for relative comparison between similar scenarios, and should only be used with caution for other purposes such as predicting material properties or temperature control.

Controlling temperature from measurements, whether relative or absolute, is not a straightforward task. In the situation where a desired surface temperature profile can be established, from e.g. material data and desired material structure, the temperature will still vary throughout the material, even if surface temper-

ature can be successfully controlled [77]. Since non-contact measurements can only provide surface temperature information and surface temperatures typically are lower than bulk temperature in a deposit, the bulk temperature will mostly exceed that of the desired surface temperature profile. The relation between surface and bulk temperatures is dependent on for example: deposit geometry and thermal conductivity, fixture temperature, surface emissivity and the thickness of the oxide layer. Hence, controlling bulk temperature distributions by monitoring only surface temperature is a most complex task. If simulations of heat transfer were employed for such a purpose, they will have to include the varying geometry into the simulation which makes them quite complex [78]. Temperature control, in terms of maintaining a desired surface temperature profile, for LMD-w is thus dependent on extensive numerical simulation and might not yet be practical in an industrial setting.

The actuation of desired temperature control action is yet another problem. Typically, heating is achieved by the laser or the resistive power introduced by the hot-wire current. Cooling on the other hand relies on dissipation of energy through the fixture, radiation and convection or any kind of forced cooling. In the case of Alloy 718, where it is desired to rapidly cool down the material after solidification, a few options are available for managing temperature. It is possible to minimise total energy input by depositing with a high deposition rate, e.g. high P_L , v_w and v_t . It is also possible to try to cool the workpiece and the deposit as much as possible during deposition by means of active cooling. However, cooling of the workpiece will require alterations of process parameters, typically by increasing P_L since more energy is dissipated from the weld pool. Also cooling will introduce higher thermal gradients which may cause higher residual stresses. In a short unpublished study when Alloy 718 was deposited onto a water cooled fixture, no significant reduction in cracking was seen compared to the uncooled case.

The fact that temperature control generally is ill-suited for the LMD-w process does not mean that temperature measurements are not important. To the contrary, temperature measurements are instrumental in finding good control strategies for LMD-w and other AM processes. Utilising simulation models for predicting resulting geometry and material properties, as proposed by Raghavan et al. [77], is a possible way to predict how measurable and controllable parameters affect the end result. Such knowledge can be used for designing suitable control strategies, both general and tailored to specific applications. In order to accurately calibrate such simulation models to reflect reality, temperature measurements are very important for comparison. When calibrating a simulation model, most often absolute temperature data is required. Thus, any bias or other kind of error, which may not be a significant problem when maintaining constant temperature in a feedback-loop, can have a big impact on the simulation model.

The conclusion of this reasoning is that, not only is it important to measure temperature within AM. For calibrating simulation models it must also be measured as absolute and not relative temperature, and it must be measured accurately.

4.4 Summary

A number of process control strategies are available for LMD-w with regards to maintaining stable deposition and achieving the desired geometry. They range from manual control, which while being the simplest control scheme still is very complex to perform, to the even more intricate iterative learning control. ILC adopts a strategy of stepwise buildup of process characteristics and appropriate control action. In addition to these two control schemes, the concept of resistance in-process control is introduced. Its intended use is to either serve as a complement to manual control, be used in a feedback-controller for robot z-position, or to be used as a tool-to-workpiece distance input signal to an iterative learning controller. Resistance measurements have successfully been implemented for LMD-w-control both for avoiding droplet formation and for topography control when coupled to an ILC controller.

Temperature control is another important factor in achieving desired deposit characteristics. Even though the controller could be of a simple design, a temperature control system requires a desired temperature which may or may not be constant. This desired temperature would typically be derived from numerical simulations and is therefore not obtained with ease. As discussed in the following chapter however, temperature measurements are far from trivial and might limit the applicability of temperature control for LMD-w.

Chapter 5

Temperature measurements

Temperature is a central process property in many industrial applications. It is a determining factor for material properties and process characteristics. Temperature information is also often central for understanding a process and process results. In this chapter, temperature measurements are discussed from both theoretical and practical viewpoints.

5.1 Contact thermometry

For measuring the temperature of an object, a multitude of options are available when it is possible to put a measurement probe in physical contact with said object [79]. One could employ thermistors, platinum resistance thermometers such as Pt-100 or Pt-1000, thermocouples, liquid-in-glass thermometers, noise thermometry, diodes or yet another out of many techniques. For applications to LMD-w however, contacting probes are not an option due to reasons outlined in Section 4.3. The lack of contacting options only leave non-contacting alternatives, such as described in the following sections.

5.2 Radiation thermometry fundamentals

Any object above 0 K will emit electromagnetic radiation. For an idealised object, called a blackbody, the radiation is quantified by Planck's law [80, 81]:

$$r_P(T, \lambda) = \frac{C_1}{\lambda^5 (e^{C_2/(\lambda T)} - 1)} \quad (5.1)$$

where $C_1 = 1.191 \times 10^8 \text{ W}\mu\text{m}^4\text{m}^{-2}\text{sr}^{-1}$ and $C_2 = 1.4388 \times 10^4 \mu\text{m K}$ [81, 82]. T denotes temperature in Kelvin and λ denotes wavelength in μm . Planck's law describes the energy exerted from an object dependent on its temperature (T) and wavelength (λ), but independent of emission angle [83]. The angles θ and ϕ used

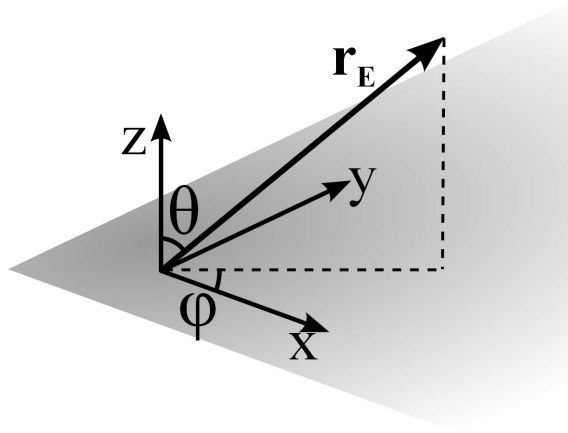


Figure 5.1: Direction of emitted radiation is denoted with angles θ and ϕ . These are defined in a euclidian coordinate system arbitrarily rotated around the z-axis, which is normal to the material surface.

for denoting the emission angle in a certain emission direction are illustrated in Figure 5.1.

By collecting the radiance r_P , in a specified spectral interval $\{\lambda_{\text{start}} \dots \lambda_{\text{end}}\}$ and in a certain direction, from a blackbody with a detector with known characteristics, Planck's law (5.1) can be inverted in order to give the temperature T of the blackbody. This is the basis for most non-intrusive temperature measurements [81] with some exceptions such as line spectra to continuum comparisons and band-edge thermometry [84, 85].

5.3 Emissivity

No real object can be considered a true blackbody. Instead the radiance emitted from a real object, r_E , must also be described by the object's emissivity ε . The emissivity of an object is defined by how the true radiation emitted differs from that described by Planck's law:

$$\varepsilon(T, \lambda, \theta, \phi) \equiv \frac{r_E(T, \lambda, \theta, \phi)}{r_P(T, \lambda)} \quad (5.2)$$

Note that emissivity is not a scalar quantity for a certain object but a function of temperature, angles and wavelength [81].

When relating radiance to temperature through Planck's law (5.1), it is necessary to take emissivity into account, since it affects any radiance measurement made on any physical object. With unknown emissivity, it is not possible to de-



Figure 5.2: Changes in reflectivity, and emissivity, are apparent for this welded steel specimen.

duce the object's temperature, T , only by measuring radiance. However, if the emissivity, ϵ , is known, it is possible to make accurate temperature measurements provided radiance measures such as described later in Section 5.4.

When consulting literature for emissivity values for a certain material, there are several measures which might be given [83]. These are *directional spectral emissivity* which is defined as in (5.2), *directional total emissivity* which is an integral over all wavelengths at certain angles θ and ϕ . There is also *hemispherical spectral emissivity* and *hemispherical total emissivity*, which both are integrals over a hemisphere with the latter also being integrated over all wavelengths. When using a value of emissivity taken from literature, it is important to know which value is required for the application and which type of value is actually given.

Material dependence

As a result of the first law of thermodynamics (conservation of energy) the hemispherical total emissivity of an object is complementary to the object's hemispherical total reflectivity, Γ , such that $\epsilon + \Gamma = 1$. As apparent even to the layman, different objects have different reflectivities, as shown in Figure 5.2, and thus different emissivities. The material studied is therefore of great importance when conducting non-contacting temperature measurements.

Dependence on surface composition

Most often, the material studied is known. Common practice is that a value of the material's emissivity is read from a table and used for creating temperature estimates from radiance measurements. However, as shown in Paper 1, the surface composition of the material greatly affects the measured emissivity.

Oxidation, crystalline reorganisation or diffusive processes might all cause the emissivity of an object not only to be different from literature but also to vary with time [81, 86, 87].

Temperature dependence

Emissivity is related to the material's complex refractive index. By knowing the incidence angle and the complex refractive index, $n + \kappa i$, of every material in the optical path, it is possible to calculate the material's emissivity even for layered structures [83, 88]. However, the complex refractive index of a material, besides being wavelength dependent, typically exhibits some kind of temperature dependence due to electron-phonon collisions [89]. This implies that emissivity is temperature dependent as well. This is also the case for several industrially relevant materials such as silicon, titanium, zirconium and Alloy 718 [74, 90–93]. The dependence of emissivity on temperature can be problematic since measurement of one property is usually used for discerning the other as described below and in Section 5.4.

Emissivity measurements

There are a number of ways of measuring or estimating the emissivity of a material. A few examples are given in this section. The first and maybe the most intuitive is to measure an object's temperature (T) by some means and at the same time measure the emitted radiance with some instrument such as a pyrometer, which is described in the following section. By employing the following relation

$$\varepsilon = \varepsilon_i \frac{e^{C_2/(\lambda_c T)} - 1}{e^{C_2/(\lambda_c T_p)} - 1}. \quad (5.3)$$

the object's true emissivity ε can be derived from the instrument's emissivity setting, ε_i , the reference absolute temperature, T , and the temperature reading given by the instrument, T_p for the waveband centre wavelength λ_c [87]. This concept of measuring emissivity and calibrating a pyrometer is further elaborated on in Paper 1 and also implemented by del Campo et al. [94] as well as Shur and Peletskii [95]. Another approach is investigated by e.g. Corwin and Rodenburgh II who measured reflectance and related this to emissivity as described in Section 5.3 [96, 97]. Through the relation between complex refractive index and emissivity, mentioned above in this section, it is also possible to use ellipsometric measurements of complex refractive indices in order to calculate material emissivity [86, 88]. This method is however not employed in this thesis.

5.4 Pyrometry

Temperature measurement instruments which measure "relatively high temperatures, as in furnaces" are, as described in *the Britannica Concise Encyclopaedia*, pyrometers [98]. Typically, radiance is measured and related to temperature. Historically, before the introduction of electronic radiation detectors, pyrometers were based on comparing a reference filament to the object of measure with the naked eye [83]. Modern pyrometers typically quantify radiance for a finite number of wavebands and use set emissivity estimations for deducing temperature through (5.1) or derivations of Planck's law. Rewriting the definition of emissivity in (5.2) results in

$$r(T, \lambda, \theta, \phi) = \varepsilon(T, \lambda, \theta, \phi)r_P(T, \lambda) \quad (5.4)$$

where it is obvious that the emissivity ε affects the measured radiance r , which is in turn converted into a temperature measure (T) through inversion of (5.1).

Single waveband pyrometry

The most intuitive implementation of a quantitative pyrometric method is the single waveband pyrometer. This method relies on radiance collected in a narrow waveband of the electromagnetic spectrum. Ideally, a very narrow waveband corresponding to a single wavelength is collected and is used for inversion of (5.1). However, sufficient signal levels must be achieved thus requiring a minimal wavelength interval. This requirement and optical limitations restrict the waveband from approaching a single wavelength. As previously explained in Section 5.3, the emissivity must be known for the waveband which is to be used. Also, the temperature dependence of emissivity for the certain wavelength must be established and the instrument must be properly calibrated [83]. The latter is to cancel out the instrument's sensitivity, Q , to that certain wavelength and optical attenuation, ρ , since the measured radiance, r , can be described by [83]:

$$r(T, \lambda, \theta, \phi) = \rho Q \varepsilon(T, \lambda, \theta, \phi) r_P(T, \lambda). \quad (5.5)$$

Provided a good emissivity estimate and a well calibrated instrument, the single waveband pyrometry method is a relatively cheap, simple and robust method for performing radiation temperature measurements [83]. An implicit formulation of the temperature is as follows

$$T = \arg \min_T H(\rho Q \varepsilon r_P(T) - r), \quad (5.6)$$

where H is some difference norm, such as absolute or squared differences of the difference

$$z = \rho Q \varepsilon r_P(T) - r. \quad (5.7)$$

This formulation of the single waveband pyrometry functionality enables comparison with the other kinds of pyrometry, to be described later, by formulation on a common form.

Dual waveband pyrometry

Employing more than one waveband is beneficial if the object is partially obstructed or if the emissivity is unknown but can be assumed to be constant with respect to wavelength. This assumption is a required constraint for dual waveband pyrometry, since radiance measures for two wavelengths are used for determining three unknowns, namely, $\varepsilon(\lambda_1)$, $\varepsilon(\lambda_2)$ and T . Temperature, T , is calculated through relating ratios of radiance to temperature by constructing a ratio of (5.5) for two wavelength bands with centre wavelengths λ_1 and λ_2 . Creating the following ratio

$$\frac{r(\lambda_1)}{r(\lambda_2)} = \frac{\rho(\lambda_1)Q(\lambda_1)\varepsilon(\lambda_1)r_P(T, \lambda_1)}{\rho(\lambda_2)Q(\lambda_2)\varepsilon(\lambda_2)r_P(T, \lambda_2)} \quad (5.8)$$

and assuming that $\rho(\lambda_1) = \rho(\lambda_2)$ and $Q(\lambda_1) = Q(\lambda_2)$ the following relation is found:

$$\frac{r(\lambda_1)}{r(\lambda_2)} \approx \frac{\varepsilon(\lambda_1)}{\varepsilon(\lambda_2)} \cdot \frac{r_P(T, \lambda_1)}{r_P(T, \lambda_2)} \quad (5.9)$$

If the relation $\varepsilon(\lambda_1)/\varepsilon(\lambda_2)$ is known *a-priori*, or if the object can be considered a graybody with constant emissivity with relation to wavelength, the temperature can be found from (5.9) and (5.1). This even holds for partial obstruction of the optical path, measurement on objects smaller than the measurement spot, fumes or other factors as long as $\rho(\lambda_1) = \rho(\lambda_2)$.

For comparison with the single waveband method, an implicit formulation of T is given below:

$$T = \arg \min_T H(z) \quad (5.10)$$

where this time

$$z = \frac{\varepsilon(\lambda_2)r(\lambda_1)}{\varepsilon(\lambda_1)r(\lambda_2)} - \frac{r_P(T, \lambda_1)}{r_P(T, \lambda_2)}. \quad (5.11)$$

If the emissivity ratio changes over time however, either due to temperature dependencies or due to changes in surface structure or composition, the dual waveband pyrometry method will give erroneous temperature values. Without *a-priori* knowledge of the object's emissive properties with respect to wavelength, dual waveband pyrometry will typically give less accurate readings than a single waveband pyrometer [83]. Also a dual waveband pyrometer is more sensitive to noise than the single waveband pyrometer due to the division operation performed.

Multispectral pyrometry

The concept of dual waveband pyrometry can be expanded into multispectral pyrometry. For pyrometers with multiple wavelengths, where the number of wavelengths $n > 2$, other constraints than on a constant ratio $\varepsilon(\lambda_1)/\varepsilon(\lambda_2)$ are required. The most common methods [99–105], are based on modelling spectral emissivity with some mathematical function, $\xi(\lambda)$, which has less degrees of freedom than the number of wavelengths employed, and

$$T = \arg \min_T H(z) \quad (5.12)$$

with the difference vector

$$z_i = \frac{r(\lambda_i)}{\xi(\lambda_i)} - r_P(T, \lambda_i) \quad (5.13)$$

where the formulation of ξ varies between different methods and H in this case is a summation of errors over all wavelengths λ_i in the spectrum. The many wavelengths contained in the measured spectrum allow for simultaneous determination of both T and parameters for ξ . However, as concluded by Coates as early as in the 1980's [99, 106], these methods rarely give better accuracy than single or dual waveband methods. Also, multispectral measurements require hardware which are roughly a factor of 10 more expensive than the more conventional methods.

Emissivity corrected methods

One way to perform emissivity corrected temperature measurements is to measure the surface's reflectivity as well as emitted radiation. As described in Section 5.3, emissivity and reflectivity are complementary properties always adding up to unity. By measuring reflectivity and radiance at the same wavelength it is possible to discern the correct absolute temperature even as emissivity changes [96, 97, 107]. This method requires optical path angles which do not change since that would disrupt the reflectance measurements.

Another method, which probably should be denoted semi-intrusive is the use of paints. The object is painted with a paint which has well defined emissive properties. A conventional pyrometer with appropriate emissivity settings is then used for absolute temperature measurements [108]. Apart from the need to paint the material and the risk of contamination, there is another downside to using paints for temperature measurements. As shown in Paper 1, the paint may react chemically with the object, thus altering the emissivity of the paint. The use of paints is practical in some specialised applications where reliable non-contact measurements are needed but the areas of application are limited.

From the physical theories such as Maxwell's electromagnetic wave theory, the Lorentz oscillator model, the Drude free-electron theory and derivations thereof [83,86,88,109], it is possible to calculate theoretical emissivity values for non-conductors such as oxides, conductors such as metals and for layered structures such as oxides upon metal. However, these theoretical values are based on idealised conditions and are only applicable for well defined situations.

5.5 Summary

Non-contact temperature measurements on metallic materials prove to be very challenging for high temperature applications. Due to temperature dependent emissivity and oxidation, the object's emissivity is rarely known with accuracy. A calibrated single waveband pyrometer might be used, but large errors might have to be accepted, especially in the case of significant oxidation. In the following chapter, a multispectral emissivity compensated pyrometry method developed by the author is presented.

Chapter 6

Emissivity compensated spectral pyrometry

Note In this chapter, mathematical operations on vectors are described. Besides the operators typically used for such operations, \circ and ϕ are used herein. These operators denote the Hadamard, element-wise multiplication and division operations respectively on the vector elements [110]. To some readers, these might be recognised as the `.*`- and `./`-operators used in MATLAB and Octave computer software.

A new temperature measurement method denoted Emissivity Compensated Spectral Pyrometry (ECSP) is presented in Paper 2 and Paper 3. It is based on spectral measurements of radiance and accommodates for varying emissivity in some situations without *a-priori* knowledge of emissivity.

For the purpose of brief notation,

$$\varepsilon^Q = \rho Q \varepsilon \quad (6.1)$$

is introduced for denoting compound emissivity in this chapter. This is the effective emissivity as seen by a user of a radiance measuring instrument. It includes the optical attenuation and the sensitivity coefficients of the instrument itself.

In order to explain how ECSP works, it helps to assume that the changes in emissivity in between samples are limited in magnitude, i.e.

$$|\varepsilon_k - \varepsilon_{k-1}| < D_{\max}. \quad (6.2)$$

This assumption makes it feasible to assume that any changes in emissivity over time will evolve gradually, and no larger discrete jumps or leaps will occur.

Recall that all pyrometry methods require some constraint in order to derive both temperature and emissivity from one radiance measurement, as described in Chapter 5. For ECSP, the constraint does not regard assumptions in

wavelength, such as constant emissivity ratios for dual-waveband pyrometry (see Section 5.4). Instead, the constraint is applied in temporal domain. It is assumed that emissivity does not vary extensively over time, which can be formalized by the assumption in (6.2). This fundamentally differentiates ECSP from the conventional methods presented in Section 5.4, which all apply some constraints in the wavelength dimension.

The implicit formulation of ECSP, similar to those in (5.6), (5.10) and (5.12), is

$$\hat{T} = \arg \min_T H(\mathbf{z}) \quad (6.3)$$

where

$$z_i = \beta_i \left[\frac{r(\lambda_i)}{\hat{\varepsilon}^Q(\lambda_i)} - r_P(T, \lambda_i) \right] \quad (6.4)$$

where β_i is a weight for a certain wavelength λ_i further described in Section 6.3, $H(\cdot)$ is a difference norm, and $\hat{\varepsilon}^Q$ is a compound emissivity estimate. This estimate, constructed from the previous temperature estimation \hat{T}_{k-1} and previous measured spectra \mathbf{r}_{k-1} , is the simplest available approximation

$$\hat{\varepsilon}_k^Q(\lambda_i) = \frac{r_{k-1}(\lambda_i)}{r_P(\hat{T}_{k-1}, \lambda_i)} \quad (6.5)$$

given (6.2).

6.1 ECSP functionality

The functionality of ECSP is that it, to a certain degree, discriminates between changes in measured radiance, \mathbf{r} , and identifies those as either changes in emissivity, which are arbitrary but spectrally continuous, or changes in temperature whose characteristics are given by Planck's law, (5.1). For a new measurement of spectral radiance, \mathbf{r} , the change in temperature which best explains the measured change in radiance is determined from (6.3). Based on this estimated temperature, and the measured radiance, emissivity is adapted to fit the measured radiance, assuming that the temperature estimate is correct.

Another simplified explanation is to say that ECSP tries to find the most appropriate temperature to satisfy the measured data, based on an estimation of emissivity derived from the previous sample. Given this temperature estimate, all characteristics in \mathbf{r} which may not be explained by a temperature change are instead explained by a change in spectral emissivity. In order to illustrate this, consider the following case, between sample $k = 0$ and $k = 1$, emissivity changes from 0.5 to 0.4 for all wavelengths in a wavelength range from 190 and 870 nm, corresponding to that of the hardware used in Paper 2. This is illustrated

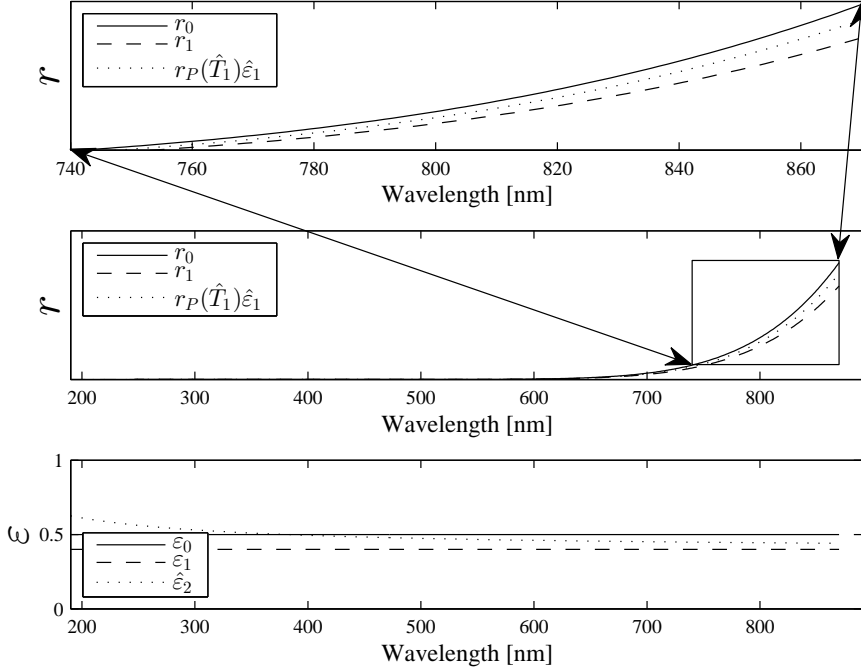


Figure 6.1: Upper two plots, measured radiances r_0 (solid line) and r_1 (dashed line), as well as the result of temperature estimation $r_P(\hat{T}_1)\hat{\varepsilon}_1^Q$ indicated by a dotted line. Bottom plot, true emissivities ε_0^Q (solid) and ε_1^Q (dashed), as well as the resulting emissivity estimation, $\hat{\varepsilon}_2^Q$, obtained at sample $k = 1$ after determining \hat{T}_1 .

in the bottom part of Figure 6.1. Please note that this is only an example for illustration purposes. A change in emissivity of 0.1 in between samples is very large and does not agree very well with (6.2) and the short sampling intervals used in practice for ECSP measurements. Between the two sampling instances, the temperature is fixed at 1000 K and $\hat{T}_0 = T_0 = 1000$ K. The measured radiance, r_0 and r_1 , for these samples are illustrated by solid and dashed lines respectively in the upper parts of Figure 6.1. In determining the temperature estimate, \hat{T}_1 , for sample $k = 1$, an estimate of compound emissivity, $\hat{\varepsilon}_1^Q$, at $k = 1$ has to be used. As introduced above in (6.5), the estimate typically used within ECSP is $\hat{\varepsilon}_1^Q = r_0 / r_P(\hat{T}_0)$. Based on r_1 and $\hat{\varepsilon}_1^Q$, \hat{T}_1 can be determined using (6.3). The result of this determination of \hat{T}_1 , in order to best explain r_1 , can be seen as the black dotted line in the upmost plot of Figure 6.1. For this particular example, \hat{T}_1 was found to be 995 K, i.e. $|\hat{T}_1| = |\hat{T}_1 - T_1| = 5$ K. Note that, in order to make the changes in r more visible, only a limited wavelength range is shown in the upper part of Figure 6.1, while the entire range is shown in the middle part.

In the lower part of Figure 6.1, indicated by a dashed black line, the emissiv-

ity estimation $\hat{\epsilon}_2^Q$ resulting from r_1 and \hat{T}_1 is seen.

This ability of the algorithm to separate temperature changes from emissivity changes is explained in some more detail in Appendix A. In Appendix A, it is also concluded that the non-linearity of Planck's law is an important factor in explaining why the algorithm works.

To put the workings of ECSP in other words: If any change in temperature results in a distinct change in measured radiance r , corresponding to r'_P , this change may be attributed to a temperature change. Otherwise, this change should be attributed to an emissivity change. Thanks to the fact that $r_P \phi r'_P$ for Planck's law is relatively low (see Appendix A), i.e. the change in r (and r_P) due to a change in T is significant, the ECSP algorithm is applicable for use with Planck's law.

There is of course a possibility to, rather than selecting only one single temperature value, create a population of temperatures, each with some certain probability measure, and from these temperatures create a population of emissivity estimates. These estimation populations could then be treated similarly to populations of particles in a particle filter, updating populations based on new measurements and the estimates' prior probabilities as time progresses [111]. This approach first and foremost requires some quantification of probability. The probability measure should ideally give an indication of when the estimates diverge from probable ones, perhaps based on the residuals of the fit obtained in (6.3). Since each single \hat{T} in the population will branch out to some number of new \hat{T} 's, the total number of \hat{T} 's will increase exponentially unless the majority of the \hat{T} 's can be eliminated at each iteration step based on their probability measure. Additionally, it should be noted that the ECSP method is already quite computationally intensive, and the proposed method of using populations might prove to be impractical due to very long computation times required.

6.2 Algorithm

A brief description of the ECSP algorithm is given in Table 6.1. For an in-depth description of the algorithm, please refer to Paper 3. The implicit expression of the ECSP method in (6.3) can beneficially be reformulated somewhat to improve the method. When noise is introduced to the measured signal, r , the noise, even if its first moment is zero, will cause an overestimation of temperature due to the nonlinearity in Planck's law which is effectively inverted in (6.3). Because of this, the following dimension-less formulation is proposed

$$\hat{T} = \arg \min_T H(z) \quad (6.6)$$

Step no	Word description	Math description
1	If initial emissivity is known, go to Step 5	
2	Collect spectrum when the temperature is known	\mathbf{r}_0, T_0
3	Filter the spectrum	$F_\lambda(F_t(\mathbf{r}_0))$
4	Calculate emissivity	$\hat{\epsilon}^\Omega = \frac{F_\lambda(F_t(\mathbf{r}_0))}{\mathbf{r}_P(T_0)}$
5	Collect spectrum for unknown temperature	\mathbf{r}_k
6	Filter the spectrum	$F_\lambda(F_t(\mathbf{r}_k))$
7	Numerically invert Planck's law	$\hat{T} = \arg \min_T H \left(\beta \left[\frac{F_\lambda(F_t(\mathbf{r}_k))}{\mathbf{r}_P(T)} - \hat{\epsilon}^\Omega \right] \right)$
8	Calculate emissivity estimate	$\hat{\epsilon}^\Omega = \frac{F_\lambda(F_t(\mathbf{r}_k))}{\mathbf{r}_P(\hat{T})}$
9	Terminate if no more samples, otherwise go to Step 5	

Table 6.1: Simplified description of the ECSP algorithm. All variables except for T are wavelength resolved vectors. A fraction line with a "o" denotes the element wise division operation. Please refer to Paper 3 for an in-depth description of the algorithm.

where

$$z_i = \beta_i \left[\frac{r(\lambda_i)}{r_P(T, \lambda_i)} - \hat{\epsilon}^\Omega(\lambda_i) \right] \quad (6.7)$$

Note that this formulation differs from that in Paper 2 and Paper 3 and does not compare as well with (5.6), (5.10) or (5.12) as the formulation in (6.3).

Recursive formulation

Introducing the functions $G_T(\hat{\epsilon}^\Omega, \mathbf{r})$ and $G_\epsilon(\hat{T}, \mathbf{r})$, corresponding to algorithm Steps 5-7 and Step 8 from Table 6.1 respectively, a simplified recursive formulation of the algorithm can be made. With samples ranging from 0 to k , and a correct first temperature estimation

$$\hat{T}_0 = T_0 \quad (6.8)$$

given *a-priori*. The first emissivity estimation becomes

$$\hat{\epsilon}_1^\Omega = G_\epsilon(\hat{T}_0, \mathbf{r}_0) = G_\epsilon(T_0, \mathbf{r}_0) = \epsilon_1^\Omega. \quad (6.9)$$

The following temperature estimation for sample 1 is

$$\hat{T}_1 = G_T(\hat{\epsilon}_1^\Omega, \mathbf{r}_1) \quad (6.10)$$

followed by the new emissivity estimation

$$\hat{\epsilon}_2^Q = G_\epsilon(\hat{T}_1, \mathbf{r}_1) \quad (6.11)$$

and so forth, resulting in

$$\hat{T}_k = G_T(\hat{\epsilon}_k^Q, \mathbf{r}_k) \quad (6.12)$$

and

$$\hat{\epsilon}_{k+1}^Q = G_\epsilon(\hat{T}_k, \mathbf{r}_k). \quad (6.13)$$

As seen above in (6.12) and (6.13), \hat{T}_k and $\hat{\epsilon}_k^Q$, are determined recursively and an error in one estimation is progressed, and possibly amplified, to the latter estimates. Note that the key enablers for application of this recursive approach is (6.8), the fact that T_0 is given *a-priori* and also that Planck's law is highly non-linear as discussed in Appendix A.

6.3 Weights and filtering

In real world situations, noise will be part of the measured spectral radiance \mathbf{r} . In order to counter this, filters are applied. Based on assumptions of limited changes both related to wavelength and time for both emissivity and radiance, see (6.2) and (5.1), low-pass filtering is applied in both spectral and temporal dimensions. In time domain, each wavelength channel is filtered with a second order Butterworth filter, whereas a Savitzky-Golay filter [112–114], is used for filtering in wavelength domain. Based on comparison of the filtered and unfiltered spectra, signal to noise ratios (SNR) and variances can be estimated for all wavelength channels, see Paper 3. The SNR and variance values are essential in deciding which wavelength channels to include in the numerical inversion (Step 7 in Table 6.1). Channels with too low SNR are not included at all, while the included channels are weighted with respect to their variances. Experiences from performed tests have given that a good formulation of the weight vector β , when $H(\cdot) = \sum_{\lambda \in \Lambda} \beta(\cdot)^2$, is

$$\beta(\lambda_i) = \frac{1}{\hat{\sigma}_{\chi_i}^2}. \quad (6.14)$$

where $\hat{\sigma}_{\chi_i}^2$ is the estimated variance of the measured radiance at λ_i . For the weighted least squares regression method, the Best Linear Unbiased Estimator (BLUE), is obtained if each weight is equal to the reciprocal of the variance of the measurement [115, 116]. This corresponds well to the empirically based findings presented in (6.14), reflecting that the weighted inversion in Step 7 in Table 6.1 is related to weighted least squares regression.

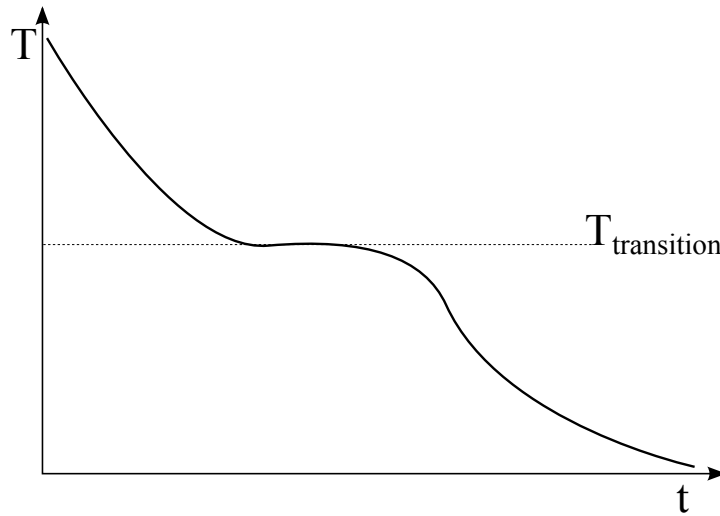


Figure 6.2: Temperature curve during cooling of a material exhibiting a phase transformation at $T_{\text{transition}}$.

6.4 Calibration

As described in Section 5.3, the temperature can be determined unambiguously from measured radiance r , if the emissivity is known. One of the fundamental problems of pyrometry is how to handle the fact the emissivity only rarely is known [81, 83]. The ECSP method constitutes a new approach to the problem but is in no way a complete solution. The fact remains that one desires to determine temperature which is one of two unknowns which affect the radiance measurement, the other one being emissivity.

The requirement for the ECSP method that T_0 (or ε_0^q) needs to be known *a-priori* constitutes a severe drawback of the method. Basically the problem comes down to the fact that one must know the temperature (or emissivity) at some point ($k = 0$) in order to measure the temperature for the other samples. This "teach-in" calibration type, where a known temperature or emissivity is used to calibrate the system at a point in time, is only available in some applications. In the situations where teach-in calibration is possible and emissivity is not expected to vary, all conventional pyrometry methods, described in Section 5.4, give good accuracy and there is no need to use ECSP. However if emissivity is expected to vary, ECSP should be considered as an alternative, if teach-in calibration is possible.

In Paper 4, a new approach for enabling teach-in calibration is presented. The fact that material phase transitions may occur during the measurement is exploited. If a material, for example, during cool down undergoes a phase transition, as illustrated in Figure 6.2, a "hump" or plateau will be seen at the phase transition temperature $T_{\text{transition}}$. This hump, and thus the phase transition, can

be automatically identified from radiance measurements in a number of ways as described in Paper 4 and in [117]. If the phase transition temperature is known, this temperature can be used as T_0 and allows for applying the algorithm both forwards and backwards in time. These techniques for automatic calibration are not restricted to use with ECSP, but are also well suited for teach-in calibration of multispectral pyrometry as described in Section 5.4.

6.5 Sensitivity analysis

In the following section, a sensitivity analysis study is presented in the form of a number of simulated scenarios, Scenario 1 to Scenario 5. The purpose of the sensitivity analysis is to illuminate both the limitations and the benefits of the ECSP method. For this purpose, all scenarios except Scenario 4 are simulated without any artificial measurement noise. The absence of noise is to illuminate the ECSP method's dynamics rather than its sensitivity to noise. Additionally, all filtering and weighting of wavelengths normally carried out for the ECSP method, see Paper 3 for details, are left out in order to make a fair comparison to other methods. The multispectral method simulated in this study, assumes graybody emissivity, i.e. constant emissivity for all wavelengths.

Reflecting the spectrometer used in Paper 2, 2048 wavelengths are simulated between 190 and 870 nm for ECSP and multispectral pyrometry. The temperature ramp is identical for all scenarios, except for Scenario 2, in which constant temperature is simulated. The simulated test set comprises of 1000 samples. With the sampling rate in Paper 2 (50 Hz), this corresponds to a duration of 20 s. During the first 50 samples, temperature is kept constant, followed by a linear increase in temperature from 1000 K to 1500 K during 700 samples, followed by a constant temperature for the remaining 250 samples as indicated in the uppermost part of Figure 6.3. This is a temperature range which, in terms of signal strength, is suitable for the wavelength range of the simulated instrument.

The simulated instruments' accuracies are illustrated in the result plots by the absolute relative error

$$\left| \frac{\hat{T} - T}{T} \right|, \quad (6.15)$$

expressed in percent. All pyrometry methods are calibrated with regard to emissivity at the first sample, $k = 0$, for each simulation scenario, meaning that the first temperature and emissivity estimations are correct. The emissivity calibration is then retained throughout each simulation for the conventional pyrometry methods, while the emissivity estimation in the ECSP method is gradually altered.

Scenario 1: Constant emissivity, varying temperature

The results of the simulated scenario with constant emissivity is shown in Figure 6.3. All methods give negligible errors as might be expected.

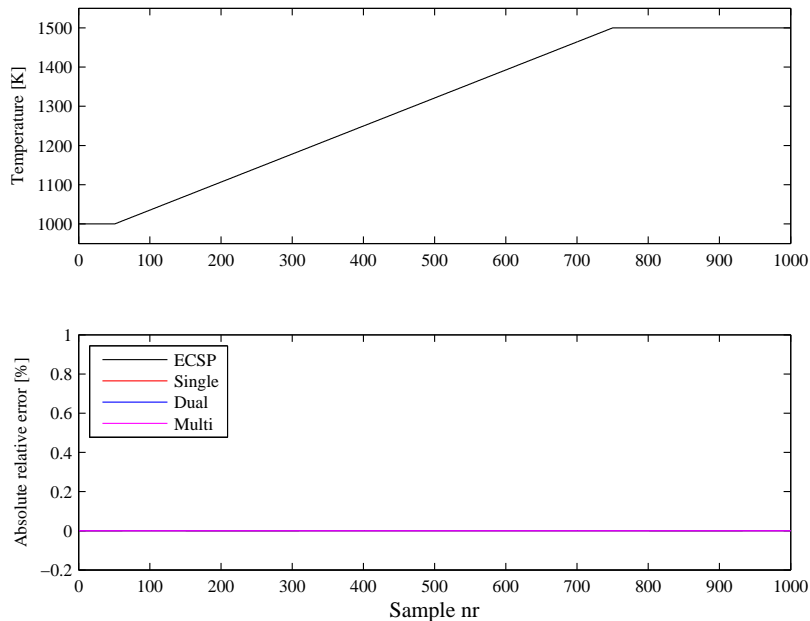


Figure 6.3: Results from Scenario 1 with constant emissivity. All methods give negligible errors. Note that no noise is introduced in the simulation.

Scenario 2: Time varying graybody, constant temperature

This scenario encompasses varying emissivity that changes linearly over time, from 0.3 to 0.7, over a range of 1000 samples. Although a somewhat idealised situation, this scenario might be representative of some real world conditions. The results from this simulation are presented in Figure 6.4. Note that due to the assumption of graybody emissivity, both the multispectral method and the dual waveband method performs without estimation errors. Temperature is not varied throughout this scenario. It is also worth noticing that if instead of 1000 samples, a lower number of samples are used for simulating the same magnitude of emissivity change, the resulting errors remain the same.

Scenario 3: Time varying graybody, varying temperature

For this scenario, where emissivity varies as a graybody over time, emissivity varies linearly from 0.3 to 0.5 from sample 0 to sample 300, followed by con-

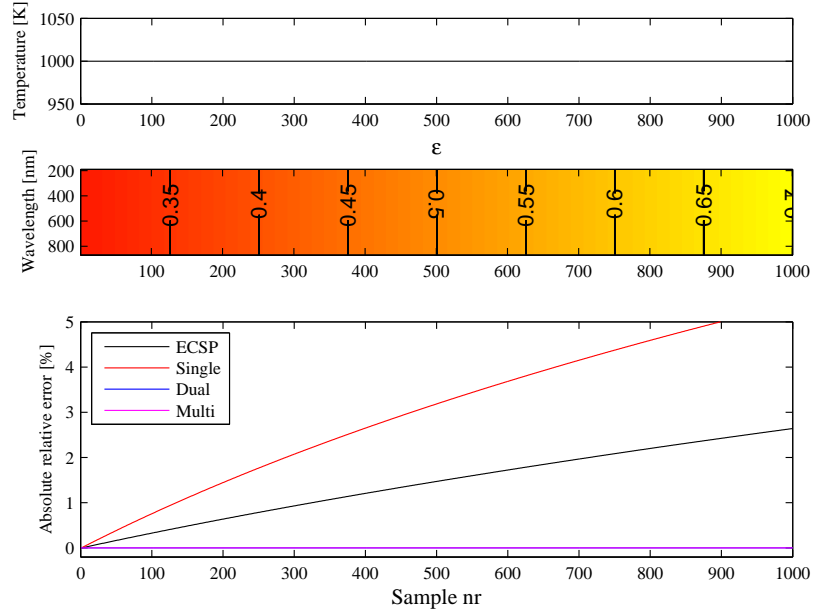


Figure 6.4: Results from Scenario 2 with time varying graybody emissivity and constant temperature. Note that no noise is introduced in the simulation.

stant emissivity for 200 samples, another linear increase to 0.7 followed by another 200 samples of constant emissivity as seen in Figure 6.5. This choice of simulated emissivity is made in order to illustrate how both varying and constant emissivity affects the temperature estimate. Note that emissivity is the same for all wavelengths for a certain sample instance. The emissivity changes simulated in this scenario could be caused by e.g. gradual obstruction of the optical path, an articulated temperature dependence of emissivity of the material or oxidation.

As seen in Figure 6.5, and as expected for a graybody, the simulated dual color and multispectral pyrometers are superior to all other methods for this idealised scenario. The ECSP method steadies at a constant temperature and does not drift for the last samples when all parameters are constant, even though it is a recursive method. This can be explained by the fact that

$$\hat{\boldsymbol{\epsilon}}_{k+1}^{\text{Q}} = G_{\epsilon}(\hat{T}_k, \mathbf{r}_k) \quad (6.16)$$

and

$$\hat{T}_{k+1} = G_T(\hat{\boldsymbol{\epsilon}}_{k+1}^{\text{Q}}, \mathbf{r}_{k+1}) = G_T(\hat{\boldsymbol{\epsilon}}_k^{\text{Q}}, \mathbf{r}_k) = \hat{T}_k \quad (6.17)$$

for the two subsequent samples k and $k+1$ when temperature and emissivity are constant, and $\hat{\boldsymbol{\epsilon}}^{\text{Q}}$ contains no noise.

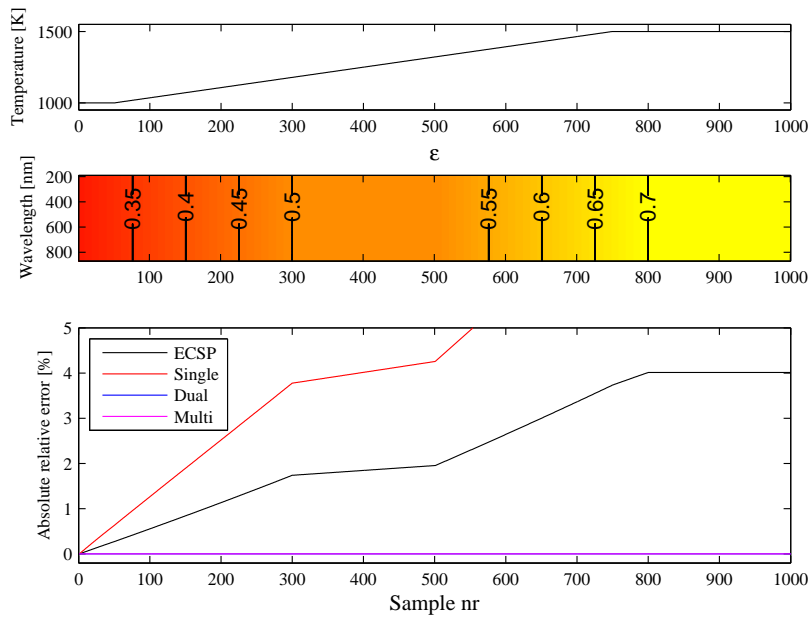


Figure 6.5: Results from Scenario 3 with time varying graybody emissivity. Note that no noise is introduced in the simulation.

Scenario 4: Time varying graybody, varying temperature - with added noise

Along with Scenario 3, another simulation was performed. It was identical to Scenario 3 except for the fact that noise is introduced. In order to have constant noise levels independent of temperature and wavelength, proportional gaussian noise with a standard deviation of 0.5 % of the signal amplitude is added. Note that the proportional behaviour of the added noise does not reflect what might be expected in reality, but is added only to illustrate how the ECSP algorithm is affected by noisy measurements. If a constant amplitude additive noise was added, its impact would very much depend on the temperature and the resulting radiance amplitude. Since no filtering is applied in the simulation, the added noise amplitude of 0.5 % should, in this particular case, be compared to the noise remaining after filtering during normal measurements where filtering is performed.

The results of Scenario 4 are presented in Figure 6.6. It shows strong resemblance to Figure 6.5 just as might be expected, but exhibits fluctuations in the temperature estimations, especially for the single- and dual waveband methods. When noise is introduced, like in this scenario, the ECSP estimates will drift somewhat, even when all parameters are constant such as after sample 800. This effect is barely visible in Figure 6.6, and is therefore shown magnified in Figure 6.7. The drift is of minor importance for the ECSP method as long as noise levels and the number of samples resemble those in this scenario. For details into

the impact of noise in ECSP measurements, please refer to Paper 3.

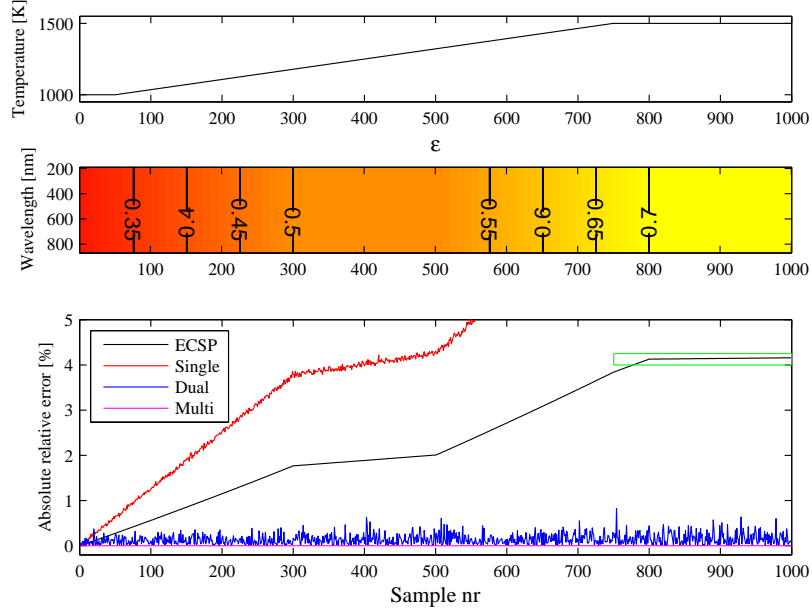


Figure 6.6: Results from Scenario 4 with added noise. Note that noise is introduced in the simulation, equivalent to 0.5 % of the signal strength. Compare to Figure 6.5. A magnification of the area indicated with green is shown in Figure 6.7.

Scenario 5: Varying spectral emissivity, varying temperature

Scenario 5 is similar to Scenario 3 in that no noise is added, the difference lies in that the spectral emissivity in Scenario 5 varies not only with samples (k) but also with wavelength (λ). Again, the minimum emissivity is 0.3 and the maximum is 0.7. The function used to generate the emissivity set, as seen in the middle part of Figure 6.8, is

$$\varepsilon^Q(k, \lambda) = 0.5 + 0.2(\underline{k}\underline{\lambda} - \underline{\lambda}) \quad (6.18)$$

where the normalised time $\underline{k} = (k - k_1)/(k_{1000} - k_1)$ and normalised wavelength $\underline{\lambda} = (\lambda - \lambda_1)/(\lambda_{2048} - \lambda_1)$.

In Figure 6.8, the similarity in errors of ECSP and the multispectral method can be seen. Both these methods perform temperature estimation based on the same information and use similar approaches, compare (5.12) and (6.3). While ECSP exhibits a slightly better result compared to multispectral pyrometry in this case, this outcome depends on how the spectral emissivity, $\varepsilon^Q(k, \lambda)$, changes with time. In some cases the multispectral method proves to be superior but experience suggests that ECSP is better in a majority of these situations. However,

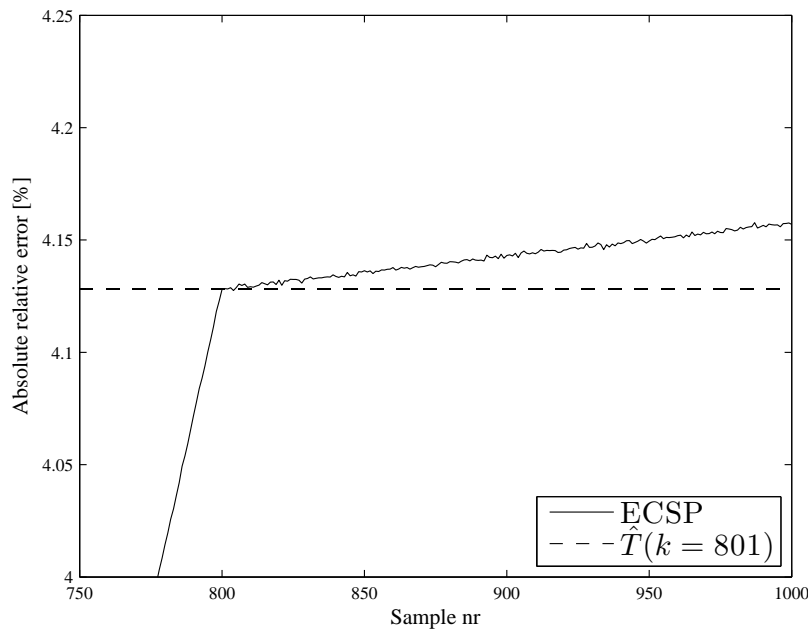


Figure 6.7: Magnification of the area indicated with green in Figure 6.6 with results from Scenario 4. The temperature $\hat{T}(k = 801)$ is indicated with a dashed black line in order to show the drift for the ECSP method (solid black line).

using ECSP comes with the tendency for drift as seen for Scenario 2 with added noise in Figure 6.6.

Conclusion - sensitivity analysis simulation study

ECSP gives quite similar performance to the multispectral pyrometry methods but has the advantage that it somewhat adapts to varying emissivity and gives more accurate temperature estimations. Due to the fact that the calculations are iterative and without any feedback, the method is prone to divergence and drift with time provided that noise is present in measurement data. However, for the scenarios simulated above, which correspond to moderately fast changes in temperature and emissivity for shorter time spans, the inherent divergence of the ECSP method does not cause significant estimation errors. This should nevertheless be a concern when utilising ECSP measurements, long periods of measuring without recalibrating should be avoided. In Paper 3, it is shown that the accumulated root mean square error, due to noise, depends as a square root of the number of samples since it is a summation of temperature estimation errors, each one normally distributed around zero.

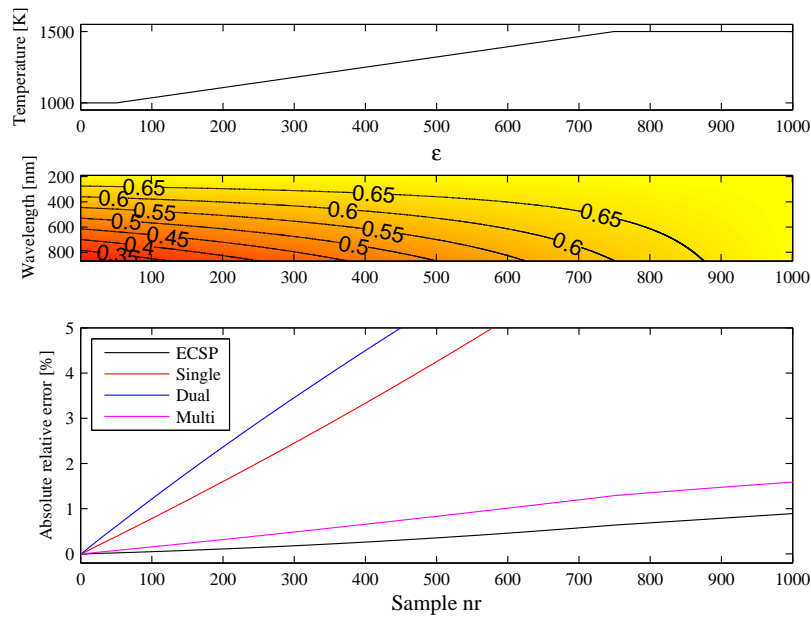


Figure 6.8: Results from Scenario 5 with time varying spectral emissivity. Note that no noise is introduced in the simulation.

6.6 ECSP results

ECSP has been successfully applied to a number of measurement situations, in Paper 2, in Paper 4 and in [117]. Thermal cycling of Ti6Al4V with oxidation is described in Paper 2. Errors proved to typically be below 1 % of absolute temperature. This translates to actual errors of approximately 10 °C in the interesting temperature range. In Figure 6.9, the results for the thermal cycling of Ti6Al4V is shown. The measurement situation is illustrated by Figure 6.10 where the oxidation of the object is clearly seen. In Paper 3, simulations of measurements are performed with variable noise levels, changing emissivity and changing temperature. These results indicate that the main limiting factor for accurate temperature estimations is the signal to noise ratio. This has the effect that higher temperatures typically give higher accuracy provided a fixed spectral range. Apart from the published results, a number of tests have been successfully performed for induction hardening of steel and for Molecular Beam Epitaxy (MBE) deposition of GaN on SiC. In both of these latter situations, emissivity changes are considerable and have previously proved to be difficult to compensate for within pyrometric measurements.

In Section 6.5 a short simulation study is presented, aimed at illustrating the dynamics of the ECSP method, mainly for cases without simulated measurement

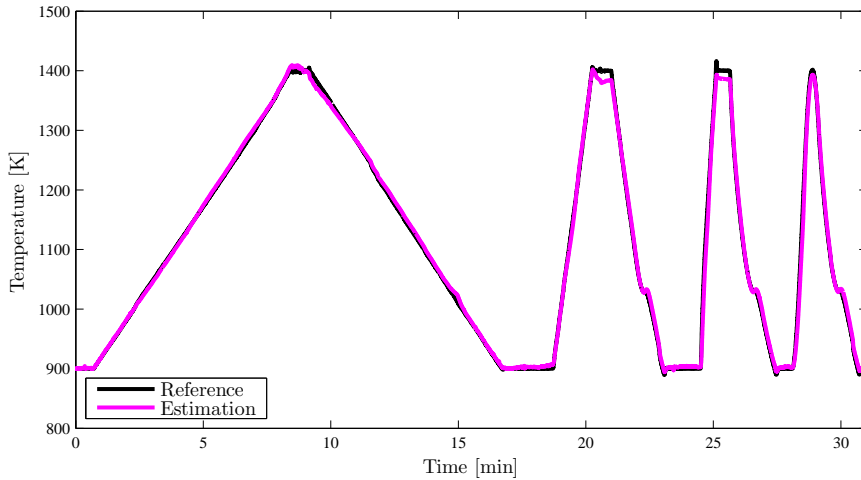


Figure 6.9: ECSP-measurements compared to thermocouple reference. Results from Paper 2.

noise. The ECSP method is shown to give similar results to the multispectral pyrometry method described in Section 5.4, but also exhibits an ability to adapt to varying emissivity.

A PCT patent application has been filed for the ECSP method with reference number PCT/EP2012/071393.

6.7 ECSP for LMD-w monitoring

As described earlier in Section 4.3, calibration of simulation models is a considerable motivation for measuring temperature within the LMD-w process. The accurate measurements made possible with the ECSP method, even for oxidising metal, are well suited as inputs for calibrating such simulation models. Inaccuracy caused by surface oxidation such as described in Paper 1 is minimised and absolute temperatures, which are usually required for model calibration, are measured. Simulation models for LMD-w have previously been calibrated using thermocouples [78], which are constrained to static measurement points on the substrate since they cannot be mounted onto the deposit before it is actually being built.

However, when using the ECSP method together with LMD-w, there are a few problems which are encountered. In order to calibrate the ECSP method, at least one phase transition, such as liquid to solid, has to be observed during processing [118]. This can be achieved by directing the spectrometer onto the cooling material at a fixed point and in such a way record the cooling behaviour and identify the phase transition. After depositing a bead, the robot pauses in a



Figure 6.10: Induction heated titanium specimen. Oxide visible as bluish taint on base plate.

position in which the spectrometer is focused onto a certain point of the recently deposited bead, as the bead cools down. In this way, measurements can be made on every new bead if the spectrometer is also mounted onto the robot with a fixed relative distance to the laser focus and wire feeder as shown in Figure 6.11.

The setup proposed in the above paragraph is however problematic because of the robot dynamics. When the deposition is halted, the robot set speed is decreased to zero, the laser is turned off and spectrometer measurements start. Due to dynamics during the retardation of the robot, the robot and the position of the spectrometer measurement spot moves relative to the substrate even when the robot is not supposed to move any longer. Since the spatial thermal gradients are high on the substrate, even the slightest movement of the measurement spot gives rise to significant temperature signal changes. This effect is illustrated in Figure 6.12, in which a second order system is used to model the positioning dynamics of the robot. The effects of the robot dynamics severely limit the possibilities to identify phase transitions, since distinguishing them from phase transitions in the spectrometer data proves to be difficult. Using the same hardware as in Paper 2 and a sampling rate of 66 Hz, the liquid to solid transition of Ti6Al4V could not be confidently identified in a not-published study conducted by the author.

6.8 Summary

The Emissivity Compensated Spectral Pyrometry (ECSP) method, developed within the scope of this thesis, is a new pyrometry method, which adapts to varying emissivity of a material during temperature measurements. In order to solve the problem of estimating temperature from radiance where emissivity is unknown, ECSP does not use a wavelength-domain constraint like the conven-

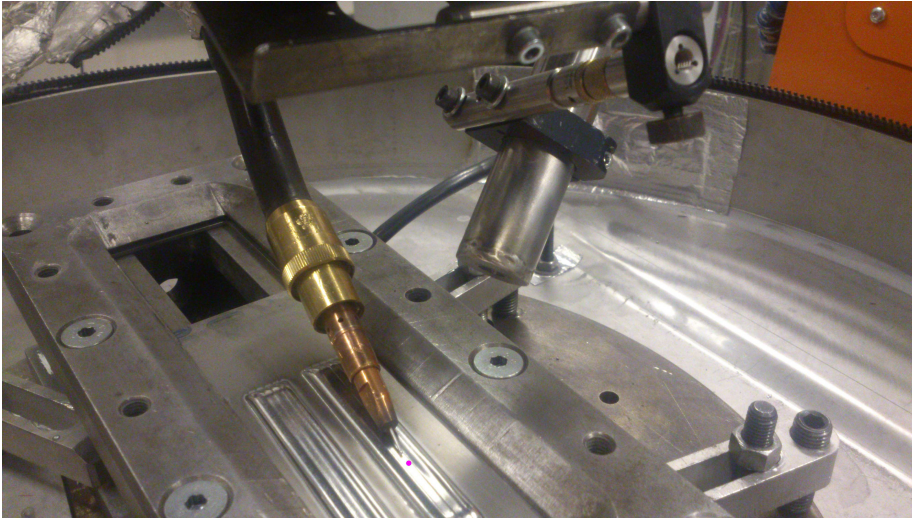


Figure 6.11: Spectrometer mounted onto robot. Measurement spot indicated with magenta.

tional pyrometry methods. The method instead uses a temporal constraint, assuming that the changes in emissivity are limited with regard to time. This leads to an emissivity compensating pyrometry method, accomplished through collection of spectrally resolved radiance measurements, which are processed with an adaptive algorithm based on the temporal constraint. Due to the fact that ECSP requires "teach-in" calibration and exhibits a tendency to drift in practical situations, it should only be used for particular situations where its advantages exceed its disadvantages. Such situations may be where a phase transition can be identified, allowing for automatic calibration, and emissivity is expected to vary significantly over time in an unknown way. In these suitable situations however, it proves to be more accurate than conventional pyrometry methods.

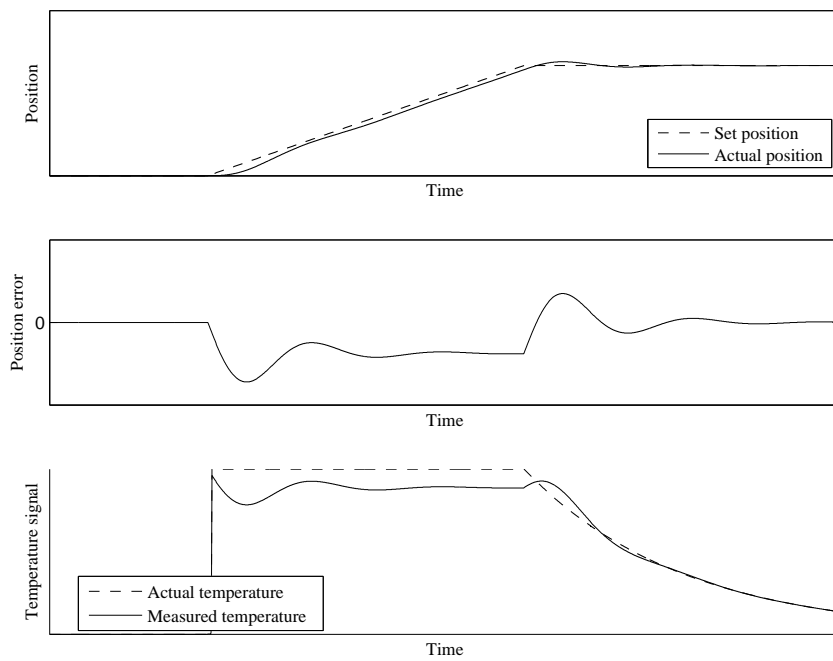


Figure 6.12: Illustration of temperature response for LMD-w bead deposition as a result of robot dynamics. Temperature is assumed to depend linearly on position error, i.e. positive position error results in higher temperature signal.

Chapter 7

Summary of included papers

In this chapter, the papers appended in the second part of this thesis are summarised.

Paper 1

P. Hagqvist, F. Sikström, and A-K. Christiansson
Emissivity estimation for high temperature radiation pyrometry on Ti-6Al-4V
Measurement, **46(2)**:871-880, Feb 2013, 46(2):871-880, Feb 2013

Author's contribution: Principal author. Devised and carried out experiments. Analysed data and proposed theoretical explanations of found results.

Paper addresses research questions **Q1** and **Q2**.

This paper discusses the difficulties in emissivity calibration for non-contact temperature measurements on Ti6Al4V. Prior work in the area of determining Ti-alloy emissivities is briefly reviewed and discussed. A narrow waveband pyrometer is used for radiance measurements and used for emissivity calibrations by also measuring the true temperature of the object with two different methods. Platinum thermocouples proved to be useful as temperature references up to 1723 K. An emissivity reference paint proved to evaporate or diffuse into the material at elevated temperatures around 1473 K. The result of the emissivity calibration showed hysteresis of emissivity with regard to temperature and time. This hysteresis, it is argued, is the result of surface oxidation which affects the resulting surface emissivity. From this, it is concluded that emissivity calibration can only successfully be employed for Ti6Al4V if the oxidation state is well defined and the calibration is carried out at a similar oxidation state.

Paper 2

P. Hagqvist, F. Sikström, A-K. Christiansson and Bengt Lennartson
Emissivity compensated spectral pyrometry for varying emissivity
metallic measurands

Measurement Science and Technology, **25**:025010 2013, Feb 2014

Author's contribution: Principal author and idea originator. Devised and carried out experiments. Implemented algorithm and compiled results.

Paper addresses research questions **Q2** and **Q3**.

Paper 2 introduces and evaluates a new method for non-contact temperature measurements called Emissivity Compensated Spectral Pyrometry (ECSP). A standard UV-Vis spectrometer is used together with an adaptive algorithm for measurements of absolute temperature which are compensated with regard to varying spectral emissivity. This is achieved by using the abundant radiance information supplied by the spectrometer. The paper presents the main principles of ECSP and validates the method by performing measurement trials on a heated metallic specimen. ECSP proves to give accurate temperature values, compared to a thermocouple reference, even when the specimen clearly oxidises.

Paper 3

P. Hagqvist, F. Sikström, A-K. Christiansson and Bengt Lennartson
Emissivity compensated spectral pyrometry - algorithm and sensitivity analysis

Measurement Science and Technology, **25**:025011 2013, Feb 2014

Author's contribution: Principal author. Devised, carried out and evaluated simulations.

Paper addresses research question **Q3**.

In this paper, the ECSP method introduced in Paper 2 is further elaborated upon. Details regarding filters and numerical inversion procedures are discussed. The algorithm is presented in detail in equation form as opposed to the text used in Paper 2. Computer simulations are employed for investigating the method's performance with regard to noise levels and changes in temperature and emissivity. An error model is introduced and its implications are discussed. Estimations

of expected errors are created from theoretical reasoning and confirmed through simulation results.

Paper 4

P. Hagqvist and A-K. Christiansson

Automatic detection of material phase transitions from spectroscopic data

Proceedings of IECON 2013 - 39th Annual Conference on IEEE Industrial Electronics Society. pages 2384-2389, Vienna AUT, Nov 2013

Author's contribution: Principal author and idea originator. Devised and carried out experiments. Conceived and implemented automatic detection methods. Presented paper orally at conference.

Paper addresses research questions **Q1**, **Q2** and **Q3**.

Automatic methods for detecting material phase changes from spectral data are presented in this paper. Such methods are vital for applying the ECSP temperature measurement method discussed in Paper 2 and Paper 3 in an industrial context. Sectioning with derivatives, steady-state identification and cross-correlation are the methods investigated for conducting the automated detection. All three of these methods proved to accurately identify the liquidus-solidus transition of a solidifying copper sample. It is concluded that the methods may be used in conjunction for increased robustness. The importance of automatic phase detection is discussed along with the possible alternatives for initiating the ECSP algorithm.

Paper 5

P. Hagqvist, A. Heralić, A-K. Christiansson and Bengt Lennartson
Resistance measurements for control of laser metal wire deposition
Optics and Lasers in Engineering, **54**:62-67, Mar 2014

Author's contribution: Principal author and idea originator. Devised, carried out and evaluated experiments. Integrated existing and new hardware and software for collecting measurements and controlling LMD-w.

Paper addresses research questions **Q1** and **Q4**.

In Paper 5, the concept of resistance monitoring for automatic control of LMD-w is investigated. From theoretical reasoning and prior knowledge, the method's usability for control of LMD-w is discussed. An empirical model relating the wire and weld-pool resistance to tool-to-workpiece distance is created. This model is used for real-time control of LMD-w using a PI-controller. Promising results are presented along with a discussion on future development and limitations of the control strategy.

Paper 6

P. Hagqvist, A. Heralić, A-K. Christiansson and Bengt Lennartson
Resistance based iterative learning control of additive manufacturing with wire
Resubmitted after revision to *Mechatronics*, Jan 2015

Author's contribution: Principal author, devised, carried out and evaluated experiments in cooperation with A. Heralić. Integrated existing and new hardware and software for collecting measurements and controlling LMD-w using an iterative learning controller based on resistance measurements.

Paper addresses research questions **Q1** and **Q4**.

The principal contribution in Paper 6 is the implementation of an iterative learning controller for geometric control of an LMD-w deposit, based on resistance measurements. Also, the publication demonstrates the benefits of using a wheatstone bridge for measuring the resistance within LMD-w.

Chapter 8

Conclusions and future work

Finding instrumentation and estimation solutions suitable for LMD-w is the core objective of this work. In response to this, a survey of suitable measurement techniques has been performed. Especially temperature measurement methods and resistance measurements have been thoroughly investigated and found to be of use. Due to the complex process and difficulties in utilising sensitive equipment within the process chamber, no other new instrumentation attempts have been made.

Resistance based process monitoring and control shows promise with regard to maintaining a nominal distance between the tool and the workpiece. A functional first generation feedback controller was implemented with a satisfactory outcome. However, when attempting to generalise this result, in order to control a more application-like deposition situation, the method of feedback control based on resistance proved to lack in distance accuracy and was limited by the actuator response time. Instead, using the distance information obtained through *in-situ* resistance measurements for feed forward control seems to be a more viable route. When coupling resistance based distance measurements to an iterative learning control system, good geometrical accuracy together with a stable deposition process is obtained. This methodology should be further investigated in order to discern its limitations and capabilities, but due to its simplicity, it is a very attractive solution when automating LMD-w. Also the possibilities of fusing different data such as from resistance measurements and from image analysis should be investigated for serving as input to an LMD-w control system in the future.

Regarding temperature measurements, much work has been directed towards non-contact temperature measurements on varying emissivity specimens. For LMD-w, Ti6Al4V is an important alloy due to its use within the aerospace industry [3]. It is an alloy which easily oxidises even when processed in argon atmosphere due to residual oxygen. The surface oxidation and oxide migration into the bulk both affect the resulting material emissivity. This is in addition to

the dependence of material phase and temperature the emissivity of Ti6Al4V exhibits by itself. An attempt was made in Paper 1 to calibrate a single waveband pyrometer for measurements on Ti6Al4V for use with LMD-w. It was found that this approach resulted in relatively large errors and that conventional pyrometry methods all give very limited accuracy for oxidising objects. In response to this, a new method which utilises spectral radiance information has been developed. It is shown in both experimental trials as well as simulations, to compensate for varying emissivity and to give more accurate temperature readings than conventional pyrometry techniques. This method, which is denoted Emissivity Compensated Spectral Pyrometry (ECSP), has been proven successful for measurements on Ti6Al4V and copper. An auxiliary method that automatically detects material phase transitions has also been developed, limiting the dependence on conventional calibration for ECSP instruments. The applicability of the technology for other industrially relevant materials such as steel or semiconductors has not fully been determined, but ECSP shows promise for some of the tested applications such as induction hardening of steel and semiconductor processing. The application of ECSP for these purposes and a thorough investigation regarding the method's suitability should be conducted in the future.

Conclusions have also been made regarding the usefulness of obtainable temperature information for LMD-w. With measurements that are limited to the surface, temperature information can only with the help of tuned simulations give bulk temperature estimates. Since such simulations are complex and therefore not feasible for every deposition trial, bulk temperature histories will not, at least in the near future, typically be produced based on radiation thermometry measurements within LMD-w. Bulk temperature histories are of great importance for material properties and one of two main reasons for performing accurate absolute temperature measurements within LMD-w. The other reason is to calibrate or tune simulation models, which can be used for either estimating temperature histories or for getting deeper insight into LMD-w fundamentals. Absolute temperature measurements are therefore of limited interest unless there is a model to be tuned. However, relative temperature measurements such as for comparing two trials might still be of interest for selection of suitable process parameters for a certain geometry. For these measurements however, lower accuracy measurements, such as provided by a single-waveband pyrometer, might suffice.

One substantial conclusion which has been drawn regarding the topic of non-intrusive instrumentation and estimation for control of LMD-w is that it is truly a multidisciplinary topic. The practical challenges require that knowledge from a multitude of disciplines is fused, in order to find solutions to problems. This thesis has, to varying extent, dealt with for example: physics, surface science, materials science, control theory, signal processing, robotics and welding. This multidisciplinary approach has proved fruitful. Progress within the field has been

made as a result of the work leading up to this thesis. This is in the form of more reliable temperature measurement solutions for metallic materials and new control solutions for LMD-w based on resistance measurements.

Appendix

Appendix A

The importance of Planck's law for ECSP

In this appendix, the importance of the properties of Planck's law for the functionality of the ECSP method is illustrated by mathematical approximations and assumptions of ideal cases. It is meant to give some further insight into how and why the ECSP method works.

In order to illustrate how some of the properties of Planck's law (5.1) affect the temperature estimates made with the ECSP method, first introduce some imagined radiance function r_x , which is used with the ECSP algorithm. The function r_x will replace Planck's law (r_P) in the equations that follow in order to show how the formulation of r_x affects the resulting temperature estimates. Also, define

$$\tilde{T}_k = T_k - \hat{T}_k \quad (\text{A.1})$$

as the temperature error at sample k .

First, assume that r_x is only a function of temperature and not of wavelength. As a result of this, $r_x(T)$ will end up being a scalar function $r_x(T)$ instead of a wavelength resolved vector. As introduced in (6.6), the temperature estimation is in ECSP found by the following implicit relation

$$\hat{T} = \arg \min_T H(z) \quad (\text{A.2})$$

with z as introduced in (6.7) and with the measured radiance r

$$z_i = \beta_i \left[\frac{r(\lambda_i)}{r_P(T, \lambda_i)} - \hat{\varepsilon}^Q(\lambda_i) \right]. \quad (\text{A.3})$$

With a scalar r_x , the above relations are satisfied by the scalar relation for each time instance k

$$\beta \left[\frac{r_k}{r_x(\hat{T}_k)} - \hat{\varepsilon}_k^Q \right] = 0. \quad (\text{A.4})$$

For any $\beta \neq 0$, this is equivalent to

$$\frac{r_k}{r_x(\hat{T}_k)} = \hat{\varepsilon}_k^Q. \quad (\text{A.5})$$

This expression may be rewritten using r_x as an analogue to r_P in the definition $r_k = r_P(T_k) \circ \varepsilon_k^Q$ as introduced in (5.5), resulting in

$$\frac{r_x(T_k)\varepsilon_k^Q}{r_x(\hat{T}_k)} = \hat{\varepsilon}_k^Q. \quad (\text{A.6})$$

Using a Taylor expansion of $r_x(\hat{T}_k)$ around $r_x(T_k)$ results in

$$\frac{r_x(T_k)\varepsilon_k^Q}{r_x(T_k) - \tilde{T}r'_x(T_k)} \approx \hat{\varepsilon}_k^Q \quad (\text{A.7})$$

where r'_x denotes the temperature derivative of r_x . Solving this equation for \tilde{T}_k yields the temperature error

$$\tilde{T}_k \approx \frac{r_x(T_k)}{r'_x(T_k)} \left(1 - \frac{\varepsilon_k^Q}{\hat{\varepsilon}_k^Q} \right) \quad (\text{A.8})$$

which also can be written as

$$\tilde{T}_k \approx \frac{r_x(T_k)}{r'_x(T_k)} \left(\frac{\varepsilon_k^Q - \hat{\varepsilon}_k^Q}{\hat{\varepsilon}_k^Q} \right) \quad (\text{A.9})$$

in order to further illuminate that it is the emissivity estimation error $\varepsilon_k^Q - \hat{\varepsilon}_k^Q$ that governs the temperature estimation error \tilde{T}_k . What conclusions may be drawn from the above expression? First, the trivial observation that $\tilde{T}_k = 0$ in the case that $\varepsilon_k^Q = \hat{\varepsilon}_k^Q$ confirms the findings presented in Scenario 3 in Chapter 6 that with a correct emissivity estimation, the temperature estimation will be correct. Second, the ratio of r_x to its temperature derivative r'_x determines how much any error in the estimation of ε_k affects \tilde{T}_k . Thus, a r_x with $r'_x = 0$ will give infinite errors. This agrees with the intuitive notion that if r_x does not change with temperature, the method is not at all appropriate for estimating temperature. On the other hand, if r'_x is large, \tilde{T}_k will be small.

Given the definition of \hat{T}_k given in (A.1), \hat{T}_k may be expressed as

$$\hat{T}_k = T_k - \tilde{T}_k. \quad (\text{A.10})$$

This expression can be used for calculating $\hat{\varepsilon}_{k+1}^Q$ as outlined in Table 6.1

$$\hat{\varepsilon}_{k+1}^Q = \frac{r_k}{r_x(\hat{T}_k)}. \quad (\text{A.11})$$

The expression to the right of the equality sign is, for the scalar case, equal to (A.5):

$$\hat{\varepsilon}_{k+1}^Q = \frac{r_k}{r_x(\hat{T}_k)} = \hat{\varepsilon}_k^Q. \quad (\text{A.12})$$

Which results in

$$\hat{\varepsilon}_{k+1}^Q = \hat{\varepsilon}_k^Q. \quad (\text{A.13})$$

This may seem a surprising result, but it is actually rather intuitive. Recall that in this example, rather than solving for a multitude of wavelengths, we are solving a scalar problem, looking for the temperature which best satisfies our measured radiance r_k given the emissivity $\hat{\varepsilon}_k^Q$. In the scalar case, r_x is a bijective function. This implies that there exists a function r_x^{-1} such that $T = r_x^{-1}(r_x(T))$ and $r_x(T) = r_x(r_x^{-1}(r_x(T)))$ [119]. This leads to that in the scalar case:

$$\hat{T}_k = r_x^{-1} \left(\frac{r_k}{\hat{\varepsilon}_k^Q} \right) \quad (\text{A.14})$$

from (A.5), and

$$\hat{\varepsilon}_{k+1}^Q = \frac{r_k}{r_x(\hat{T}_k)} \quad (\text{A.15})$$

from (A.11). Inserting (A.14) into (A.15) gives

$$\hat{\varepsilon}_{k+1}^Q = \frac{r_k}{r_x \left(r_x^{-1} \left(\frac{r_k}{\hat{\varepsilon}_k^Q} \right) \right)} = \hat{\varepsilon}_k^Q \quad (\text{A.16})$$

once again arriving at the expression in (A.13) for the scalar case. The vectorised case will now be analysed using the same approach as in (A.14) to (A.16).

Calculating \hat{T} for the vectorised case through the minimisation in (A.2) is an overdetermined problem. Since exact solutions to such problems are mere exceptions, a residual vector

$$\delta_k = \frac{r_k}{\hat{\varepsilon}_k^Q} - r_x(\hat{T}_k) \quad \forall \lambda \in \{\lambda_1 \dots \lambda_n\} \quad (\text{A.17})$$

typically exists, i.e. $\delta \neq \mathbf{0}$ where $\mathbf{0}$ is a vector of zeros. Rewriting (A.17) results in

$$r_x(\hat{T}_k) = \frac{r_k}{\hat{\varepsilon}_k^Q} - \delta_k \quad \forall \lambda \in \{\lambda_1 \dots \lambda_n\}. \quad (\text{A.18})$$

Thus, for each wavelength, the scalar \hat{T}_k is (redundantly) determined for each wavelength by

$$\hat{T}_k = r_x^{-1} \left(\frac{r_k}{\hat{\varepsilon}_k^Q} - \delta \right) \quad \forall \lambda \in \{\lambda_1 \dots \lambda_n\} \quad (\text{A.19})$$

while the vector $\hat{\varepsilon}_{k+1}^Q$ is still for each wavelength determined by

$$\hat{\varepsilon}_{k+1}^Q = \frac{r_k}{r_x(\hat{T}_k)} \quad \forall \lambda \in \{\lambda_1 \dots \lambda_n\}. \quad (\text{A.20})$$

Inserting (A.19) into (A.20), results in

$$\hat{\epsilon}_{k+1}^Q = \frac{r_k}{r_x \left(r_x^{-1} \left(\frac{r_k}{\hat{\epsilon}_k^Q} - \delta \right) \right)} \neq \hat{\epsilon}_k^Q \quad \forall \lambda \in \{\lambda_1 \dots \lambda_n\}, \quad (\text{A.21})$$

proving that it is required that $\delta \neq \mathbf{0}$ in order to obtain $\hat{\epsilon}_{k+1}^Q \neq \hat{\epsilon}_k^Q$.

In the case where an exact solution is found for the overdetermined problem in (A.2), the residual vector $\delta = \mathbf{0}$ and consequently $\hat{\epsilon}_{k+1}^Q = \hat{\epsilon}_k^Q$. Such an exact solution can only be produced (for noise-free measurements) if emissivity does not change between samples i.e: $\epsilon_k^Q = \epsilon_{k-1}^Q$. Since an exact solution implies that emissivity does not change, there is reason to keep the emissivity estimate $\hat{\epsilon}_k^Q$ also when calculating $\hat{\epsilon}_{k+1}^Q$. This intuitively corresponds to that $\delta = \mathbf{0}$ leads to $\hat{\epsilon}_{k+1}^Q = \hat{\epsilon}_k^Q$ in this special case. Normally however, this will not be the case for the overdetermined problem created when using multispectral measurements. The utilisation of multiple wavelengths will typically give non-zero residuals and consequently result in an update of $\hat{\epsilon}_k^Q$ that can not be achieved by using only a single wavelength with the ECSP method.

The above equations (A.19) to (A.21) prove that multispectral measurements are required in order to achieve emissivity estimate updates with the ECSP method and that the method can not be successfully used only with a single wavelength. Apart from being a necessity in order to obtain "new" emissivity estimates, the use of many wavelengths also enable using the weight vector β in order to best employ wavelengths with minimal $\frac{r_x(T_k)}{r'_x(T_k)}$ -quotients in order to minimise temperature estimation errors.

Due to the impact of $\frac{r_x(T_k)}{r'_x(T_k)}$ in (A.8) and (A.9), it is interesting to try to quantify it for Planck's law, i.e. $r_x = r_P$. Planck's law (5.1) can be simplified provided that the wavelength and temperature ranges employed ensure that $C_2 \gg \lambda T$, where the constant $C_2 = 0.014388 \text{ K m}$ [81–83]. This approximation is called Wien's approximation and is

$$r_P(T_A, \lambda) \approx \frac{C_1}{\lambda^5 (e^{C_2/(\lambda T_A)})} \quad (\text{A.22})$$

where $C_1 = 1.191 \times 10^8 \text{ W}\mu\text{m}^4\text{m}^{-2}\text{sr}^{-1}$. Using the approximation in (A.22) gives that

$$\frac{r_P(T_k, \lambda)}{r'_P(T_k, \lambda)} \approx \frac{T_k^2 \lambda}{C_2}. \quad (\text{A.23})$$

This result helps in quantifying (A.8) when the wavelength is known and the temperature is known approximately. In Paper 2, it is found that $\frac{T_k^2 \lambda}{C_2} \approx 38 \text{ K}$ for the wavelengths and temperature ranges used therein.

Returning to (A.8), it is seen that the remaining unknown in this expression is

$$1 - \frac{\varepsilon^{\text{Q}}(\lambda)_k}{\hat{\varepsilon}^{\text{Q}}(\lambda)_k} = 1 - \frac{\varepsilon(\lambda)_k}{\hat{\varepsilon}(\lambda)_k} = \frac{\hat{\varepsilon}(\lambda)_k - \varepsilon(\lambda)_k}{\hat{\varepsilon}(\lambda)_k} = \frac{-\tilde{\varepsilon}(\lambda)_k}{\hat{\varepsilon}(\lambda)_k} \quad (\text{A.24})$$

since $\varepsilon^{\text{Q}} = \rho\mathbf{Q} \circ \varepsilon$ and $\tilde{\varepsilon} = \varepsilon - \hat{\varepsilon}$. This value will reflect how correct the emissivity estimation used actually is. If the estimation deteriorates with time, as experienced with the ESCP method, $\tilde{\varepsilon}$ will increase and thus result in an increase in \tilde{T} .

The above approximations and derivations illustrate how crucial it is that the temperature derivative of Planck's law is relatively large when using the ECSP method. It is also shown that ECSP requires wavelength resolved measurements, something which is possible thanks to that Planck's law dictates a wavelength dependence of radiance and that this radiance can be measured using spectrometers.

References

- [1] A. Kleinert, “Der messende luchs : Zwei verbreitete fehler in der galilei-literatur,” *NTM*, vol. 17, no. 2, pp. 199–206, 2009.
- [2] E. Toyserkani, A. Khajepour, and S. Corbin, *Laser cladding*. CRC Press, 2005.
- [3] A. Heralić, “Monitoring and control of robotized laser metal-wire deposition,” Doctoral Thesis, Chalmers University of Technology, 2012.
- [4] T. Wohler, “Additive manufacturing 101: Part IV,” 2010.
- [5] Renishaw plc, “Laser melting systems,” Feb. 2013, <http://www.renishaw.com/en/laser-melting-systems-15240>.
- [6] Phenix Systems, “PXS | phenix systems additive manufacturing using laser sintering,” Feb. 2013, <http://www.phenix-systems.com/en/pxs>.
- [7] Arcam AB, “Additive manufacturing | arcam AB,” Feb. 2013, <http://www.arcam.com/technology/additive-manufacturing/>.
- [8] Sciaky Inc, “Sciaky, inc. | electron beam welding | direct manufacturing | additive manufacturing.” Oct. 2014, http://www.sciaky.com/additive_manufacturing.html.
- [9] A. Spierings, G. Levy, L. Labhart, and K. Wegener, “Production of functional parts using SLM - opportunities and limitations,” in *Innovative Developments in Virtual and Physical Prototyping - Proceedings of the 5th International Conference on Advanced Research and Rapid Prototyping*, 2012, pp. 785–790.
- [10] M. Cronskär, M. Bäckström, and L. Rännar, “Production of customized hip stem prostheses – a comparison between conventional machining and electron beam melting (EBM),” *Rapid Prototyping Journal*, vol. 19, no. 5, pp. 365–372, Jul. 2013.

REFERENCES

- [11] Arcam AB, “Electron beam melting - EBM process, additive manufacturing | arcam AB,” Feb. 2013, <http://www.arcam.com/technology/electron-beam-melting/>.
- [12] ———, “Arcam q20,” Oct. 2014, <http://www.arcam.com/technology/products/arcam-q20/>.
- [13] Trumpf GmbH, “Deposition welding - TRUMPF laser technology,” Feb. 2013, <http://www.trumpf-laser.com/en/solutions/applications/laser-welding/deposition-welding.html>.
- [14] Concept Laser GmbH, “Concept laser - home,” Feb. 2013, <http://www.concept-laser.de/en/home.html>.
- [15] ExOne Inc, “ExOne,” Feb. 2013, <http://www.exone.com/>.
- [16] EOS GmbH, “EOS metall-laser-sinter-systeme,” Feb. 2013, <http://www.eos.info/en/products/systems-equipment/metall-laser-sinter-systeme-kopie-1.html>.
- [17] BeAM Machines, “HOME - BeAM machines,” Feb. 2013, <http://www.beam-machines.com/>.
- [18] Optomec, “Optomec - additive manufacturing technology overview,” Feb. 2013, <http://www.optomec.com/Additive-Manufacturing-Technology/Overview>.
- [19] Fraunhofer IWS, “Coaxial laser wire cladding head COAXwire,” Dec. 2014, http://www.iws.fraunhofer.de/en/business_fields/thermal_coating_additive_manufacturing/laser_cladding/system_technology/COAXwire.html.
- [20] Lincoln Electric, “Laser systems,” Dec. 2014, <http://automation.lincolnelectric.com/laser-systems/>.
- [21] R. Miranda, G. Lopes, L. Quintino, J. Rodrigues, and S. Williams, “Rapid prototyping with high power fiber lasers,” *Materials & Design*, vol. 29, no. 10, pp. 2072–2075, 2008.
- [22] W. Syed and L. Li, “Effects of wire feeding direction and location in multiple layer diode laser direct metal deposition,” *Applied Surface Science*, vol. 248, no. 1-4, pp. 518–524, 2005.
- [23] W. Syed, A. Pinkerton, and L. Li, “A comparative study of wire feeding and powder feeding in direct diode laser deposition for rapid prototyping,” *Applied Surface Science*, vol. 247, no. 1-4, pp. 268–276, 2005.

REFERENCES

- [24] E. Brandl, B. Baufeld, C. Leyens, and R. Gault, "Additive manufactured Ti-6Al-4V using welding wire: comparison of laser and arc beam deposition and evaluation with respect to aerospace material specifications," *Physics Procedia*, vol. 5, no. Part 2, pp. 595–606, 2010.
- [25] E. Brandl, F. Palm, V. Michailov, B. Viehweger, and C. Leyens, "Mechanical properties of additive manufactured titanium (ti-6al-4v) blocks deposited by a solid-state laser and wire," *Materials & Design*, vol. 32, no. 10, pp. 4665–4675, Dec. 2011.
- [26] E. Brandl, A. Schoberth, and C. Leyens, "Morphology, microstructure, and hardness of titanium (Ti-6Al-4V) blocks deposited by wire-feed additive layer manufacturing (ALM)," *Materials Science and Engineering: A*, vol. 532, pp. 295–307, 2012.
- [27] Norsk Titanium AS, "Game changing technology for the production of complex titanium components - norsk titanium," Feb. 2013, <http://www.norsktitanium.no/>.
- [28] F. Bonaccorso, L. Cantelli, and G. Muscato, "An arc welding robot control for a shaped metal deposition plant: Modular software interface and sensors," *Industrial Electronics, IEEE Transactions on*, vol. 58, no. 8, pp. 3126–3132, Aug. 2011.
- [29] B. Baufeld, O. Van der Biest, and R. Gault, "Additive manufacturing of Ti-6Al-4V components by shaped metal deposition: Microstructure and mechanical properties," *Materials & Design*, vol. 31, pp. S106–S111, 2010.
- [30] G. Escobar-Palafox, R. Gault, and K. Ridgway, "Robotic manufacturing by shaped metal deposition: state of the art," *Industrial Robot: An International Journal*, vol. 38, pp. 622–628, 2011.
- [31] G. Muscato, G. Spampinato, and L. Cantelli, "A closed loop welding controller for a rapid manufacturing process," *2008 IEEE International Conference on Emerging Technologies and Factory Automation, Proceedings*, pp. 1080–1083 1517, 2008.
- [32] P. Colegrove and S. Williams, "High deposition rate high quality metal additive manufacture using wire + arc technology," <http://www.norsktitanium.no/en/News/~media/NorskTitanium/Titanidum%20day%20presentations/Paul%20Colegrove%20Cranfield%20Additive%20manufacturing.ashx>.

REFERENCES

- [33] Cranfield University, “Revolutionary 3d printing,” Dec. 2013, <http://www.cranfield.ac.uk/about/media-centre/news-archive/news-2013/revolutionary-3d-metal-production-process-developed-at-cranfield.html>.
- [34] A. Adebayo, “Characterisation of integrated WAAM and machining processes,” Doctoral Thesis, Cranfield University, Dec. 2013.
- [35] P. A. Colegrove, F. Martina, M. J. Roy, B. A. Szost, S. Terzi, S. W. Williams, P. J. Withers, and D. Jarvis, “High pressure interpass rolling of wire+ arc additively manufactured titanium components,” in *Advanced Materials Research*, vol. 996. Trans Tech Publ, 2014, pp. 694–700.
- [36] J. Ding, P. Colegrove, J. Mehnen, S. Ganguly, P. M. Sequeira Almeida, F. Wang, and S. Williams, “Thermo-mechanical analysis of wire and arc additive layer manufacturing process on large multi-layer parts,” *Computational Materials Science*, vol. 50, no. 12, pp. 3315–3322, Dec. 2011.
- [37] C. G. Pickin, S. W. Williams, and M. Lunt, “Characterisation of the cold metal transfer (CMT) process and its application for low dilution cladding,” *Journal of Materials Processing Technology*, vol. 211, no. 3, pp. 496–502, Mar. 2011.
- [38] F. Martina, J. Mehnen, S. W. Williams, P. Colegrove, and F. Wang, “Investigation of the benefits of plasma deposition for the additive layer manufacture of ti–6al–4v,” *Journal of Materials Processing Technology*, vol. 212, no. 6, pp. 1377–1386, Jun. 2012.
- [39] F. Martina, S. W. Williams, and P. Colegrove, “Improved microstructure and increased mechanical properties of additive manufacture produced Ti-6Al-4V by inter pass cold rolling,” in *Proceedings of the 24th International Freeform Fabrication Symposium*, Austin, TX, USA, 2013.
- [40] P. S. Almeida and S. Williams, “Innovative process model of ti–6al–4v additive layer manufacturing using cold metal transfer (CMT),” in *Proceedings of the Twenty-first Annual International Solid Freeform Fabrication Symposium*, Austin, TX, USA, 2010.
- [41] P. Kazanas, P. Deherkar, P. Almeida, H. Lockett, and S. Williams, “Fabrication of geometrical features using wire and arc additive manufacture,” *Proceedings of the Institution of Mechanical Engineers, Part B: Journal of Engineering Manufacture*, p. 0954405412437126, Feb. 2012.

REFERENCES

- [42] J. Mehnen, J. Ding, H. Lockett, and P. Kazanas, "Design study for wire and arc additive manufacture," *International Journal of Product Development*, vol. 19, no. 1, pp. 2–20, Jan. 2014.
- [43] F. Wang, S. Williams, and M. Rush, "Morphology investigation on direct current pulsed gas tungsten arc welded additive layer manufactured Ti6Al4V alloy," *The International Journal of Advanced Manufacturing Technology*, vol. 57, no. 5-8, pp. 597–603, Nov. 2011.
- [44] J. R. Davis and ASM International Handbook Committee, *Metals Handbook Desk Edition 2nd Edition*, 2nd ed. Boca Raton, FL: CRC Press, Dec. 1998.
- [45] J. Andersson, "Weldability of precipitation hardening superalloys – influence of microstructure," Doctoral thesis, Chalmers University of Technology, 2011.
- [46] M. Doubenskaia, M. Pavlov, S. Grigoriev, E. Tikhonova, and I. Smurov, "Comprehensive optical monitoring of selective laser melting," *Journal of Laser Micro Nanoengineering*, vol. 7, no. 3, pp. 236–243, 2012.
- [47] M. Doubenskaia, M. Pavlov, S. Grigoriev, and I. Smurov, "Definition of brightness temperature and restoration of true temperature in laser cladding using infrared camera," *Surface and Coatings Technology*, vol. 220, pp. 244–247, 2013.
- [48] M. Gharbi, P. Peyre, C. Gorny, M. Carin, S. Morville, P. Le Masson, D. Carron, and R. Fabbro, "Influence of various process conditions on surface finishes induced by the direct metal deposition laser technique on a Ti-6Al-4V alloy," *Journal of Materials Processing Technology*, vol. 213, no. 5, pp. 791–800, 2013.
- [49] M. Iravani-Tabrizipour and E. Toyserkani, "An image-based feature tracking algorithm for real-time measurement of clad height," *Machine Vision and Applications*, vol. 18, no. 6, pp. 343–354, 2007.
- [50] J. Liu and L. Li, "In-time motion adjustment in laser cladding manufacturing process for improving dimensional accuracy and surface finish of the formed part," *Optics & Laser Technology*, vol. 36, no. 6, pp. 477–483, Sep. 2004.
- [51] I. Smurov, M. Doubenskaia, and A. Zaitsev, "Comprehensive analysis of laser cladding by means of optical diagnostics and numerical simulation," *Surface and Coatings Technology*, vol. 220, pp. 112–121, Apr. 2013.

REFERENCES

- [52] L. Song, V. Bagavath-Singh, B. Dutta, and J. Mazumder, "Control of melt pool temperature and deposition height during direct metal deposition process," *International Journal of Advanced Manufacturing Technology*, vol. 58, no. 1-4, pp. 247–256, 2012.
- [53] E. Toyserkani and A. Khajepour, "A mechatronics approach to laser powder deposition process," *Mechatronics*, vol. 16, no. 10, pp. 631–641, 2006.
- [54] I. Eriksson, P. Gren, J. Powell, and A. F. Kaplan, "New high-speed photography technique for observation of fluid flow in laser welding," *Optical Engineering*, vol. 49, no. 10, pp. 100 503–100 503, 2010.
- [55] M. Doubenskaia, P. Bertrand, and I. Smurov, "Optical monitoring of Nd:YAG laser cladding," *Thin Solid Films*, vol. 453, pp. 477–485, 2004.
- [56] A. Medrano, J. Folkes, J. Segala, and I. Pashbya, "Fibre laser metal deposition with wire: parameters study and temperature monitoring system," in *Proc. of SPIE Vol.*, vol. 7131, 2009, pp. 221–227.
- [57] D. Salehi and M. Brandt, "Melt pool temperature control using LabVIEW in Nd:YAG laser blown powder cladding process," *The International Journal of Advanced Manufacturing Technology*, vol. 29, no. 3, pp. 273–278, 2006.
- [58] K. H. Leong, K. L. Ho, and H. C. Han, "Monitoring laser cladding," in *ICALEO 2005 Congress Proceedings*. Laser Institute of America, 2005, pp. 895–899.
- [59] G. Bi, B. Schürmann, A. Gasser, K. Wissenbach, and R. Poprawe, "Development and qualification of a novel laser-cladding head with integrated sensors," *International Journal of Machine Tools and Manufacture*, vol. 47, no. 3–4, pp. 555–561, Mar. 2007.
- [60] G. Bi, A. Gasser, K. Wissenbach, A. Drenker, and R. Poprawe, "Characterization of the process control for the direct laser metallic powder deposition," *Surface and Coatings Technology*, vol. 201, no. 6, pp. 2676–2683, 2006.
- [61] D. Hu and R. Kovacevic, "Sensing, modeling and control for laser-based additive manufacturing," *International Journal of Machine Tools and Manufacture*, vol. 43, no. 1, pp. 51–60, 2003.
- [62] L. Song and J. Mazumder, "Feedback control of melt pool temperature during laser cladding process," *IEEE Transactions on Control Systems Technology*, vol. 19, no. 6, pp. 1349–1356, 2011.

REFERENCES

- [63] M. Zeinali and A. Khajepour, “Development of an adaptive fuzzy logic-based inverse dynamic model for laser cladding process,” *Engineering Applications of Artificial Intelligence*, vol. 23, no. 8, pp. 1408–1419, Dec. 2010.
- [64] Y. M. Zhang, P. J. Li, Y. W. Chen, and A. T. Male, “Automated system for welding-based rapid prototyping,” *Mechatronics*, vol. 12, no. 1, pp. 37–53, 2002.
- [65] M. Ericsson, P. Nylén, F. Danielsson, and H. Carlsson, “Off-line programming of robots for metal deposition,” in *Proceedings of the 7th international conference on Trends in Welding Research*, Pine Mountain, Georgia, May 2005, pp. 629–634.
- [66] J. Nurminen, “Hot-wire laser cladding: Process, materials and their properties,” Doctoral Thesis, Tampere University of Technology, 2008.
- [67] A. Heralić, A. Christiansson, K. Hurtig, M. Ottosson, and B. Lennartson, “Control design for automation of robotized laser metal-wire deposition,” in *17th IFAC World Congress, Seoul, Korea, 2008*.
- [68] R. Aune, L. Battezzati, R. Brooks, I. Egry, H.-J. Fecht, J.-P. Garandet, K. C. Mills, A. Passerone, P. N. Quested, and E. Ricci, “Surface tension and viscosity of industrial alloys from parabolic flight experiments—results of the ThermoLab project,” *Microgravity-Science and Technology*, vol. 16, no. 1-4, pp. 11–14, 2005.
- [69] P. J. Webster, L. G. Wright, K. D. Mortimer, B. Y. Leung, X. Z. Joe, and J. M. Fraser, “Automatic real-time guidance of laser machining with inline coherent imaging,” *Journal of Laser Applications*, vol. 23, no. 2, p. 022001, 2011.
- [70] J. F. Andersen, J. Busck, and H. Heiselberg, “Applications of high resolution laser radar for 3-d multispectral imaging,” in *Proceedings of SPIE*, vol. 6214, Orlando, FL, USA, 2006, pp. 62 140U–62 140U–10.
- [71] M. Abderrahim, A. Khamis, S. Garrido, and L. Moreno, “Accuracy and calibration issues of industrial manipulators,” in *Industrial Robotics: Programming, Simulation and Applications*, K.-H. Low, Ed. Mammendorf, Germany: pro literatur Verlag, 2007.
- [72] A. Heralić, M. Ottosson, K. Hurtig, and A.-K. Christiansson, “Visual feedback for operator interaction in robotized laser metal deposition,” in *Proceedings of the 22nd international conference on surface modification technologies*, 2008, pp. 297–304.

REFERENCES

- [73] A. Heralić, A.-K. Christiansson, and B. Lennartson, “Height control of laser metal-wire deposition based on iterative learning control and 3d scanning,” *Optics and Lasers in Engineering*, vol. 50, no. 9, pp. 1230–1241, Sep. 2012.
- [74] G. Pottlacher, H. Hosaeus, E. Kaschnitz, and A. Seiffter, “Thermophysical properties of solid and liquid inconel 718 alloy,” *Scandinavian Journal of Metallurgy*, vol. 31, no. 3, pp. 161–168, Jun. 2002.
- [75] G. Bi, A. Gasser, K. Wissenbach, A. Drenker, and R. Poprawe, “Identification and qualification of temperature signal for monitoring and control in laser cladding,” *Optics and Lasers in Engineering*, vol. 44, no. 12, pp. 1348–1359, 2006.
- [76] A. Crespo, “Modelling of heat transfer and phase transformations in the rapid manufacturing of titanium components,” in *Convection and Conduction Heat Transfer*, A. Ahsan, Ed. InTech, Oct. 2011.
- [77] A. Raghavan, H. L. Wei, T. A. Palmer, and T. DebRoy, “Heat transfer and fluid flow in additive manufacturing,” *Journal of Laser Applications*, vol. 25, no. 5, p. 052006, Nov. 2013.
- [78] M. Edstorp, “Numerical simulation of heat transfer and fluid flow during laser metal wire deposition,” in *2011 ICALEO Congress Proceedings*. Orlando, FL, USA: Laser Institute of America, Oct. 2011.
- [79] P. R. N. Childs, J. R. Greenwood, and C. A. Long, “Review of temperature measurement,” *Review of Scientific Instruments*, vol. 71, no. 8, p. 2959, 2000.
- [80] M. Planck, *The theory of heat radiation*. Philadelphia, PA: P. Blakiston’s Son & Co, 1906.
- [81] R. Siegel and J. R. Howell, *Thermal radiation heat transfer*. London: Taylor & Francis, 2002.
- [82] H. Preston-Thomas, “The international temperature scale of 1990(ITS-90),” *Metrologia*, vol. 27, no. 1, pp. 3–10, 1990.
- [83] Z. M. Zhang, B. K. Tsai, and G. Machin, Eds., *Radiometric Temperature Measurements, Volume 43: II. Applications*, 1st ed. Academic Press, Dec. 2009.
- [84] G. J. Bastiaans and R. A. Mangold, “The calculation of electron density and temperature in ar spectroscopic plasmas from continuum and line

REFERENCES

- spectra,” *Spectrochimica Acta Part B: Atomic Spectroscopy*, vol. 40, no. 7, pp. 885–892, 1985.
- [85] R. Sacks, D. Barlett, C. Taylor, and J. Williams, “Growth related interference effects in band edge thermometry of semiconductors,” *Journal of Vacuum Science and Technology B: Microelectronics and Nanometer Structures*, vol. 23, no. 3, pp. 1247–1251, 2005.
- [86] T. Iuchi, T. Furukawa, and S. Wada, “Emissivity modeling of metals during the growth of oxide film and comparison of the model with experimental results,” *Applied Optics*, vol. 42, no. 13, pp. 2317–2326, May 2003.
- [87] P. Hagqvist, F. Sikström, and A.-K. Christiansson, “Emissivity estimation for high temperature radiation pyrometry on Ti-6Al-4V,” *Measurement*, vol. 46, no. 2, pp. 871–880, Feb. 2013.
- [88] P. Pigeat, D. Rouxel, and B. Weber, “Calculation of thermal emissivity for thin films by a direct method,” *Physical Review B*, vol. 57, no. 15, pp. 9293–9300, Apr. 1998.
- [89] K. Ujihara, “Reflectivity of metals at high temperatures,” *Journal of Applied Physics*, vol. 43, no. 5, pp. 2376–2383, 1972.
- [90] N. M. Ravindra, S. Abedrabbo, W. Chen, F. M. Tong, A. K. Nanda, and A. C. Speranza, “Temperature-dependent emissivity of silicon-related materials and structures,” *Semiconductor Manufacturing, IEEE Transactions on*, vol. 11, no. 1, pp. 30–39, 1998.
- [91] G. Teodorescu, P. D. Jones, R. A. Overfelt, and B. Guo, “High temperature emissivity of high purity titanium and zirconium,” in *Proceedings of the Sixteenth symposium on thermophysical properties*, Boulder, CO, USA, 2006.
- [92] N. D. Milošević and K. D. Maglić, “Thermophysical properties of solid phase titanium in a wide temperature range,” *High Temperatures - High Pressures*, vol. 37, pp. 184–204, 2008.
- [93] P.-F. Paradis and W.-K. Rhim, “Non-contact measurements of thermophysical properties of titanium at high temperature,” *The Journal of Chemical Thermodynamics*, vol. 32, no. 1, pp. 123–133, Jan. 2000.
- [94] L. del Campo, R. B. Pérez-Sáez, L. González-Fernández, X. Esquisabel, I. Fernández, P. González-Martín, and M. J. Tello, “Emissivity measurements on aeronautical alloys,” *Journal of Alloys and Compounds*, vol. 489, no. 2, pp. 482–487, 2010.

REFERENCES

- [95] B. A. Shur and V. E. Peletskii, “The effect of alloying additions on the emissivity of titanium in the neighborhood of polymorphous transformation,” *High Temperature*, vol. 42, no. 3, pp. 414–420, May 2004.
- [96] R. R. Corwin and A. Rodenburgh II, “Temperature error in radiation thermometry caused by emissivity and reflectance measurement error,” *Applied Optics*, vol. 33, no. 10, pp. 1950–1957, Apr. 1994.
- [97] B. K. Tsai, J. Bodycomb, D. DeWitt, K. Kreider, and W. Kimes, “Emissivity compensated pyrometry for specular silicon surfaces on the NIST RTP test bed,” in *12th IEEE International Conference on Advanced Thermal Processing of Semiconductors, 2004. RTP 2004*, 2004, pp. 167–172.
- [98] Britannica Concise Encyclopedia, “Pyrometer,” Jan. 2006.
- [99] P. B. Coates, “Multi-wavelength pyrometry,” *Metrologia*, vol. 17, no. 3, pp. 103–109, Jul. 1981.
- [100] T. Duvaut, “Comparison between multiwavelength infrared and visible pyrometry: Application to metals,” *Infrared Physics & Technology*, vol. 51, no. 4, pp. 292–299, Mar. 2008.
- [101] T. Duvaut, D. Georgeault, and J. L. Beaudoin, “Multiwavelength infrared pyrometry: optimization and computer simulations,” *Infrared Physics & Technology*, vol. 36, no. 7, pp. 1089–1103, Dec. 1995.
- [102] T. Fu, X. Cheng, M. Zhong, and T. Liu, “The theoretical prediction analyses of the measurement range for multi-band pyrometry,” *Measurement Science and Technology*, vol. 17, no. 10, pp. 2751–2756, Oct. 2006.
- [103] H. Madura, M. Kastek, and T. Piątkowski, “Automatic compensation of emissivity in three-wavelength pyrometers,” *Infrared Physics & Technology*, vol. 51, no. 1, pp. 1–8, Jul. 2007.
- [104] C.-D. Wen, “Investigation of steel emissivity behaviors: Examination of multispectral radiation thermometry (MRT) emissivity models,” *International Journal of Heat and Mass Transfer*, vol. 53, no. 9-10, pp. 2035–2043, Apr. 2010.
- [105] C.-D. Wen and I. Mudawar, “Emissivity characteristics of polished aluminum alloy surfaces and assessment of multispectral radiation thermometry (MRT) emissivity models,” *International Journal of Heat and Mass Transfer*, vol. 48, no. 7, pp. 1316–1329, Mar. 2005.

REFERENCES

- [106] P. B. Coates, “The least-squares approach to multi-wavelength pyrometry,” *High Temperatures. High Pressures*, vol. 20, no. 4, pp. 433–441, 1988.
- [107] P. Herve, J. Cedelle, and I. Negreanu, “Infrared technique for simultaneous determination of temperature and emissivity,” *Infrared Physics & Technology*, vol. 55, no. 1, pp. 1–10, 2012.
- [108] R. Brandt, C. Bird, and G. Neuer, “Emissivity reference paints for high temperature applications,” *Measurement*, vol. 41, no. 7, pp. 731–736, Aug. 2008.
- [109] N. M. Ravindra, B. Sopori, O. H. Gokce, S. X. Cheng, A. Shenoy, L. Jin, S. Abedrabbo, W. Chen, and Y. Zhang, “Emissivity measurements and modeling of silicon-related materials: an overview,” *International journal of thermophysics*, vol. 22, no. 5, pp. 1593–1611, 2001.
- [110] G. P. Styan, “Hadamard products and multivariate statistical analysis,” *Linear Algebra and its Applications*, vol. 6, pp. 217–240, 1973.
- [111] F. Gustafsson, *Statistical sensor fusion*. Lund: Studentlitteratur, 2010.
- [112] A. Savitzky and M. Golay, “Smoothing and differentiation of data by simplified least squares procedures,” *Analytical Chemistry*, vol. 36, no. 8, pp. 1627–1639, 1964.
- [113] H. H. Madden, “Comments on the savitzky-golay convolution method for least-squares-fit smoothing and differentiation of digital data,” *Analytical Chemistry*, vol. 50, no. 9, pp. 1383–1386, 1978.
- [114] P. Hagqvist, F. Sikström, A.-K. Christiansson, and B. Lennartson, “Emissivity compensated spectral pyrometry—algorithm and sensitivity analysis,” *Measurement Science and Technology*, vol. 25, no. 2, p. 025011, Feb. 2014.
- [115] A. C. Aitken, “On least squares and linear combinations of observations,” *Proceedings of the Royal Society of Edinburgh*, vol. 55, pp. 42–48, 1935.
- [116] B. Everitt, *The Cambridge dictionary of statistics*, 2nd ed. Cambridge, UK ; New York: Cambridge University Press, 2002.
- [117] P. Hagqvist, H. Kristoffersen, and A.-K. Christiansson, “Temperature monitoring of induction hardening using spectral pyrometry,” in *Proceedings of the sixth Swedish production symposium*. Gothenburg: Swedish Production Academy, Sep. 2014.

REFERENCES

- [118] P. Hagqvist and A.-K. Christiansson, “Automatic detection of material phase transitions from spectroscopic data,” in *Proceedings of IECON 2013 - 39th Annual Conference on IEEE Industrial Electronics Society*. Vienna, AUT: IEEE, 2013, pp. 2384–2389.
- [119] L. Råde and B. Westergren, *Mathematics handbook for science and engineering*. Berlin; New York: Springer, 2004.